UNIVERSIDAD SAN FRANCISCO DE QUITO USFQ

Colegio de Ciencias e Ingeniería

Physics-based sound synthesis of the vibrations of a cantilever steel beam using the finite element method
Trabajo de investigación
.

David Andrés Rivadeneira Bolaños

Ingeniería Mecánica

Trabajo de titulación presentado como requisito
para la obtención del título de
Ingeniero Mecánico

Quito, 19 de mayo de 2017

UNIVERSIDAD SAN FRANCISCO DE QUITO USFQ

COLEGIO DE CIENCIAS E INGENIERÍA

**HOJA DE CALIFICACIÓN
DE TRABAJO DE TITULACIÓN**

Physics-based sound synthesis of the vibrations of a cantilever steel beam using the finite element method

David Andrés Rivadeneira Bolaños

Calificación:

Nombre del profesor, Título académico   Patricio Chiriboga, Ph.D

Firma del profesor   _____

Quito, 19 de mayo de 2017

Derechos de Autor

Por medio del presente documento certifico que he leído todas las Políticas y Manuales de la Universidad San Francisco de Quito USFQ, incluyendo la Política de Propiedad Intelectual USFQ, y estoy de acuerdo con su contenido, por lo que los derechos de propiedad intelectual del presente trabajo quedan sujetos a lo dispuesto en esas Políticas.

Asimismo, autorizo a la USFQ para que realice la digitalización y publicación de este trabajo en el repositorio virtual, de conformidad a lo dispuesto en el Art. 144 de la Ley Orgánica de Educación Superior.

Firma del estudiante: _____

Nombres y apellidos: David Andrés Rivadeneira Bolaños

Código: 00107263

Cédula de Identidad: 1722318803

Lugar y fecha: Quito, 19 de mayo de 2017

RESUMEN

El diseño de instrumentos musicales a través de la historia ha sido un proceso lento de prueba y error, y para mejorar y optimizar su diseño con más rapidez sería muy útil saber cómo cambiaría su sonido al cambiar determinadas características del instrumento. Esto normalmente requeriría construir un prototipo del instrumento primero, lo cual toma demasiado tiempo y dinero. Sin embargo, este paso se podría obviar si se construye un modelo computacional del instrumento que pueda reproducir su sonido. En el presente trabajo se construyó un modelo computacional bidimensional de un instrumento musical sencillo: una viga en voladizo rodeada de aire, y mediante elementos finitos, se calculó el sonido producido por la viga al darle una excitación inicial. El sonido sintetizado se comparó con una grabación con micrófono del sonido producido por una viga en voladizo real para verificar que la onda de sonido haya sido calculada correctamente. Las frecuencias en las ondas de sonido sintetizada y grabada se compararon en el rango de frecuencias desde 100 hasta 2000 hz ya que la onda de sonido grabada tenía la mayor parte de sus frecuencias en este rango, y se halló que las frecuencias en ambas ondas de sonido difirieron en un máximo de 8.08 %, lo cual fue atribuido en parte a variaciones en las propiedades elásticas de la viga. Se halló también que el amortiguamiento de las frecuencias en ambas ondas fue más grande para frecuencias altas que para frecuencias bajas. Se concluyó que la onda de sonido sintetizada logró representar satisfactoriamente las frecuencias del sonido real a pesar de haber usado un modelo bidimensional para la viga, el cual tenía implícita la suposición de que la viga tenía un ancho idealmente infinito. Además de mejorar instrumentos musicales ya existentes, la metodología presentada en este trabajo podría usarse para crear instrumentos nunca antes imaginados.

Palabras clave: Síntesis de sonido, Elementos finitos, Acústica, Simulación, Espectrograma, Viga en voladizo, Vibraciones.

ABSTRACT

Through history, the design of musical instruments has been a slow process of trial and error, and to improve and optimize their design more quickly, it would be very useful to know how their sound would change when changing specific characteristics of the instrument. This would normally require the building of a prototype of the instrument, which would require time and money. This step, however, could be avoided if a computational model of the instrument that could reproduce its sound was build. In the present work, a 2-dimensional computational model of a simple musical instrument: a cantilever beam surrounded by air, was built, and using finite elements, the sound produced by the beam when giving it an initial excitation was calculated. The synthesized sound was compared to a microphone recording of the sound produced by a real cantilever beam to verify that the synthesized soundwave had been calculated correctly. The frequencies in the synthesized and recorded soundwaves were compared in the frequency range from 100 to 2000 hz since the recorded soundwave had most of its frequencies in this range, and it was found that the frequencies in both soundwaves differed by a maximum of 8.08 %, which was attributed in part to variations of the elastic properties of the beam. It was also found that the damping of the frequencies in both soundwaves was larger for larger frequencies than for lower frequencies. It was concluded that the synthesized soundwave represented satisfactorily the frequencies contained in the real sound, despite having used a 2-dimensional beam model to accomplish this, which had implicitly the assumption that the beam had an infinite width. Besides improving already existing musical instruments, the methodology presented in this work could be used to create instruments never imagined before.

Key words: Sound synthesis, Finite element method, Acoustics, Simulation, Spectrogram, Cantilever beam, Vibrations.

TABLE OF CONTENTS

TABLE INDEX

FIGURE INDEX

1 INTRODUCTION

Music and musical instruments have always been part of every culture from the origin of mankind and they have characterized them in both the artistic and historical ways. The development of musical instruments in every culture has required years of development in the past, based on trial and error (Fletcher & Rossing, 1998), which has made their evolution a slow process, and it's not until recently that an engineering approach considering the physics of sound production is being used to guide and accelerate the design of musical instruments. An example of this is the course offered by the University of Michigan in which the fundamentals of music acoustics and hands on experimentation are used by college students to design musical instruments (Bertrand, Kaczmarek, & Wilen, 2015).

To optimize the design of a musical instrument, first it's necessary to listen to its sound, and then make modifications to the shape or materials used in the design. To do this, the instrument would normally first have to be built and then played but this would require a large amount of time, and expenses in material and the construction process. An alternative to overcome this would be to build a mathematical model of the instrument and calculate the sound produced by it using sound synthesis techniques. This would make building the instrument unnecessary, thus allowing building expenses to be avoided. Besides, the instrument's sound would be known in the time it takes to synthesize it, which would ideally take less time than building the instrument. Additionally, the effect of changes to the instrument's properties such as geometry and materials could be done easily by changing few parameters in the mathematical model.

The synthesis of sound is a field of its own and several sound synthesis techniques have been developed. These techniques can be classified into abstract techniques, and the more modern

physical modeling techniques. Abstract techniques focus on synthesizing new sounds either by processing prerecorded samples of existing sounds, or by adding mathematical functions representing simple sounds, and they don't consider the behavior of musical instruments in the generation of sound. Physical modeling techniques, unlike abstract techniques, start from a physical model that describes the behavior of an instrument, and by using this model, they synthesize the produced sound. By using an underlying physical model of an instrument, physical modeling techniques give a more realistic sound than abstract techniques (Bilbao, Numerical Sound Synthesis, 2009).

The most important physical modeling techniques are: 1) digital waveguide synthesis, which uses concepts from digital signal processing to model instruments; 2) lumped mass-spring networks, which models the behavior of an instrument by discretizing it into a large network consisting of point masses, springs, and damping elements; and 3) direct simulation techniques, which solve the partial differential equations describing the motion of a continuous structure by means of numerical methods, to obtain the sound produced by them (Bilbao, Numerical Sound Synthesis, 2009). The advantage of direct simulation techniques over other physical modeling techniques is that they need the least amount of assumptions regarding the physical behavior or geometry of the structure, so they are very general.

Among the different direct simulation techniques, the most popular is the use of finite difference methods (FDMs), which have been used in the sound synthesis of musical instruments of simple geometry, like the cymbal and gong (Bilbao, Percussion Synthesis Based on Models of Nonlinear Shell Vibration, 2010). The drawback of FDMs is that they don't work very well for modeling instruments of irregular geometries (Bilbao, Numerical Sound Synthesis, 2009). The finite element method (FEM), which is another direct simulation technique, however, doesn't have this limitation and is more general. Musical instrument sound synthesis with the FEM hasn't been done much due to its high

computational cost, however some examples include the sound synthesis produced by striking plates of arbitrary shapes (Bruyns, 2006) using modal dynamics; the sound synthesis of a broken bell, where the sound is synthesized from the velocities of the bell's surface (Debut, Carvalho, Figueiredo, Antunes, & Silva, 2015); and the sound synthesis of ideophones, where the vibrations of vibraphone bars are calculated with the FEM and the resulting sound pressure is calculated using an analytical acoustic formulation involving simple pressure sources distributed on the surface of the bars (Bestle, Eberhard, & Hanss, 2017).

In the present work, it is sought to develop and verify a sound synthesis approach using the FEM that models the behavior of both the vibrating structure and the surrounding fluid. The procedure was developed and applied to synthesize the sound produced by the vibrations of a simple structure surrounded by air, in this case a cantilever beam, which is a simplified approximation of a musical instrument known as mbira. A 2D fully coupled acoustic-structural FE model of a beam vibrating in an unbounded domain of air was made in the software Abaqus and is explained in chapter 3; the beam was given an initial excitation, and the soundwave, or acoustic pressure, produced by the resulting vibrations was calculated at a particular location in the air domain as a function of time. Infinite acoustic elements were used in conjunction to finite acoustic elements to model the surrounding air.

To validate the presented synthesis procedure, microphone measurements of the vibrations of an actual cantilever beam were made and are shown in chapter 4, and these measurements were compared with the soundwave obtained from the FE model in chapter 5. The frequency values and their damping in each soundwave were compared in the time and frequency domains using MATLAB. Finally, aural comparisons of the FE and recorded soundwaves were made by playing both sounds.

The present work is unique in that it makes use of acoustic finite and infinite elements to model the behavior of the air as a continuum, which, in the knowledge of the author, hasn't been done before using infinite elements, although the Boundary Element Method (BEM) has been used instead (Bestle, Eberhard, & Hanss, 2017).

The approach presented here can be used to investigate the changes in the sound produced by a musical instrument by making changes to its material and geometrical properties. Also, it could be used to listen to the sound produced by a musical instrument that for some reason, like being broken, cannot be played (Debut, Carvalho, Figueiredo, Antunes, & Silva, 2015), or that doesn't yet exist. Furthermore, it can also be applied in areas other than music, like computer graphics, where synthetic environments from the real world are imitated, and the sound produced by interacting objects forms part of these environments (O'Brien, Shen, & Gatchalian, 2002).

2 LITERATURE REVIEW AND THEORY

This chapter is divided into three sections. Section 2.1 is a review of topics related to the present work, such as previous and current work on physical modeling sound synthesis, and numerical methods used to model unbounded fluid domains in fluid-structure interaction problems, such as the one addressed in this work. The following two sections explain the basic theory used in the present work: section 2.2 gives an explanation of the modal dynamics finite element procedure, which calculates the vibrations of a structure as a function of time by decoupling these vibrations into the motions of the eigenmodes of the structure; section 2.3 presents basic acoustic theory, which is used by Abaqus to synthesize sound, and additionally, some psychoacoustic basic theory is given at the end of section 2.3, which will be referenced in chapter 5. Finally, in section 2.4 the Short Time Fourier

Transform, used to analyze the frequency content of a time domain signal over time, is explained, since it will also be used in chapter 5.

2.1 Literature review

In this section, previous and current work on the field of sound synthesis using the FEM are summarized. Moreover, since the present work also uses the FEM to synthesize sound, some references are cited that illustrate the use of different numerical methods in conjunction with the FEM to discretize the fluid surrounding the structure that produces the sound. The literature referencing the numerical methods is presented first, and the previous and current work in sound synthesis are summarized later.

The sound radiation of a structure represents an acoustic-structure interaction problem and to solve these types of problems computationally, the finite element method (FEM) can be used provided that the acoustic and structural domains being modeled are of finite dimensions. The problem of a structure radiating sound in an open space filled by fluid, however, implies that the fluid domain is unbounded, so FEM cannot be used on its own to solve these types of problems, and needs to be used in conjunction with another type of numerical method. By coupling FEM with the BEM, the issue can be overcome easily as explained in the literature (Fahy & Gardonio, 2006).

Another way that the FEM can handle unbounded domains is by using it in conjunction with either infinite elements or nonreflecting boundary conditions. The brief entitled "Sound Radiation Analysis of Automobile Engine Covers", summarized by Simulia, shows the use of acoustic infinite elements and nonreflecting boundary conditions in the finite element program Abaqus by calculating the acoustic radiations of two car engine valve covers. The results from using either infinite elements or nonreflecting boundary conditions were compared. Also, the use of infinite elements was validated with an experiment. Additionally,

the performance advantages of using infinite elements instead of the BEM are discussed. Further details can be found in the reference (Lu, D'Souza, & Chin, 2005).

In the field of numerical simulations of acoustic-structure interaction problems, some research has been done on the sound radiated by simple representative structures such as plates. The work by Nowak calculates the acoustic radiation of the individual modes of vibration of an aluminum baffled plate surrounded by a semi-infinite water domain with the FEM, where both the plate and the water are discretized with finite elements (Nowak & Zielinski, 2012). This can have applications in military technology where the reduction of noise radiated from submarines, which are composed of simpler structures like plates, is desirable. The sound radiation in water of the first 8 plate's eigenmodes, each vibrating at its natural frequency, was calculated both in the near field (near the structure) and the far-field (far from the structure). This work is important in that it shows how the natural frequencies of the plate change when it's coupled to a dense fluid such as water in comparison to when it's surrounded by a lighter fluid such as air, in which case the natural frequencies only change a little from the values obtained when the plate is in vacuum. It's important to consider this effect when modeling a coupled structural-acoustics problem with the FEM: if the structure is surrounded by a dense fluid, the fluid forces affect significantly the behavior of the structure, so both the structure and fluid are strongly coupled and their motions must be calculated simultaneously in the FE model. In contrast, if a light fluid surrounds the structure, the forces of the fluid don't affect the behavior of the structure significantly, so the fluid and structure are weakly coupled and the structure's motions can be calculated in vacuum with the FEM, and then used to drive the pressure values in the fluid.

In the field of sound synthesis using physical modeling techniques, there are a few works and one example is that of Bruyns (Bruyns, 2006). In this work, the sound produced by striking plate structures of rectangular and letter-like shapes with rods was synthesized. To do this, a

linear finite element model of the structures was created and the resulting motions from striking them at specific locations were obtained as a composition of their eigenmodes oscillating at the corresponding eigenfrequencies. Then, having calculated the motions of the structures, the sound produced by them was synthesized by treating the finite elements in their surfaces as small pistons, each pushing on the surrounding air. The finite element model was then validated by comparing the radiated sound pressure from the model at specific locations, with the sound pressure recorded from experiments in which the same structures were hit by a rod at the same locations. The author goes on to develop a small graphical user interface in which a user can obtain the soundwave produced by hitting an arbitrarily shaped object.

Sound synthesis of musical instruments can be used for purposes other than design optimization. For example, a work has been done in which the sound of a broken medieval bell that can no longer be played was synthesized using the FEM (Debut, Carvalho, Figueiredo, Antunes, & Silva, 2015). The purpose of the work was to get an idea of how the bell sounded when it was in good state. To do this, an FE linear model of the bell and the clapper used to strike it was made to calculate the surface vibrations of the bell. The contact between the clapper and the bell was modeled with Hertz's contact formulation. The bell's material properties were obtained by performing nondestructive tests on part of the bell, averaging the elastic properties of the different material phases in the microstructure. The sound was synthesized directly from the normal surface velocities of the bell without modeling the surrounding air. Additionally, the clapper's elastic properties were varied to know the effect on the synthesized sound. The procedure for obtaining material properties in this work could be used for obtaining very accurate property values if desired.

Most recently, a work on the field of sound synthesis of idiophones such as vibraphone bars has been done (Bestle, Eberhard, & Hanss, 2017). In this work, a sound synthesis algorithm

was developed to optimize the design of vibraphone bars: the algorithm consisted of discretizing a vibraphone bar into finite elements, and the elastic properties of the bar were obtained from experimental modal analyses with laser doppler vibrometers on an actual metal bar. The surface vibrations of the bar in vacuum given an initial excitation were calculated by combining the FEM with multibody dynamics, to account for nonlinear motions, and then used to calculate the acoustic pressure at any point in the surrounding air. The acoustic pressure was calculated by superposing the pressure radiated by simple spherical acoustic sources distributed on the surface of the bar. The algorithm was validated by comparing it with results using the BEM and microphone measurements, giving very similar results, an in a notably shorter time in comparison to the BEM model. Finally, the algorithm was used to synthesize the sound radiated by two other bars with different geometric modifications. While the far field sound calculations were very similar to those obtained with the BEM in all cases, the near field results (those in the vicinity of the vibrating structure) were not as similar, so there lies the disadvantage of the described algorithm, which might come from modeling the air pressure as the superposition of discrete spherical pressure sources, instead of modeling the air as a continuum.

2.2 Finite element equations for dynamic problems and solution procedures

In this section, the FE equation that describes the motions of structures in time, under general loading conditions, is introduced. Also, two methods used to solve the equation, namely direct integration and modal dynamics, are introduced.

The equation of equilibrium that governs the linear response of a displacement-based system of finite elements is given by equation (1):

$$M\ddot{U} + C\dot{U} + KU = R \tag{1}$$

Equation (1) is a set of coupled ordinary differential equations where M, C, K, & R are the system's mass, damping, stiffness and vector of externally applied forces respectively, and U is the vector of nodal displacements, of order n. There are two methods that can be used to solve equation (1): direct integration is the first, and mode superposition the second. These methods are introduced in the sequel.

2.2.1 Direct integration.

In direct integration, equation (1) is solved using numerical step-by-step integration without transforming the equation set into another equivalent form before doing the integration. The solution is sought for a given finite time period and it's approximated at discrete time values within this period separated by a time increment Δt that is not necessarily constant. Direct integration is an expensive solution method if the system consists of a large number of degrees of freedom (DOF), which in this case are the nodal displacements in vector U, and is mainly used when the time response of the system is sought for a small time period. The solver Abaqus/Explicit from Abaqus solves equation (1) by using the central difference direct integration scheme, and in addition it can account for the nonlinear effects caused by the large displacement FE formulation. This solver was used in the calculation of the soundwave radiated by the free vibrations of a cantilever beam, which is explained in section 3.7.

2.2.2 Modal dynamics.

If only the linear-displacement time response of a structure is sought, the mode superposition solution method can be used. This method first decouples the system of equations in equation (1); this implies that the system reduces to n individual linear ordinary differential equations (ODEs), each of which can be solved independently from one another. The solution then is carried out by numerically integrating each ODE. In what follows, the process of decoupling equation (1) is shown and details can be found in the reference (Bathe, 1996).

The decoupling of equation (1) begins by making a change of variables from U to X as shown in equation (2)

$$U = PX \tag{2}$$

and then substituting equation (2) into equation (1) before premultiplying the resulting equation by P^T. This gives equation (3)

$$\tilde{M}\ddot{X} + \tilde{C}\dot{X} + \tilde{K}X = \tilde{R} \tag{3}$$

where

$$\tilde{M} = P^T M P; \quad \tilde{C} = P^T C P; \quad \tilde{K} = P^T K P; \quad \tilde{R} = P^T R \tag{4}$$

The matrix P in equations (2) and (4) is a square matrix, and can be determined from the solution of the undamped unforced version of equation (1) shown in equation (5)

$$M\ddot{U} + KU = 0 \tag{5}$$

The general solution to equation (5) is of the form shown in equation (6)

$$U = \varphi\sin(\omega(t - t_0)) \tag{6}$$

where φ is called an eigenvector, t is the time variable, t_0 is a constant & ω is called a natural frequency. By substituting equation (6) into equation (5) and simplifying, equation (7) is obtained. This last equation, which must be solved for φ and ω, is known as a generalized eigenproblem.

$$K\varphi = \omega^2 M\varphi \tag{7}$$

This equation has n solution pairs of the form $(\omega_1^2, \varphi_1); (\omega_2^2, \varphi_2); \dots ; (\omega_n^2, \varphi_n)$.

All solutions to equation (7) can be condensed into a single expression, shown in equation (8)

$$K\Phi = M\Phi\Omega^2 \tag{8}$$

Where the matrices Φ and Ω^2 are defined in equations (9) and (10)

$$\Phi = [\varphi_1 \ \varphi_2 \ \cdots \ \varphi_n] \tag{9}$$

$$\Omega^2 = \begin{bmatrix} \omega_1^2 & 0 & 0 & 0 \\ 0 & \omega_2^2 & 0 & 0 \\ 0 & 0 & \ddots & 0 \\ 0 & 0 & 0 & \omega_n^2 \end{bmatrix} \tag{10}$$

The eigenvectors have the property of being M-Orthonormal, which means that equation (11) holds:

$$\varphi_i^T M \varphi_j = \begin{cases} 1 & if \ i = j \\ 0 & if \ i \neq j \end{cases} \tag{11}$$

This equation can be expressed for all eigenvectors as in equation (12), where I is the identity matrix

$$\Phi^T M \Phi = I \tag{12}$$

Premultiplying equation (8) by Φ^T and then substituting equation (12) in the previous equation gives equation (13).

$$\Phi^T K \Phi = \Omega^2 \tag{13}$$

By comparing equations (12) & (13) with equation (4), it can be seen that Φ works as a suitable P matrix. By making the substitution $P = \Phi$ in equation (3), equation (14) is obtained, which is the decoupled version of equation (1) since the new system matrices, $\widetilde{M}$ & $\widetilde{K}$, (see equation (4)) are diagonal, and the matrix $\widetilde{C}$ can be made diagonal.

$$\ddot{X} + \Phi^T C \Phi \dot{X} + \Omega^2 X = \Phi^T R \tag{14}$$

The n components $x_i(t)$ of vector X in the preceding equation are called generalized displacements, and can be obtained in a transient modal dynamic analysis in Abaqus.

Equation (2) can be rewritten using equation (9) as in equation (15). In practice, not all n modes in equation (15) are used to synthesize $U(t)$, but only those whose associated generalized displacements are relatively large in comparison to the others. This is done to simplify the analysis of large problems.

$$U(t) = \Phi X = \sum_{i=1}^{n} \varphi_i x_i(t) \tag{15}$$

If damping can be assumed to be proportional, in other words, if $\varphi_i^T C \varphi_j = 2\xi_i \omega_i \delta_{ij}$ where ξ_i is a modal damping variable known as damping ratio and δ_{ij} is the Kroneker delta ($\delta_{ij} = 1 \; if \; i = j, \delta_{ij} = 0 \; if \; i \neq j$), then matrix $\tilde{C}$ in equation (4) is diagonalized and the system of ordinary differential equations (ODE) in equation (14) is decoupled. Each of the n decoupled equations without the vector of nodal forces is of the form given in equation (16). As a note, to each eigenvector, and consequently, to each natural frequency ω_i, corresponds one damping ratio ξ_i.

$$\ddot{x}_i + 2\xi_i \omega_i \dot{x}_i + \omega_i^2 x_i = 0 \tag{16}$$

In case of overdamping, the solution to equation (16) is given in equation (17), where δ_i, Θ_i, and $\omega_{d,i}$ are constants dependent on initial conditions.

$$x_i(t) = \Theta_i e^{-\xi_i \omega_i t} \cos(\omega_{d,i} t + \delta_i) \tag{17}$$

Damping in a FE model is usually defined in terms of Rayleigh damping, given in matrix form in equation (18), where C, M and K are the matrices from equation (1), and α and β are constants to be defined by two known damping ratios ξ_i corresponding to two different frequencies ω_i.

$$C = \alpha M + \beta K \tag{18}$$

The equation relating the damping ratios and the α and β constants, which are known as mass and stiffness proportional damping respectively, is given in equation (19)

$$\xi_i = \frac{\alpha + \beta \omega_i^2}{2\omega_i} \tag{19}$$

2.3   The linear wave equation for an acoustic medium, and basic psychoacoustics

In this section, the linear acoustic wave equation that Abaqus solves with the FEM is introduced. The linear, lossless wave equation governs the behavior of acoustic waves when viscosity effects can be neglected, and the variations of pressure with respect to the steady state (atmospheric) pressure are small. The detailed derivation of this equation can be found in (Kinsler, Frey, Coppens, & Sanders, 2000). Below, a brief overview of how this equation is obtained is given.

The linear, lossless wave equation is the combination of the linear Euler's equation (a force equation), the linear continuity equation, and the equation of state of a fluid medium in an acoustic process. These equations are given below.

The linear Euler's equation, given in equation (20) assumes that viscous effects within the fluid can be neglected and is valid for acoustic processes of small amplitude. In this equation, ρ_0 represents the steady-state density of the acoustic medium, $\vec{u}$ represents the velocity vector of the particles of the acoustic medium, and p represents the acoustic pressure, which is defined as the pressure above the pressure of the medium in equilibrium conditions: if $\wp$ is the absolute pressure (a function of time and space), and $\wp_0$ is the pressure in steady-state

conditions (atmospheric air pressure in our case), then $p = \wp - \wp_0$. All the variables defined in equation (20) and in equations (21) - (23) are a function of space and time.

$$\rho_0 \frac{\partial \vec{u}}{\partial t} = -\nabla p \tag{20}$$

The linear continuity equation is given in equation (21). In this equation, ρ is the density of the medium as a function of time and space; s is the condensation, defined as $s = \frac{(\rho - \rho_0)}{\rho}$.

$$\rho_0 \frac{\partial s}{\partial t} + \nabla \cdot (\rho_0 \vec{u}) = 0 \tag{21}$$

The equation of state for a fluid medium in an acoustic process is given in equation (22), where $\mathcal{B}$ is the adiabatic bulk modulus of the medium.

$$p = \mathcal{B}s \tag{22}$$

Taking the time derivative of equation (21), taking the divergence of equation (20), combining these two equations, and substituting equation (22) in the resulting equation gives the linear lossless wave equation, given in equation (23). Where, c is the speed of sound, defined as $c = \sqrt{\frac{\mathcal{B}}{\rho_0}}$.

$$\frac{\partial^2 p}{\partial t^2} = c^2 \nabla^2 p \tag{23}$$

This concludes the derivation of the linear, lossless wave equation. In the remainder of this section, some basic concepts of psychoacoustics are given.

Figure 1 shows the so called equal loudness level contours plot. The figure consists of several curves known as equal loudness level contours, each of which is composed of points of coordinates $(frequency, SPL)$, where $frequency$ represents the frequency of a pure sinusoidal tone, and SPL is the sound pressure level, which is an increasing function of the acoustic pressure p of the same tone.

The exact formula for SPL is given in equation (24), where P_{RMS} is the RMS value of the acoustic pressure p, and P_{ref} is equal to $2e-5\ Pa$ for acoustic pressure in air (Kinsler, Frey, Coppens, & Sanders, 2000).

$$SPL = 20log_{10}\left(\frac{P_{RMS}}{P_{ref}}\right)\ [dB] \qquad (24)$$
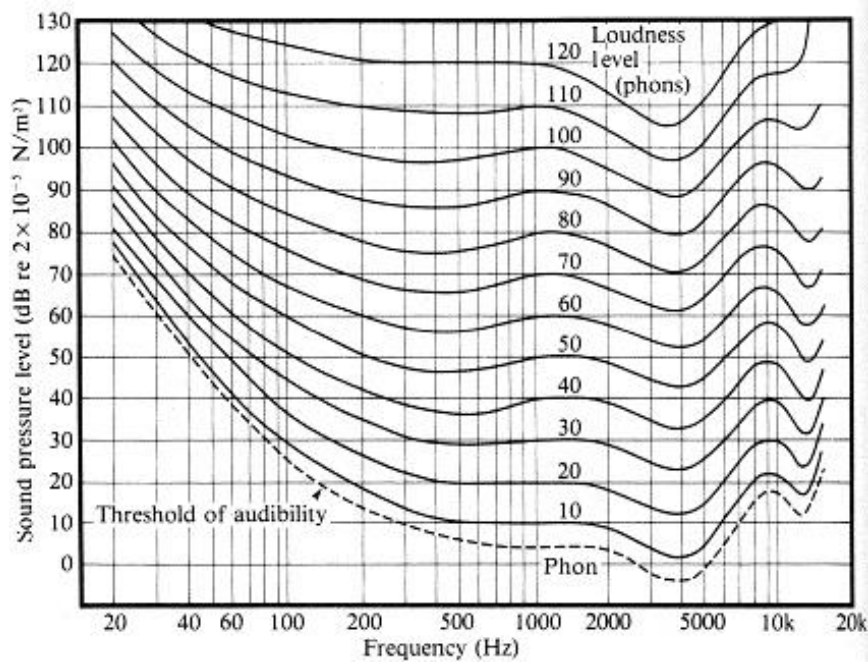
Figure 1: Equal loudness level contours plot

Each curve in Figure 1 corresponds to a tone whose sound is perceived by humans to be equally loud. For example, a 100 hz sinusoidal tone with $SPL \approx 30\ dB$ is perceived as equally loud as a 1000 hz sinusoidal tone with $SPL = 10\ dB$. The important thing to take from Figure 1 is that in the range from 0 to 10 khz, midfrequency tones need a lower SPL value to be perceived as equally loud as low and high frequency tones. And since SPL is an increasing function of the acoustic pressure, this means that midfrequency tones need a lower acoustic pressure magnitude to be perceived as equally loud as low and high frequency tones.

2.4   The Short Time Fourier Transform

To analyze how the frequency content of a time-domain signal such as an audio signal evolves over time, the Short Time Fourier Transform (STFT), or spectrogram, can be employed. This is an algorithm that divides the time signal into various segments and calculates the Discrete Fourier Transform (DFT) of each segment. This can be seen in Figure 2, which shows how a time-domain signal is divided into segments, and the DFT of each of these is calculated using a Fast Fourier Transform (FFT) algorithm. The magnitude spectrum from the DFT of each segment shows the frequency content of the corresponding segment, so the evolution over time of the frequency content of the original time-domain signal can be seen by looking at how the magnitude spectrum of the segments composing it evolves over time, which is shown at the bottom of the figure in the plot with colors which is the spectrogram, where the colors represent the magnitude of each frequency in it.
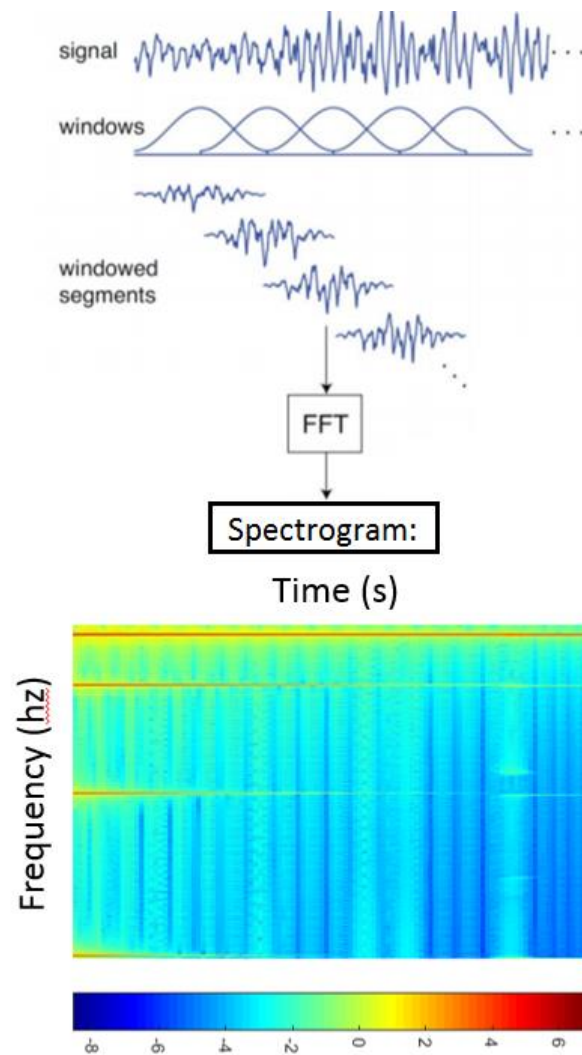
Figure 2: Diagram showing how the STFT works

3 MODELING

In the present work, the acoustic radiation of the vibrations of a cantilever beam given an initial displacement were calculated with finite elements in the form of acoustic pressure, or soundwave, at a certain point in space. Both the beam and the surrounding air were modeled with finite elements. The material and damping properties used in the FE modeling were obtained from a real-life cantilever beam system, which was also used to validate the sound synthesized from the FE model in chapter 5. The current chapter explains the FE procedures used to synthesize the sound of the vibrating beam, and how the real-life cantilever beam

system was built. The chapter is divided into several sections as explained next. Section 3.1 describes the real-life cantilever beam system that was built, consisting of a steel beam clamped at one end by a vise. Section 3.2 describes an analytical beam formulation that was used to validate a FE model of the beam (without the surrounding air). In section 3.3, a summary of the FE procedures explained in more detail in sections 3.4 through 3.8 is given. Section 3.4 describes the modeling of the beam alone in Abaqus and its validation using the analytical formulation from section 3.2. Section 3.5 describes how the air domain was meshed. Section 3.6 explains how the FE beam was initially excited for the subsequent vibration in air. In Section 3.7, the FE meshes of the beam and air from the previous two sections are combined in an acoustic-structural model that was later used to synthesize the sound from the beam's vibrations. Finally, section 3.8 explains how material damping was added to the beam in the acoustic-structural model from section 3.7 using Rayleigh damping.

3.1 Physical system description

The beam FE model presented in section 3.4 needed material and damping properties, which were measured from a real-life cantilever beam that was built by clamping a steel beam with a vise. This beam-vise assembly is henceforth referred to as the vise-beam system. This section explains how the vise-beam system was built. This includes a description of the dimensions of the beam used as well as a description of its material and how it was manufactured.

To manufacture the beam, a rectangular piece of dimensions 15 X 220 X 1 mm was cut from a SAE 430 cold-rolled steel plate using the waterjet cutting manufacturing process. This process was used because it makes clean cuts and principally because it is a cold-work process, meaning that material properties of the work material are not changed appreciably,

which was necessary since variations in the elastic modulus or yield strength of the piece were not desired.

Since a fixed condition was needed for one of the beam's ends, this end was held in place using a vise. The effective length of the beam (the length not clamped by the vise, and that radiates sound) was 86.2 mm. This length was chosen to be as large as possible to reduce the values of the beam's natural frequencies as much as possible, which would reduce the simulation time when synthesizing the acoustic soundwave using Abaqus. This is because lower frequencies allow coarser meshes to be used for both the acoustic and structural domains, to obtain accurate results, and this translates into less equations to be solved. At the same time, the length was chosen so that the first natural frequency of the beam would be easily audible, which would allow a qualitative comparison of the sound recorded in the experiment, and the sound calculated numerically by playing both sounds.

The length of the beam was chosen so that the beam would have its fundamental frequency at 110 hz. This frequency was chosen as the fundamental because it's a low audible frequency and because it corresponds to an A note on the musical scale, and this work is related to music. Due to human errors, the beam's length was chosen as 8.62 mm, which gives a fundamental frequency of 111.97 hz. The calculation of this length is shown in section 3.2.

The material for the beam was chosen to be stainless steel because it has a relatively large yield strength, and this allowed a relatively large range of possible values for the effective length of the beam to be picked from. The technical specifications that came with the material are included in attachment B.

3.2 Structural analytical model

In this section, the Euler – Bernoulli beam model is used to solve for the motions of a cantilever beam due to initial conditions. The solution involves algebraic equations

describing the natural frequencies and the mode shapes of the beam. The modes and corresponding natural frequencies are calculated and are used subsequently to validate a finite element (FE) model of the same beam (vibrating in vacuum), described in section 3.4, where the validation was done by comparing the values of the natural frequencies obtained by both methods. The details of the mathematical development given in this section can be found in (Rao, 2011).

The lateral vibrations of a beam (with no loading) of uniform cross section with an area equal to A can be modeled with equation (25), which is derived from the Euler – Bernoulli theory:

$$\frac{EI}{\rho A}\frac{\partial^4 w}{\partial x^4}(x,t) + \frac{\partial^2 w}{\partial t^2}(x,t) = 0 \tag{25}$$

Each of the constants and variables in equation (25) are defined in Table 1:

Table 1: Parameters in the Euler-Bernoulli beam equation of free motion

Variables		Constants	
w	Lateral displacement of the beam	ρ	Beam density
x	Longitudinal position along the beam	E	Young's modulus
t	time	I	Moment of inertia of the beam cross section along w (transversal) axis

Figure 3, taken from (Rao, 2011), shows the spatial disposition of variables w and x from equation (25). In the figure, the function $f(x,y)$ is equal to zero for vibrations of the beam with no loading, and it's ignored in this work.
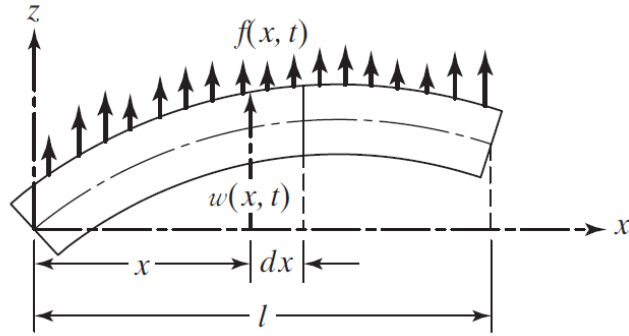
Figure 3: Figure showing the principal variables in equation (25)

The boundary conditions (BCs) in equations (26) to (29) are necessary to solve the differential equation for a cantilever beam:

Fixed (clamped) end boundary condition at $x = 0$:

$$w(0, t) = 0 \tag{26}$$

$$\left. \frac{\partial w}{\partial x} \right|_{x=0} = 0 \tag{27}$$

Free end boundary condition at $x = l$:

$$EI \left. \frac{\partial^2 w}{\partial x^2} \right|_{x=l} = 0 \tag{28}$$

$$\left\{ \frac{\partial}{\partial x} \left(EI \frac{\partial^2 w}{\partial x^2} \right) \right\} \Bigg|_{x=l} = 0 \tag{29}$$

The differential equation (25) has several solutions, w_i, which are solved for using the method of separation of variables as shown in equation (30),

$$w_i(x, t) = W_i(x) T_i(t) \tag{30}$$

where each function $W_i(x)$ is called a mode shape. The functions $T_i(t)$ can be defined using initial conditions, but it's of no interest in this work to do so because we are only interested in the mode shapes and natural frequencies, which are independent of initial conditions and serve the purpose of validating the FE model described in section 3.4.

The mode shapes are found by substituting equation (30) into equation (25) and using the BCs given in (26) - (29). The mode shapes are given in equation (31):

$$W_i(x) = C_i[\sin(\beta_i x) - \sin h(\beta_i x) - \alpha_i(\cos(\beta_i x) - \cosh(\beta_i x))] \tag{31}$$

where C_i is an arbitrary constant, and α_i is given in equation (32):

$$\alpha_i = \left(\frac{\sin(\beta_i l) + \sinh(\beta_i l)}{\cos(\beta_i l) - \cosh(\beta_i l)}\right) \tag{32}$$

Equation (33), called the frequency equation, gives the values of $\beta_i l$:

$$\cos(\beta_i l) * \cosh(\beta_i l) = -1 \tag{33}$$

Where β_i is given in equation (34):

$$\beta_i = \frac{\rho A \omega_i{}^2}{EI} \tag{34}$$

Here ω_i is the ith angular natural frequency (a positive real number) associated with the ith mode shape.

The general solution of the differential equation (25) can be expressed as the sum of the individual solutions w_i, given in (30), due to the principle of linear superposition which applies to linear differential equations. Equation (35) gives the general solution, which is a sum of an infinite number of terms; this is due to the fact that equation (33) has an infinite number of solutions, hence, there's an infinite number of mode shapes because each mode $W_i(x)$ is a function of β_i (see equation (31)).

$$w(x,t) = \sum_{i=1}^{\infty} w_i(x,t) \tag{35}$$

Figure 4 shows the first four mode shapes, obtained from equation (31) and their corresponding natural frequencies f_i, where $f_i = 2\pi\omega_i$. Only the first three modes were considered in this work as will be explained in section 4.1. The modes and frequencies in this figure correspond to a beam of length equal to 8.62 cm, which was the length of the beam used in this work. In the figure, the zero position corresponds to the fixed end of the beam and the mode shapes are shown normalized to 1.
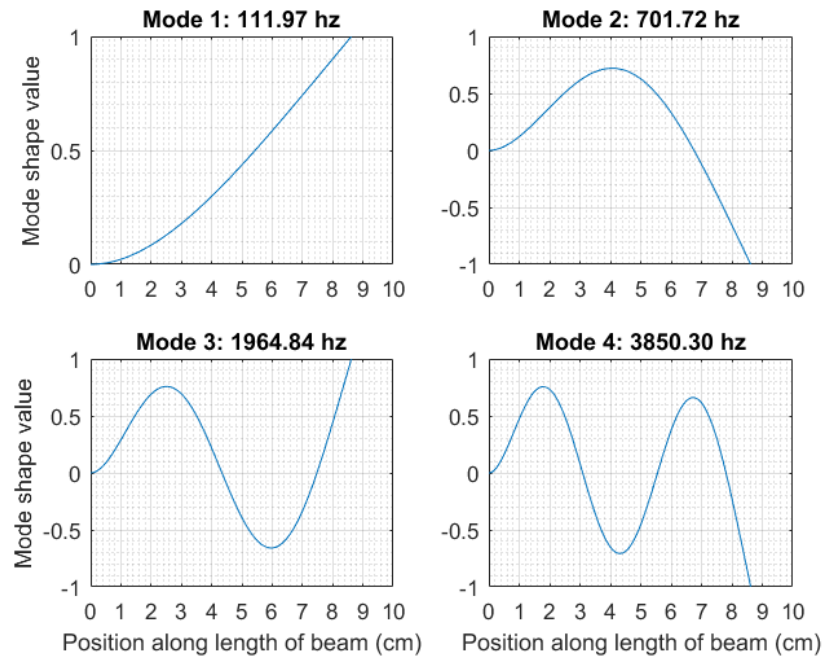
Figure 4: First 4 mode shapes and corresponding eigenfrequencies of the cantilever beam, obtained with the Euler-Bernoulli model. The length of the beam of 8.62 cm used in this work, was used to calculate the modes and frequencies in the figure.

The beam's length of 8.62 cm was calculated by solving equation (33) for $\beta_i l$, taking $i = 1$, and using equation (34) to solve for l, using $\omega_1 = 2\pi f_1$, and $f_1 = 100 \, hz$, where f_1 is defined to be the first natural frequency of the beam. In this calculation, ρ from equation (34) was taken as $7800 \frac{kg}{m^3}$ which is a theoretical value for the density of steel. However, the real

density of the beam used in this work was measured as $7539.4 \frac{kg}{m^3}$, so the fundamental frequency of the beam with the same length of 8.62 cm changed to 111.97 hz, which is only a small change. This frequency is shown in Figure 4, with the other natural frequencies.

3.3 Finite element modeling outline

The real-life cantilever beam described in section 3.1 was modeled in Abaqus (the vise was not modeled) to replicate, by using Finite Elements, the sound produced by the beam, shown in Figure 32 from section 4.1. In this section, all the finite element models created to accomplish this are described. The flowchart in Figure 5 shows a summary of the models created. In each box of the chart, the name of a model is given first, and a description of what the model does is given next. The arrows indicate the succession in which each model was used.
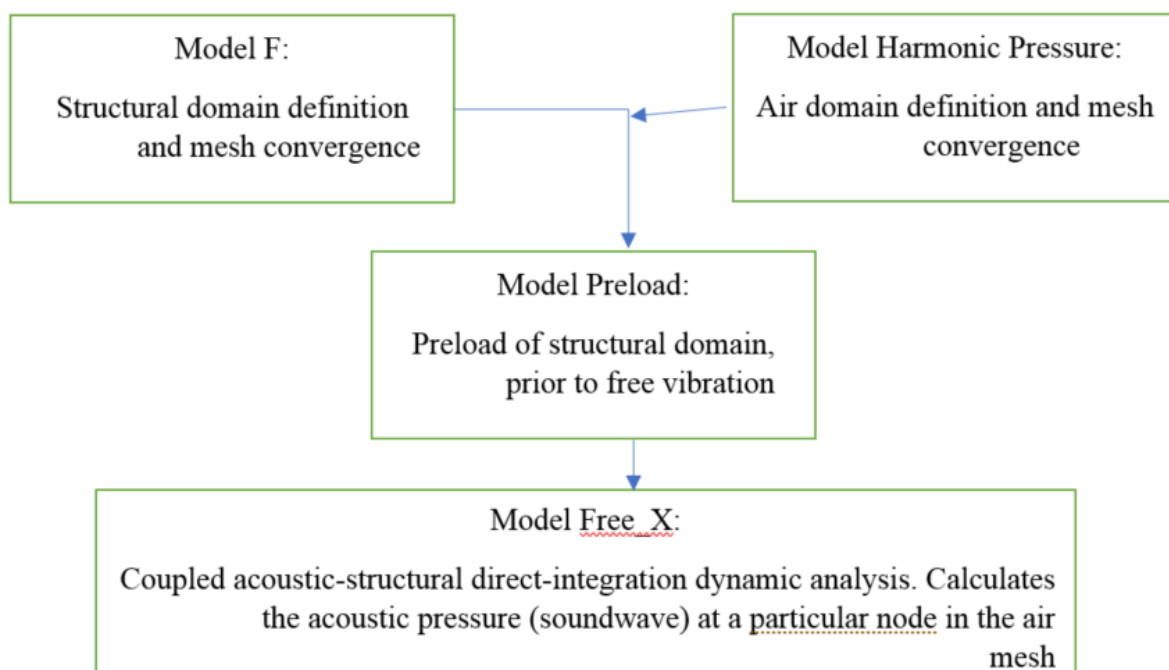
Figure 5: Flowchart indicating the different FE models made in Abaqus

Each of the models in the flowchart is described in a separate section in what follows, in the order in which they were used. First, Model F is described.

3.4 Structural FE domain definition (Model F)

In this section, the procedure used to model the FE structural domain is described. This comprises the geometric modeling, the material properties assigned to the structure, and the mesh design and convergence. The beam model is validated by comparing its natural frequencies to those obtained with the analytical Euler-Bernoulli model from section 3.2. Since the analytical model assumes a zero value for Poisson's ratio, the frequencies obtained from the FE beam model were calculated by setting Poisson's ratio equal to zero, before comparing them to those from the analytical model. It's noted that setting Poisson's ratio to zero was done only to validate the FE model, and for synthesizing the sound produced by the beam's vibrations, a nonzero value of Poisson's ratio was used.

Before describing the Abaqus modeling procedures used, it must be noted that the beam was defined in Abaqus as a 2D plain strain structure. A 2D model was used instead of a 3D model to simplify the calculations because it was found that a 3D model required too much computer resources. Defining the beam as a plain-strain structure implies that the beam's width is treated as very large (ideally infinite), as though it was a plate, and the real-life beam's width is not that large (it's smaller than the length). By using this model to synthesize sound, the resulting sound signal may have larger amplitudes than expected, since the sound synthesized would be that of a plate with a large surface area, and objects with large surface areas radiate sound more strongly (Fahy & Gardonio, 2006). Now that this has been discussed, the modeling procedure is explained next.

In Abaqus, a model was created and named F; within it, the part defining the beam was defined as a 2D deformable, solid part, and was named BEAM_PART. The dimensions given to the part are shown in Figure 6 in m. These dimensions are the same beam dimensions described in section 3.1, where the real-life cantilever beam was described.
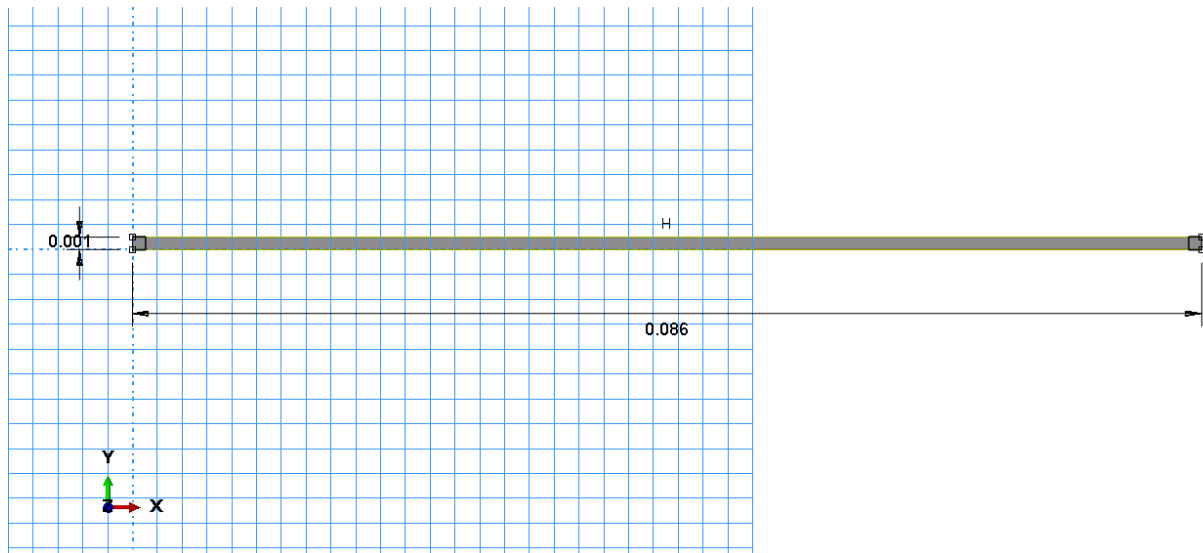
Figure 6: Beam part sketch with dimensions

Two materials were defined for the beam in Abaqus as indicated in Table 2 and Table 3. The materials in the two tables only differ in the value of Poisson's ratio: material "steel" has a nonzero Poisson's ratio value, and material "steel_v0" has Poisson's ratio equal to zero. Material "steel_v0" was used to validate the FE beam model being described, as explained at the beginning of this section, and was used only once for this purpose. For synthesizing the sound produced by the beam, material "steel" was used instead.

Table 2: Material definition for material "steel"

Name			steel
Material behaviors	**Density** $\left(\frac{kg}{m^3}\right)$		7539.4
	Elastic	**Young's modulus (Pa)**	200000000000
		Poisson's ratio	0.3

Name			steel_v0
Material behaviors	**Elastic**	Density $\left(\frac{kg}{m^3}\right)$	7539.4
		Young's modulus (Pa)	200000000000
		Poisson's ratio	0

The density assigned to the materials was calculated from the measured mass of the beam and its volume. This last was calculated using the dimensions given in section 3.1.

The elastic modulus and Poisson's ratio were determined from MatWeb (MatWeb Material Property Data, n.d.) for SAE 430 steel.

Two sections were created as shown in Table 4 and Table 5:

Table 4: Section definition of section "plane_strain_v0"

Name	plane_strain_v0
Type	Solid, Homogeneous
Material	steel_v0
Plane strain thickness (m)	0.015

Table 5: Section definition for section "plane_strain"

Name	plane_strain
Type	Solid, Homogeneous
Material	steel
Plane strain thickness (m)	0.015

Section plane_strain_v0 was assigned to part BEAM_PART.

A natural frequency extraction step was created with the characteristics shown in Table 6:

Table 6: natural frequency extraction step definition

Name	frequency
Step type	Linear perturbation, Frequency
Number of eigenvalues requested	All in frequency range
Maximum frequency of interest (cicles/s)	10000

The fixed-end condition of the structure was imposed by applying a BC to the edge of part BEAM_PART shown in Figure 7. The characteristics of the BC are shown in Table 7.
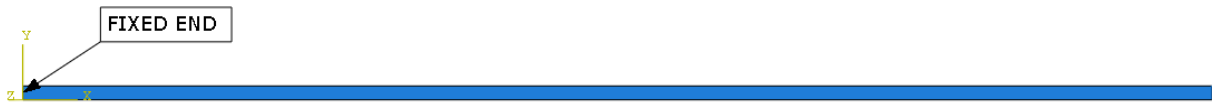
Figure 7: Edge of part BEAM_PART where "fixed" BC was applied

Table 7: BC definition used to fix one end of the beam

Name	fixed	
Step	Initial	
Category	Mechanical	
Type	Symmetry/Antisymmetry/Encastre	PINNED

The part was meshed with CPE4R elements because this is the only type of plain-strain element available for use in Abaqus explicit, which was the Abaqus solver used to synthesize the soundwave. To mesh the beam part, the sweep meshing technique was used to obtain a structured mesh, which avoids having distorted elements in the mesh that could give numerical errors when synthesizing the sound. The mesh consisted of 100 elements along the length of the part, and 4 elements along the thickness, giving a total of 400 elements for the part. Finally, a job was created and submitted.

Table 8 shows the natural frequencies obtained with Abaqus, and those calculated using the
Euler-Bernoulli beam model. A percentage error was calculated between the theoretical
results and the numerical results, using equation (36), where f_{FE} represents the frequencies
obtained using finite elements, either with the plane_strain_v0 or the plane_strain section,
and f_t represents the frequencies obtained with the theoretical (Euler-Bernoulli) model:
equation (25).

$$\%e = \frac{|f_{FE} - f_t|}{f_t} * 100 \tag{36}$$

Table 8: Natural frequencies comparison. The percent error shows the level of convergence obtained with the mesh used.

| | | Theoretical | Using finite elements | | | |
			With plane_strain_v0 section	%e	With plane_strain section	%e
Length			100		100	
Thickness			4		4	
Natural frequencies (hz)	**1**	111.97	111.96	0.01	117.48	4.92
	2	701.72	701.27	0.06	735.76	4.85
	3	1964.84	1962.06	0.14	2058.13	4.75
	4	3850.30	3840.72	0.25	4027.59	4.60
	5	6364.83	6340.30	0.39	6646.35	4.42
	6	9507.95	9455.65	0.55	9907.66	4.20

The Euler-Bernoulli model doesn't include Poisson's ratio in its formulation, so if the
frequencies extracted from a FE model are to be compared with those from the Euler-
Bernoulli model, then Poisson's ratio must be set to zero in the FE model. This was done by
assigning section plane_strain_v0 to the beam part and the results are shown in Table 8.
According to the values of %*e* for this case, the mesh has converged within an error of

approximately 0.55%, which is a low value, and this validates the beam FE model. The error obtained with the beam FE model that uses section plane_strain, which accounts for Poisson's ratio, is also shown in Table 8. The mesh density was the same as in the case in which section plane_strain_v0 was used, so the higher %e values were increased, although not by much, due to Poisson's ratio. The section "plain_strain", which makes reference to the "steel" material (with steel's actual Poisson's ratio value), will be used in subsequent Abaqus models because in reality steel's Poisson's ratio is not zero.

3.5   Definition and validation of the FE air domain (Model Harmonic Pressure)

The present section describes how a FE air part was created in Abaqus, in model Harmonic Pressure from section 3.3. Nonreflecting boundary conditions were used to truncate the part, and the considerations from section 4.1 were taken into account when defining its dimensions. The air part was then tested by applying a harmonically varying pressure source at one of its nodes and analyzing the pressure field generated in the whole mesh. The results of this test were compared to those from the same part using infinite acoustic elements instead of nonreflecting boundary conditions, which was done to verify that both the nonreflecting boundary conditions and infinite acoustic elements gave the same results. The results are given in this section. Finally, the dimensions of the air part were reduced for its subsequent use in model Free_X (see section 3.3), from which the sound produced by the beam was calculated. This was done to reduce the computational cost in that model. To validate the behavior of the reduced part, its response to the same harmonically varying pressure source was compared to that from the original air part using infinite elements. The results from these tests are described in this section. The section begins with the modeling description of the original (large) air part

An air part was created in Abaqus as a 2D, deformable part. The part's sketch with dimensions in m is shown in Figure 8. As a note, for better visibility, the sketch in the figure is just a schematic and was not drawn with the dimensions shown. The rectangular sketch in the middle of the figure is a hole where the beam part from section 3.4 will be placed later.
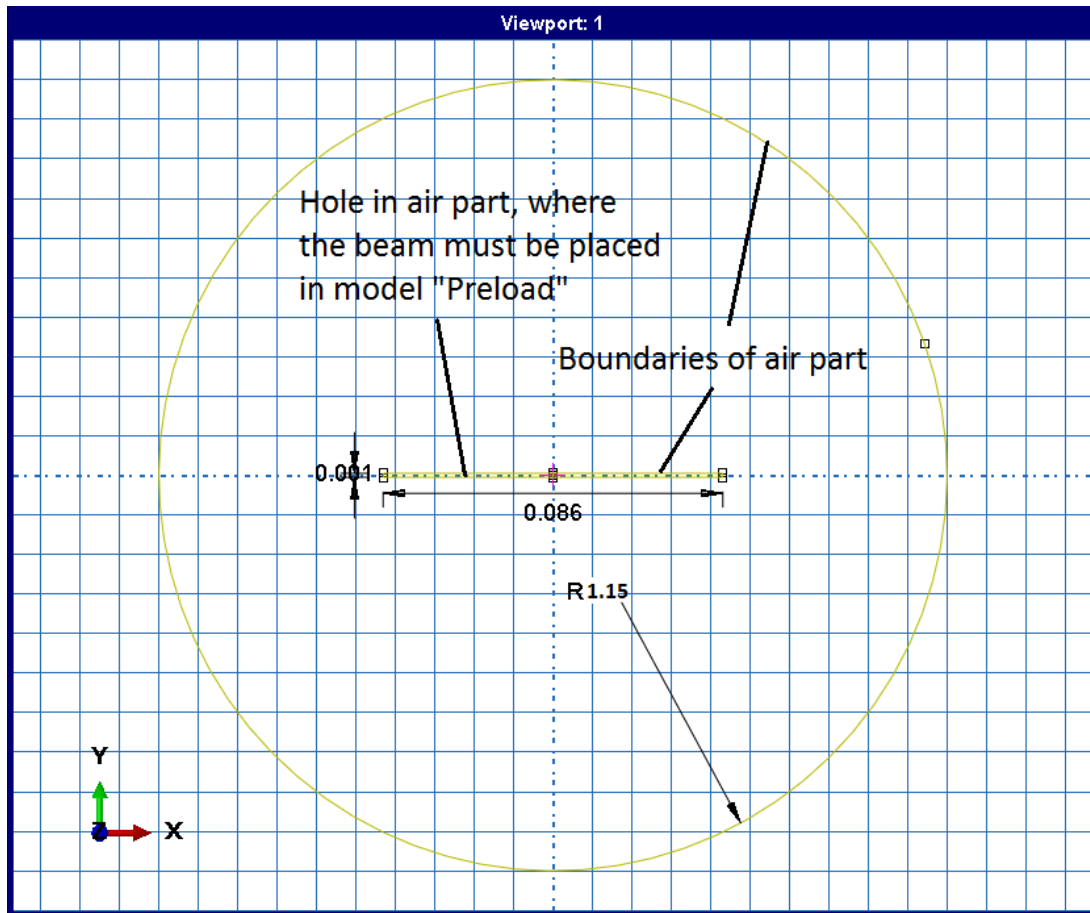
Figure 8: Skecth made to create air part

The extent of the air domain, interpreted as the radius R in Figure 8, was defined using the guidelines discussed in section 4.1. The Abaqus documentation gives an estimate of this radius which is expressed in equation (37).

$$R > \frac{c\ m_{min}}{f_{min}} = \frac{343}{3 * 100} = 1.143 \sim 1.15 \tag{37}$$

In the last equation, c represents the speed of sound; f_{min} is the minimum frequency in the system to be analyzed which in this case is 100 hz, as mentioned at the end of section 4.1; and m_{min} is a fraction that abaqus suggests setting equal to 1/3.

Figure 9 shows the part generated from the sketch in Figure 8. The part was named CIRCLE1. A reference point was defined in its center and is visible in the figure as "RP". The point is used by acoustic infinite elements yet to be defined. Also, visible in the figure are some partitions made to the part, represented by the vertical lines inside it. The partitions were made with the following objective: in Figure 9 are indicated two regions; since the synthesized soundwave was calculated at a node within these regions, it was desired to have a greater control of the mesh in these regions, so they were meshed with structured meshing, which required some partitions to be done on the part prior to meshing.
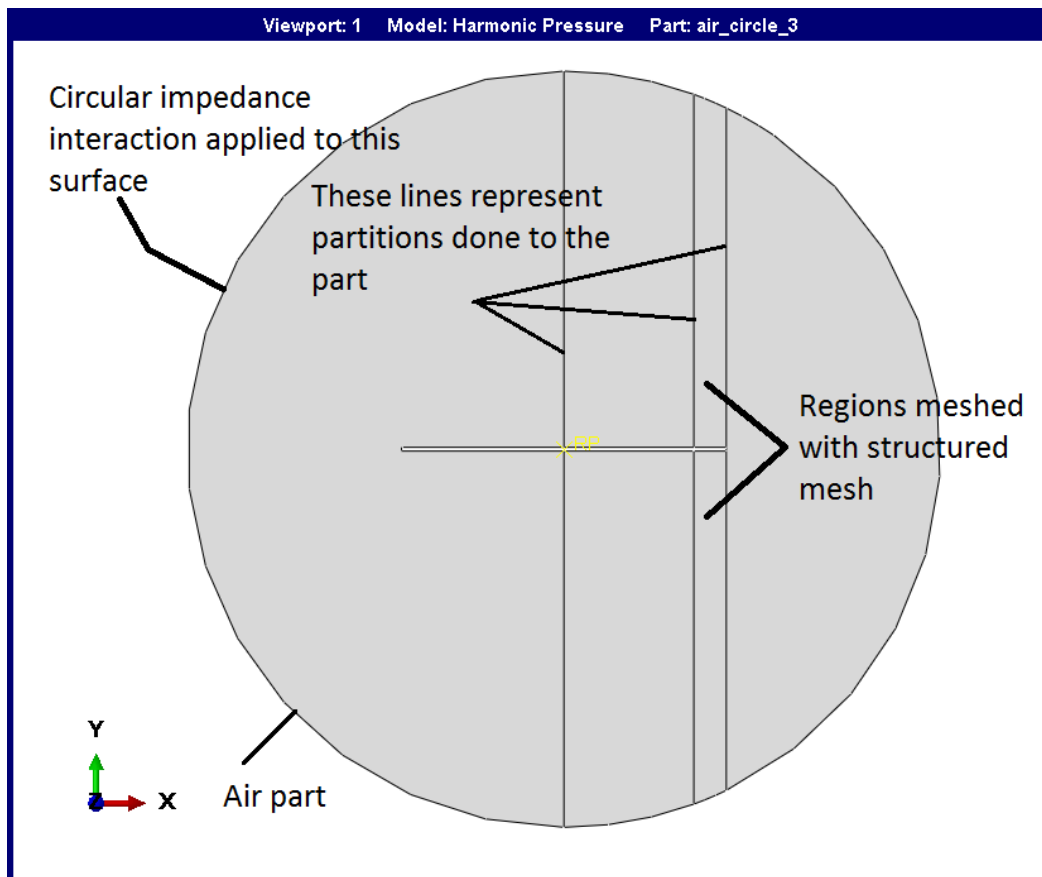
Figure 9: Part CIRCLE1 generated from the sketch in Figure 8

A material for the air was created with the properties shown in Table 9. These properties were taken from the literature (Serway & Jewett, 2005).

Table 9: Air material definition

Name			air
Material behaviors	**Density** $\left(\frac{kg}{m^3}\right)$		1.225
	Acoustic medium	**Bulk modulus (Pa)**	142000

A section was created with the properties in Table 10, and assigned to part CIRCLE1.

Table 10: Section definition for finite acoustic elements, referencing material "air"

Name	air_finite
Type	solid, homogeneous
Material	air
Plane strain thickness (m)	0.015

The part CIRCLE1 was meshed with a mixture of AC2D3 and AC2D4 elements, which were the elements available in the Abaqus standard element library. The part was meshed with a combination of these elements for more flexibility when meshing. The mesh, according to the Abaqus analysis documentation, must be defined according to the range of frequencies desired to model, which is the range from 100 hz to 2000 hz, as said at the end of section 4.1. According to the Abaqus documentation guidelines (Section 6.10.1 of Abaqus 2016 analysis documentation), the maximum mesh density to be used, expressed in terms of the maximum internodal interval L_{max} should be as given in equation (38).

$$L_{max} < \frac{c}{n_{min}f_{max}} = \frac{343m \cdot s^{-1}}{10 * 2000} = 0.01715 \qquad (38)$$

Where c represents the speed of sound, f_{max} is the maximum frequency to be analyzed, which is 2000 hz, and n_{min} is the desired number of internodal intervals per acoustic wavelength. (An acoustic wavelength is the counterpart in the spatial domain, of a periodic wave's time period). For linear elements, as in this case, L_{max} is the length of the largest element's edge Abaqus recommends using. A finer mesh than recommended was used to obtain more accurate results, and seeds of an approximate global size equal to $0.1L_{max}$ were defined in the mesh module for the whole part CIRCLE1.

To simulate the unboundedness of the air domain, a circular impedance interaction (nonreflecting boundary condition) was defined on the outer surface of the part, in the interaction module, as shown in Figure 9.

The behavior of the mesh (particularly of the nonreflecting BCs) defined for the part CIRCLE1 was tested by applying a simple harmonic pressure source near the center of the part, which was done in two cases using Abaqus' steady state dynamics analysis. In one case, the source's frequency was set equal to the lowest frequency analyzed in this work (see section 4.1), which is 100 hz, and in the other case, its frequency was set equal to the highest frequency analyzed, which is 2000 hz. By analyzing the response of the mesh at these two extremum frequencies, the response at all frequencies in between (the range of frequencies analyzed) was already tested. The criteria for determining if the mesh behaves well will be described later in this section.

To do the testing just described, a step was created as shown in Table 11. In the step definition, it's stated that only the frequencies of 100 and 2000 hz are to be analyzed in a steady state analysis.

Table 11:Steady state dynamics analysis step definition

Name	SSD	
Type	Steady-state dynamics, Direct	
Data	Lower frequency	Upper frequency
1	100	0
2	2000	0

A boundary condition (BC) was created at a node near the center of part CIRCLE1. A set was
created to reference this node, and was named pressure_source. The intention of the BC was
to make the node act as a sinusoidally (monofrequency) varying acoustic pressure source
with a magnitude arbitrarily defined as 1. The frequency of the source was in one case 100
hz, and in another, 2000 hz. These are the frequencies shown in Table 11. Figure 10 shows
the location of set pressure_source.
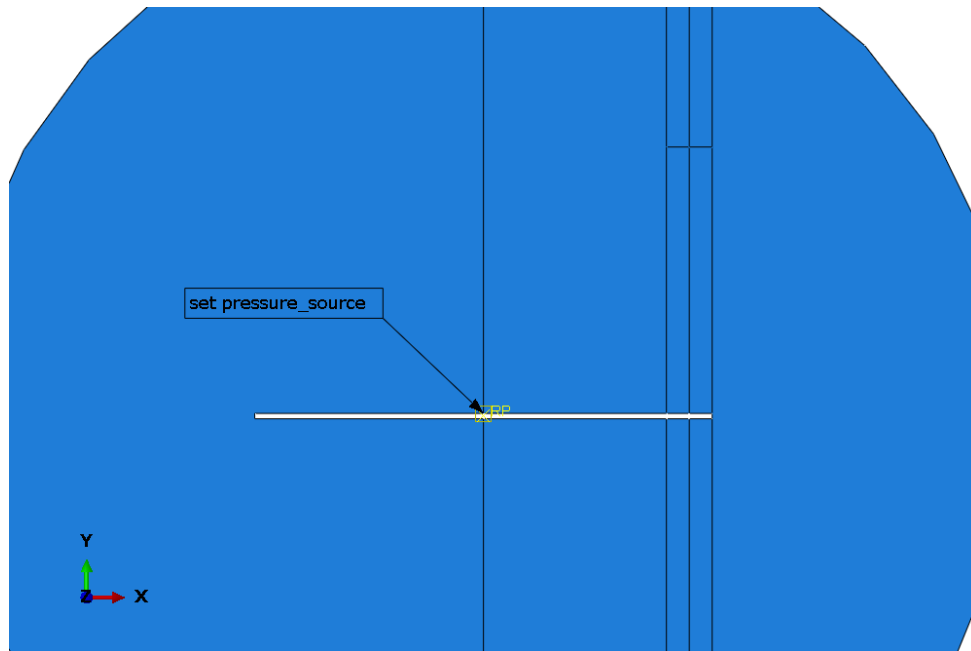
Figure 10: Location of pressure source boundary condition

The BC definition is given in Table 12. Since step SSD defined in Table 11 is a steady state
step, the results obtained with it are expressed in complex notation, and the magnitude

parameter in Table 12, must also be defined as a complex value. The value given for the real part of the magnitude defines a harmonic pressure source of magnitude equal to 1. An analysis was then created, named HP_1, and submitted. The results of the analysis are given later in the section.

Table 12: BC defining a sinusoidally time-varying acoustic pressure source

Name	sinusoidal_pressure
Step	SSD
Type	Acoustic pressure
Magnitude	$1 + 0i$
Region	pressure_source

An alternative to using the nonreflecting boundary conditions as in analysis HP_1 is using infinite elements on the (outer) surface that truncates the air domain. This alternative is more computationally expensive but yields more accurate results. An additional analysis, named HP_2 was made to validate that infinite elements and nonreflecting BCs yield the same results: infinite elements, ACIN2D2, were used instead of nonreflecting boundary conditions on the outer circular surface of part CIRCLE1 (see Figure 9). To do this, a stringer was created on this perimeter first, and section air_inf defined in Table 13 was assigned to it.

Table 13: Definition of an acoustic infinite section

Name	air_inf
Type	Acoustic,infinite
Material	air
Plane strain thickness (m)	0.015

A side-by-side comparison of the results of these two analyses is given in Figure 11 (pressure source at 2000 hz) and Figure 12 (pressure source at 100 hz): on the left of each figure are the

results of analysis HP_2 (infinite elements used), and on the right, are those of analysis HP_1 (nonreflecting BCs used). The results shown are the phase angle isolines. It's reminded that the results are given in complex form, so they consist of a magnitude and a phase. If the infinite elements/nonreflective boundary conditions behave correctly, the plot of the phase angle isolines near them, caused by the pressure source, should approach the shape of circles, as stated in section 9.1.1 of the Abaqus 2016 example problems guide. This is because a point source must produce a pressure field with circular symmetry.
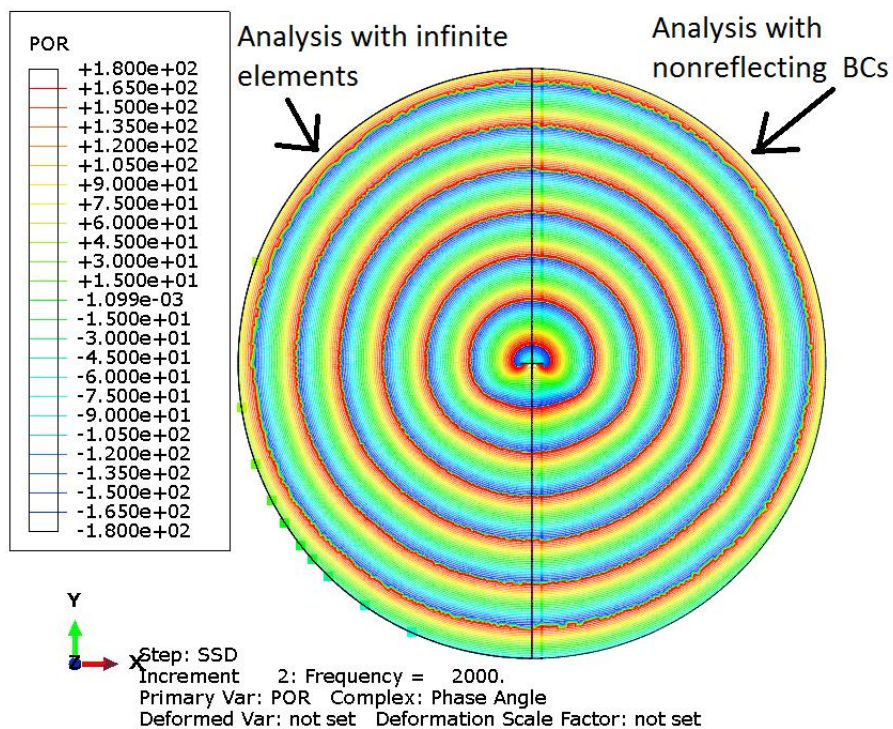
Figure 11: Phase angle comparison between analyses using infinite elements, and nonreflective boundary conditions, when a sinusoidal pressure source of 2000 hz is located near the center of the air domain.
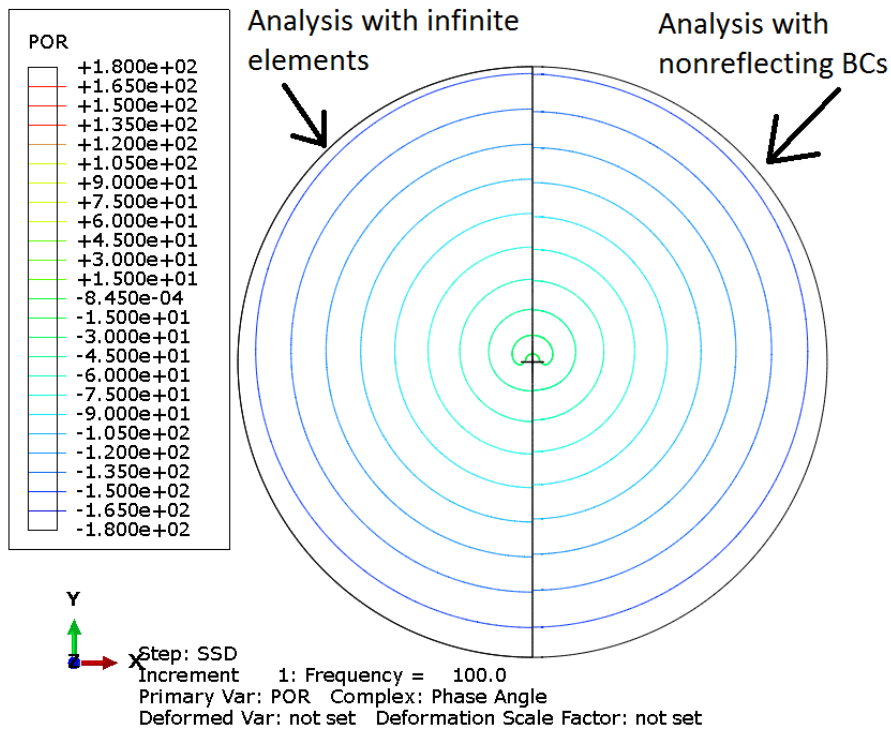
Figure 12: Phase angle comparison between analyses using infinite elements, and nonreflective boundary conditions, when a sinusoidal pressure source of 100 hz is located near the center of the air domain.

Figure 11 and Figure 12 show that, indeed, near the surface that truncates the air domain the phase angle isolines approach a circular shape. Furthermore, the isolines across the results from the two analyses show only a slight discontinuity jump. This validates that in both analyses the infinite elements/nonreflecting boundary conditions behave well, and that the results from both analyses are practically equal.

Since the air domain from the previous analyses is too large, it's not practical to use it in a coupled structural-acoustic simulation since it would slow it down significantly due to the number of nodal variables, and the fact that the direct integration procedure needed in such simulation is much more expensive than the steady state dynamics analyses described in this section. Besides, only results in the air near the beam are desired. For this reason, a smaller air domain was created by changing the radius R in Figure 8 to a value of 0.1 m. In the

remainder of this section, the reduced air part is verified to behave correctly by comparing its behavior with that of the original air part that used infinite elements.

The reduced part was named CIRCLE_3 and a new analysis named HP_3 was created with it. Infinite elements were used on this part since they should yield more accurate results than nonreflecting conditions. Figure 13 shows the air domains from analyses HP_2 (original air domain using infinite elements) and HP_3 (reduced air domain using infinite elements) side-by-side for visual comparison. On the left figure, the two domains are shown: the left half circle comes from analysis HP_2 and the right half circle from HP_3. On the right figure is shown a closer view of the left figure, near the location of set pressure_source.
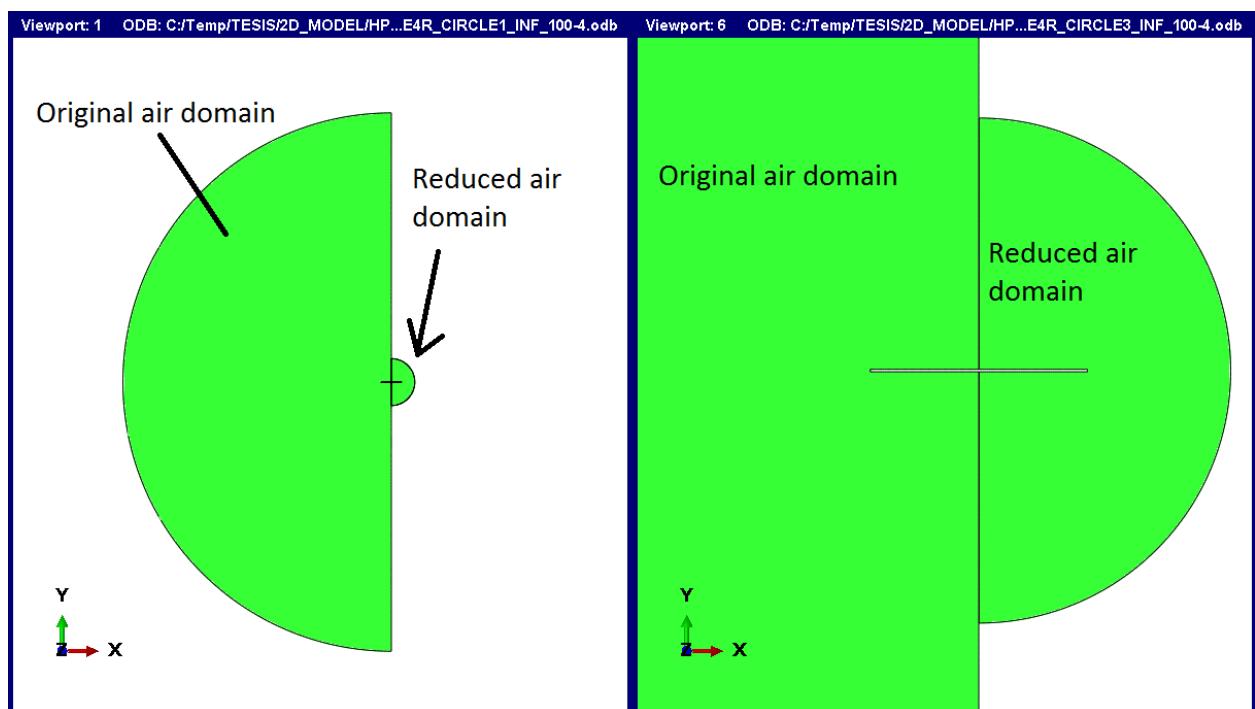
Figure 13: Comparison of the air domains used in analyses HP_2 and HP_3. The domain used in analysis HP_3 is shown as the right half circle

Like before, a phase angle isolines plot is shown in Figure 14: on the left, results are shown when the pressure source oscillates at 2000 hz, and on the right, when the frequency is equal to 100 hz.
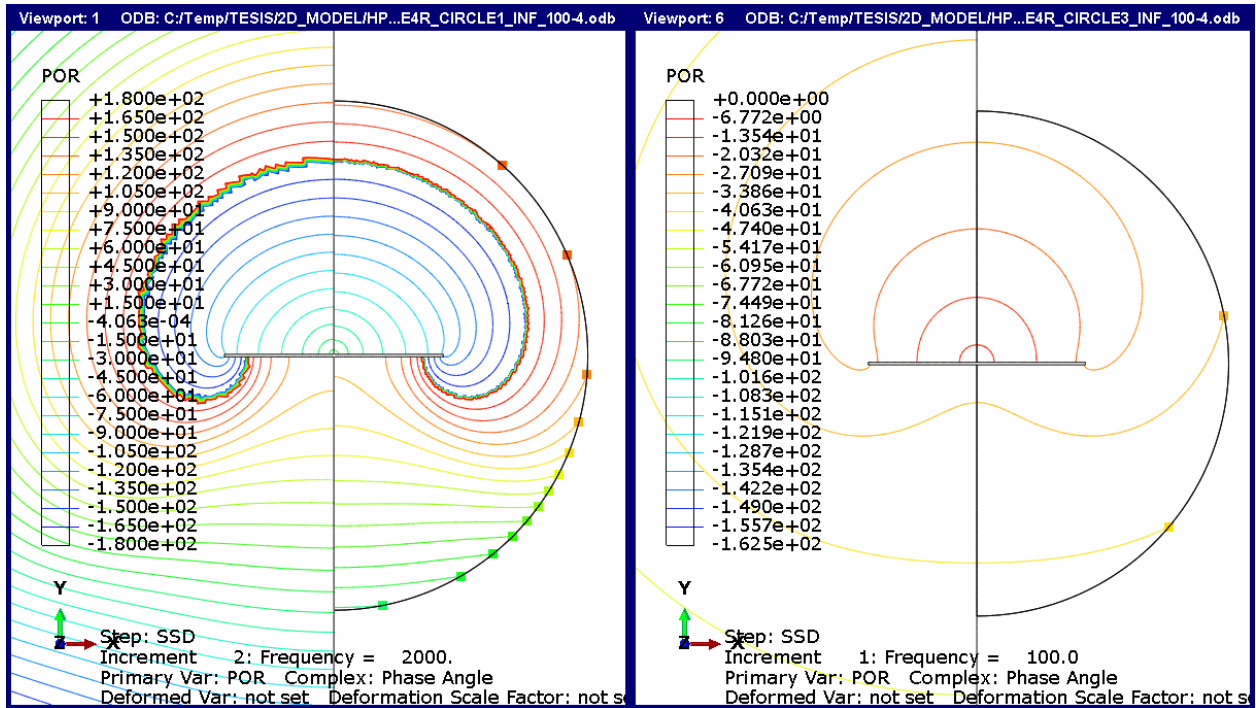
Figure 14: Phase angle isolines plot for analyses HP_2 and HP_3 when the pressure source frequency is: on the left, equal to 2000 hz; on the right, equal to 100 hz.

From Figure 14, for both frequencies the phase isolines are nearly continuous across analyses, so similarly accurate results are obtained from both.

Figure 15 shows a similar comparison as Figure 14, but instead of plotting the phase angle response, the magnitude of the solution is plotted (it is reminded here that an Abaqus steady state dynamic analysis' solution is given in complex form, which is described by a magnitude and a phase). As Figure 14, Figure 15 shows near continuity of the solution across analyses, and the results of each analysis looks almost like a mirror of the other. This further shows that almost the same level of accuracy is obtained with analysis HP_3 even though it's air domain size was reduced substantially from that used in HP_2 (or HP_1).
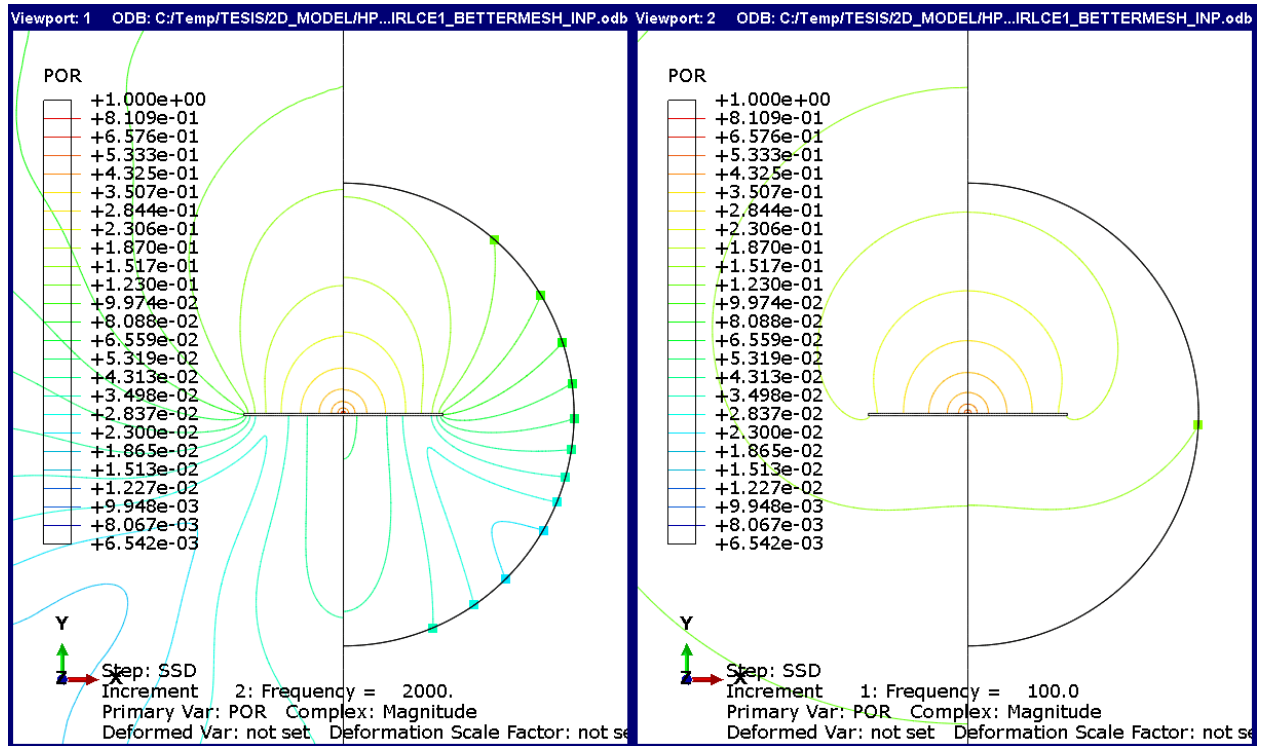
Figure 15: Magnitude isolines plot comparison between analyses HP_2 and HP_3

3.6 Preloading of the FE structure (Model Preload)

Prior to the free vibration of the beam in air, the beam must be preloaded to give it potential energy which is transferred to the air during free vibration, thus creating the soundwave that can be heard. The Preload model in section 3.3 was created to calculate the configuration of the beam after preloading it. This configuration will be referred to as the initial configuration. The initial configuration was obtained by displacing the free end of the beam in the transverse direction (y direction in Figure 7). The procedure taken to create the model, and submit an analysis derived from it, is described in this section. Up to this point, the FE beam and air domains have been modeled separately in Abaqus. From this point forward, however, the two domains must be modeled together.

To create the Preload model, the model objects shown in Table 14 were copied from model F, from section 3.4:

Table 14: Model objects copied into model Preload from model F

Object type	Object name
Part	BEAM_PART (with mesh)
Material	steel
Section	plane_strain (assigned to BEAM_PART)
BC	Fixed (assigned to the same region as in model F)

The model objects shown in Table 15 were copied from model Harmonic Pressure (section 3.5).

Table 15: Model objects copied into model Preload from model Harmonic Pressure

Object type	Object name
Part	CIRCLE_3 (with mesh)
Material	air
Section	air_finite (assigned to CIRCLE_3)

The two parts in the model were positioned in the assembly module as shown in Figure 16.
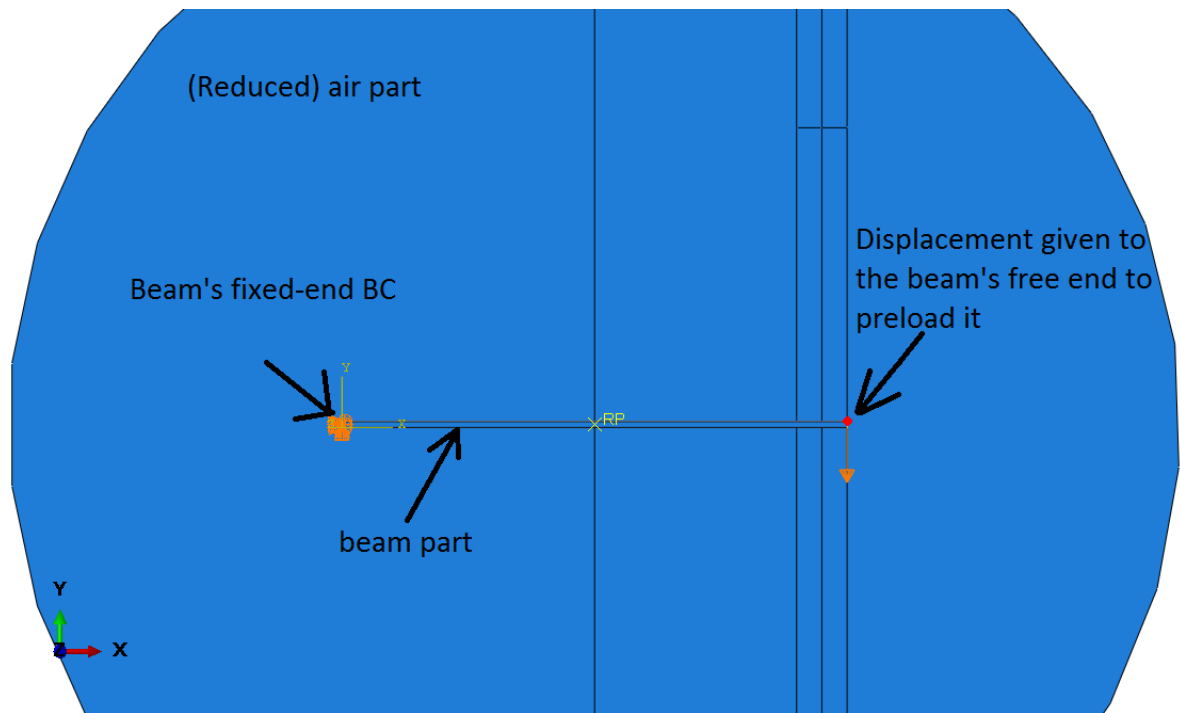
Figure 16: The two parts comprising the model, positioned in the assembly module

After this, a tie constraint was created between the surfaces of the two parts in contact with each other. This constraint is intended to model the acoustic-structural coupling between the two parts at their interface in a later model. Figure 17 shows the surfaces used in the tie constraint. The Abaqus analysis documentation dictates that for best accuracy, the master surface should be chosen as the surface with the coarser mesh. Since BEAM_PART had the coarser mesh, its surface was designated as master.
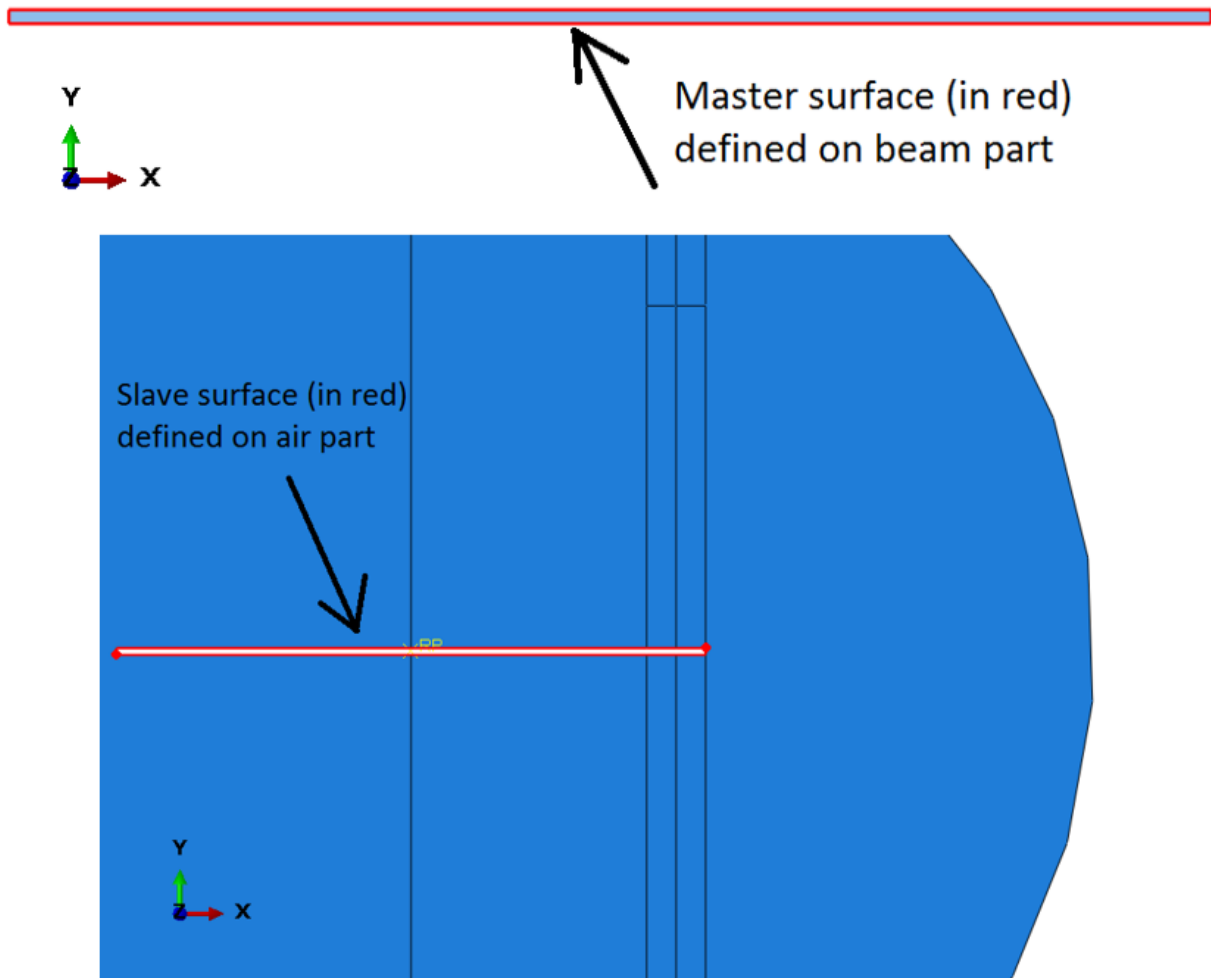
Figure 17: On top, the master surface defined on the beam part; on the bottom, the slave surface defined on the air part.

Both surfaces are highlighted in red

To preload the beam, a new step was defined with the characteristics shown in Table 16. The parameter Nlgeom was set to on to include the large displacement formulation for the beam in the FE solution.

Table 16: Step definition for model "Preload"

Name	preload
Type	Static, General
Nlgeom	On (includes nonlinear effects of large displacements)

A BC was created, with the characteristics shown in Table 17, to give the free end of the beam an initial displacement of 2 mm in the transverse direction. The BC was assigned to set free_edge, shown in Figure 18.The BC displacement value was chosen to be small, so that the acoustic waves radiated by the subsequent free vibration of the beam would be of small amplitude, which would honor the assumptions implicit in the linear wave equation (equation (23)).

Table 17: Definition of BC used to give the free end of the beam an initial displacement

Name	Initial_displacement	
Step	preload	
Category	Mechanical	
Region	free_edge (set)	
Type	Displacement/Rotation	U2 = -0.002
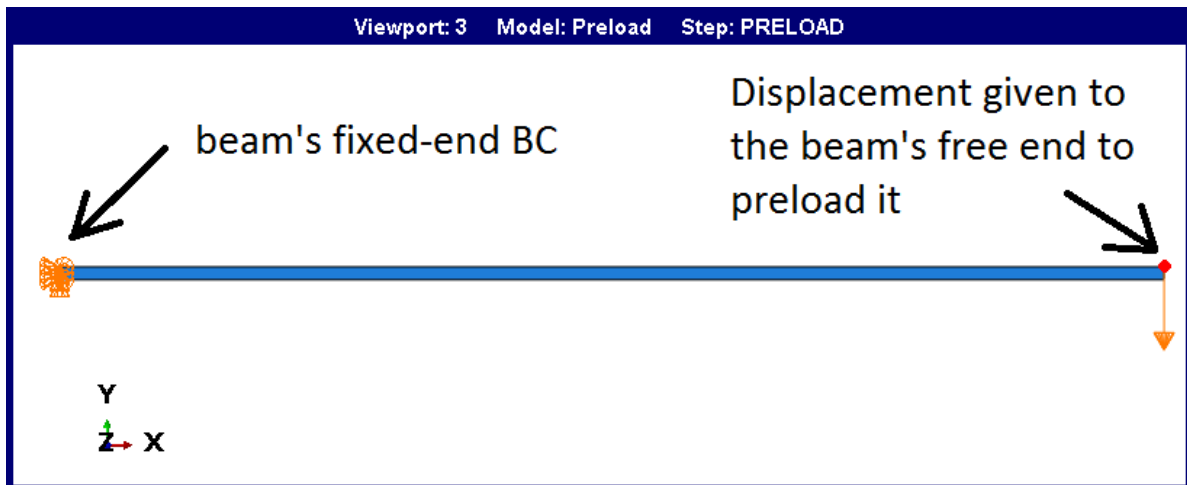
Figure 18: set "free_edge", where BC "Initial_displacement" was defined. The set is the dot highlighted in red on the right

In the current model, the air domain mesh had to adjust to the deformations that the beam underwent. To accomplish this, Arbitrary Lagrangian Eulerian (ALE) adaptive meshing was defined on the air mesh, with a frequency of 1, and 5 remeshing sweeps per increment. These meshing parameters were used because they gave good results.

While the preloading of the beam was modeled with the Abaqus standard solver (since a static, general step was used), its subsequent free vibration analysis was modeled with Abaqus/explicit as will be explained later. To transfer the results from the current analysis to the Abaqus/explicit analysis, the results at the end of the first had to be exported for use by the later, by writing the analysis results to the restart files, as explained in the Abaqus analysis documentation, in section 9.2.2.

After this, a job named P_CPE4R_CIRCLE2-100-4 corresponding to the current analysis was created and submitted. Figure 19 shows the results at the end of the analysis' step. It can be seen that the air's mesh has adjusted itself to the deformation of the beam's.
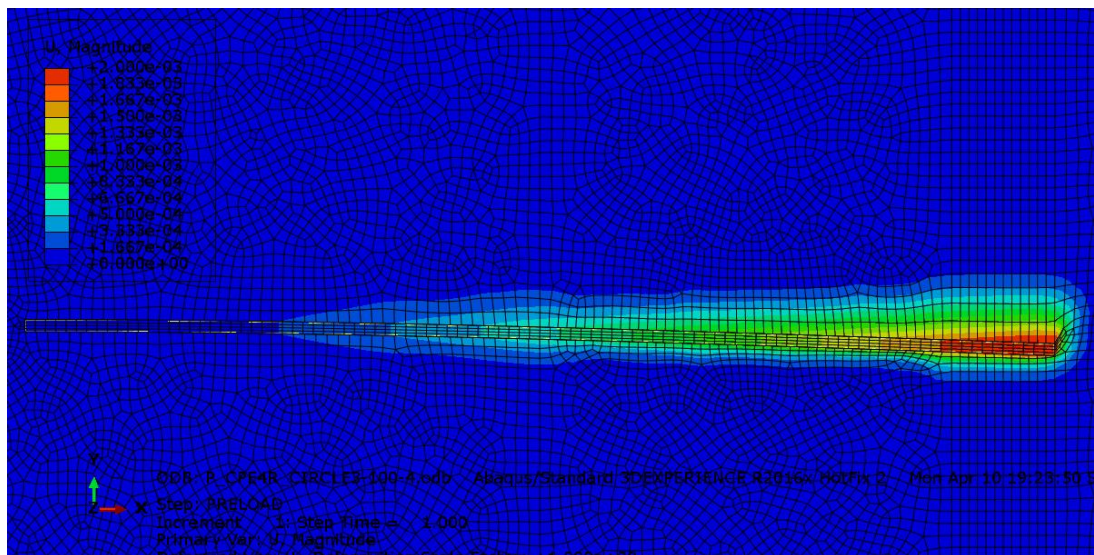
Figure 19: Model mesh at the end of the preload analysis. The adjustment of the air mesh to that of the beam can be appreciated.

3.7 Acoustic-structural coupling of FE structure and air domains (Model Free_X)

The fully-coupled acoustic-structural FE model that simulates the acoustic radiation from the beam, and thus calculates a soundwave like the one in Figure 32 from section 4.1, is

described in this section along with the procedures taken to create it. Two verifications made to the model are explained at the end of the section.

All the model objects (parts, materials, sections, and BCs) from Table 14 and Table 15 were copied into the current model, named Free_X (see section 3.3). In addition, section air_inf from model Harmonic Pressure, Table 13, was also copied into the current model. The air and beam parts were positioned in the assembly module as in Figure 16. The same tie constraint used in model Preload was defined, with the master and slave surfaces shown in Figure 17. Acoustic infinite elements, ACIN2D2, were defined on the circular outer surface of part CIRCLE_3. The finite air elements currently assigned to part CIRCLE_3 are not available in Abaqus explicit, so the element types were changed to AC2D3R and AC2D4R, from the Abaqus explicit library. These elements are different from the ones originally defined in part CIRCLE_3 in that they are reduced integration elements, and the previous ones were full integration elements. A step was created with the characteristics shown in Table 18.

For this model, an explicit direct integration step is used instead of an implicit one because, as is said in the Abaqus getting started guide, the explicit integrator is better suited for wave propagation analyses. Besides, an implicit integrator due to its formulation, requires more computer calculations for each time increment; in contrast, the explicit integrator computes each increment with relatively low cost, and the coupled acoustic-structural analysis requires a very large number of time increments to be made, so the explicit scheme is better suited.

Table 18: Direct integration step definition used in model Free_X

Name	FREE_X
Type	Dynamic, Explicit
Time period	0.1

A small time interval equal to 0.1 s was specified in the definition of the step to first verify the model by calculating the acoustic pressure at a selected node. This node conforms the set MIC, shown in Figure 20.
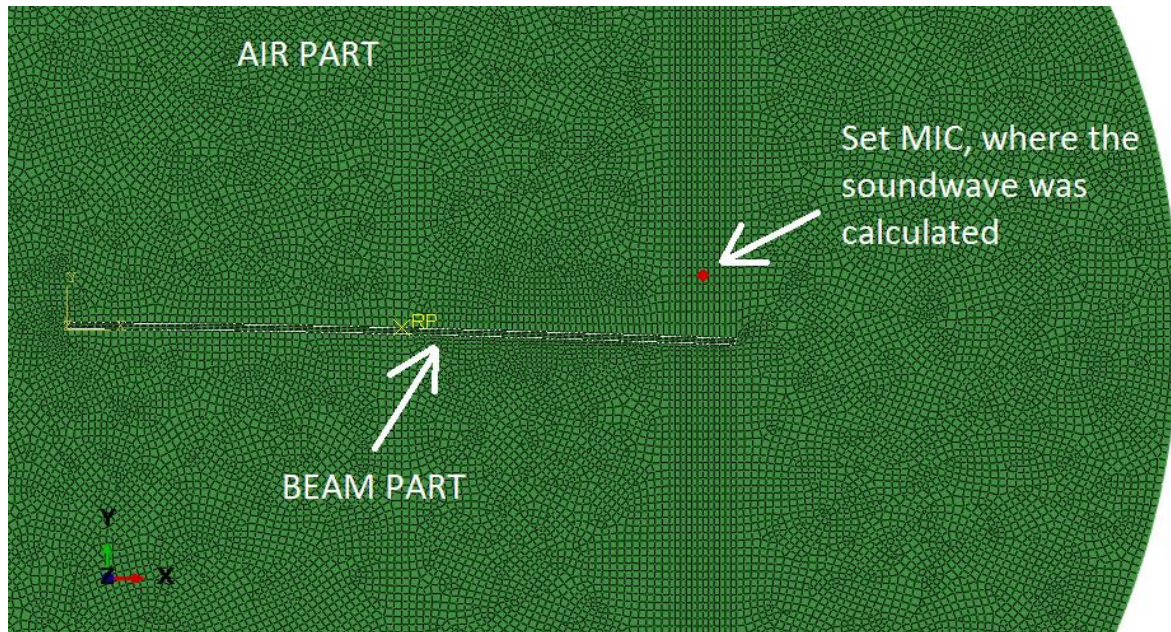
Figure 20: Set MIC, composed of the nodes where the acoustic pressure was calculated as a function of time

A predefined field was created with the characteristics shown in Table 19. This feature imports the results from model Preload from section 3.6 at the end of step "preload". In the current model, the beam is let to vibrate after removing the preload given to it, as explained in section 3.6.

Table 19: Predefined field definition used to import results from model Preload

Name	Import
Type	Initial state
Step	Initial
Instances	Beam and air instances
Update reference configuration	yes

After this, an analysis named FX_1 was submitted, which served as a verification as will be explained. Figure 21 shows the acoustic pressure as a function of time obtained for the node in Figure 20 for analysis FX_1. Since material damping was not defined for the beam when calculating the acoustic soundwave in Figure 21, the beam would vibrate with little damping (due to the infinite elements only) and therefore, the produced soundwave should be seen to oscillate in the figure with little damping. This is seen to happen in the figure, after the initial transient goes away. The DFT magnitude spectrum of this soundwave was taken and is shown in Figure 22, on top. Also, the beam's natural frequencies obtained using section plane_strain, from Table 8 are shown as vertical lines for comparison. For better visualization, a zoomed view of the DFT magnitude spectrum is shown in the bottom of the figure. As can be seen in the figure, there is a correspondence between the frequencies in the soundwave and the natural frequencies of the beam. This validates that the soundwave was calculated correctly.
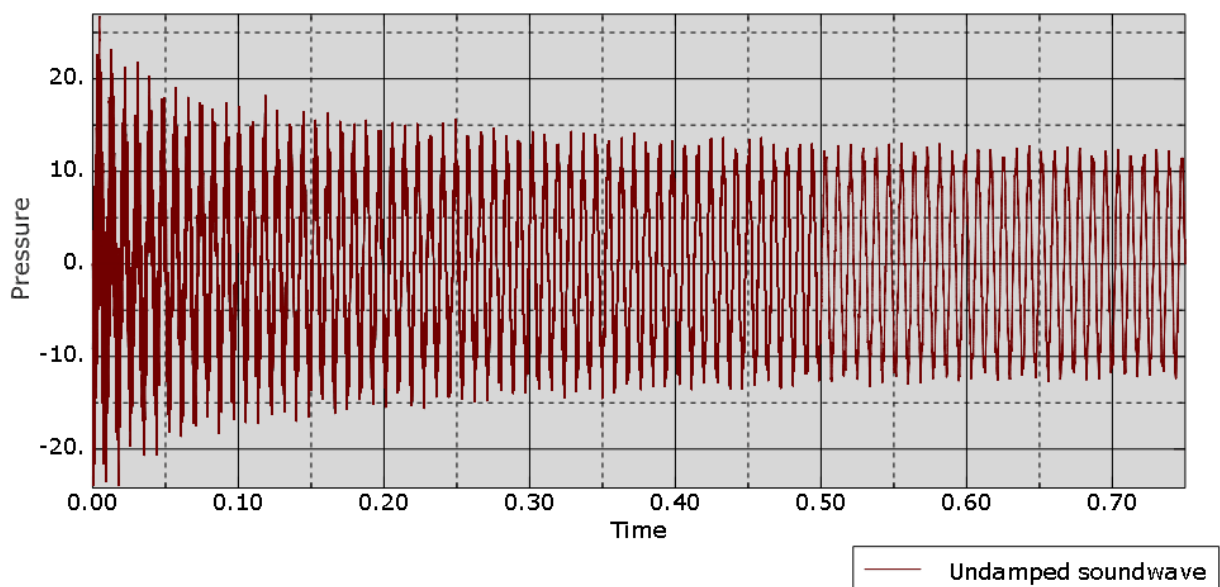
Figure 21: Soundwave from Abaqus as a function of time produced by beam vibration for the node in Figure 20. No damping was specified for the structure and actual air density was used.
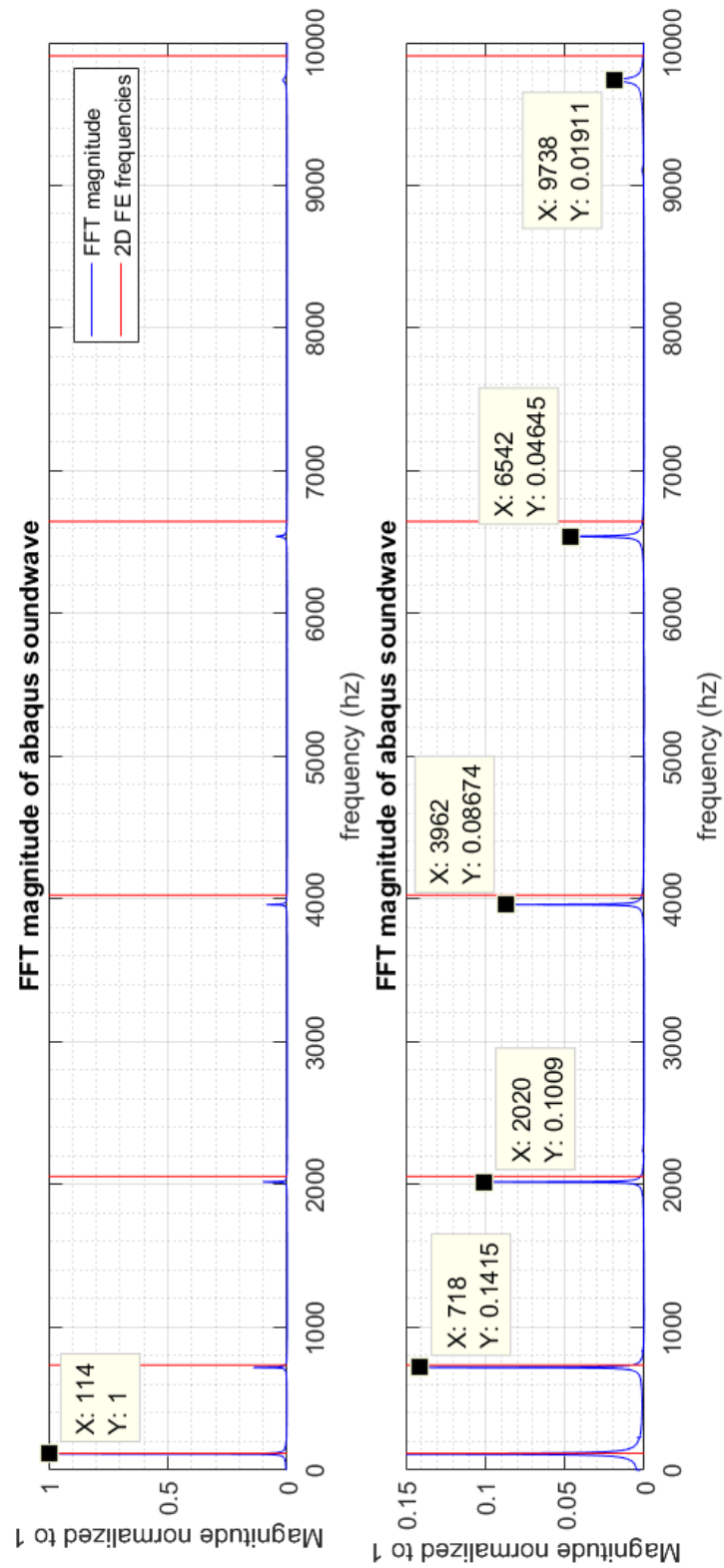
Figure 22: DFT of soundwave in Figure 21. Also, the beam's natural frequencies from Table 8 using section plane_strain are plotted for comparison

A second analysis named FX_2 was submitted with air's density changed to a much larger value, in this case chosen to be $1000\ kg/m^3$, to prove that the infinite elements were dissipating energy. If the damping provided by the infinite elements works, the transverse displacement of the free end of the beam should decay with time even though no material damping was specified. This should occur because the beam loses its energy to the surrounding air by doing work on it, and the infinite elements dissipate this energy into domain B in Figure 29 (section 4.1), which does not return, at least in part, to the finite element system. This effect is not easily appreciated if the actual air density is used, which is why its density was changed to that of water (a value in the order of magnitude of the beam's density).

In Figure 23 the transverse displacement of the node in set "free_edge" (Figure 18) is shown when the air density was changed to that of water. No damping was specified for the structure and yet, there's damping in the beam end's motion. This proves that the infinite elements are indeed dissipating energy.
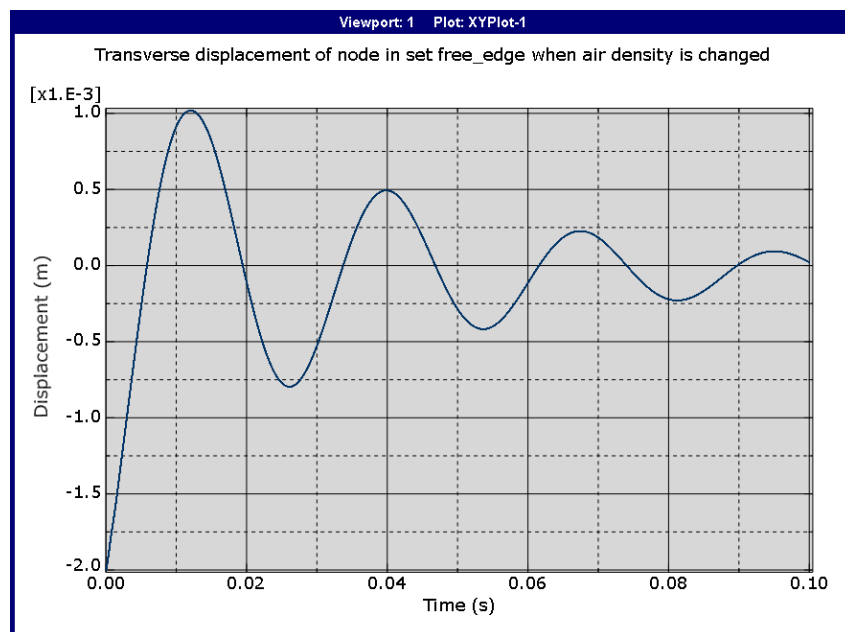
Figure 23: Transverse displacement of the free end of the beam when damping is not included in the structure. The beam vibrates in a fluid whose density is the same as water's.

3.8 Inclusion of damping in the FE structure

The FE model has two sources of damping: one comes from truncating the unbounded air domain by using either nonreflecting boundary conditions or infinite elements; the other comes from damping within the structure. The first source is completely defined when the impedance conditions or infinite elements are included in the model. The second source, however, must be defined by measuring the damping.

Damping in the structure was measured indirectly by measuring the damping in the recorded soundwave in Figure 32 from section 4.1. For this, it was assumed that the damping in the soundwave was the same as the damping in the structure. The present section explains how damping was measured from the recorded soundwave, and how it was inserted into the beam in model Free_X to calculate the numeric soundwave, which is shown in the results section. The recorded soundwave in Figure 32 is composed of several frequency components shown in Figure 33, but it can be observed from this figure, by comparing the relative magnitudes of the peaks, that the most prominent frequency component is the one associated with the lowest natural frequency of the beam, which is around 113.73 hz according to Table 8

Figure 24 shows a magnified view of the soundwave in Figure 32. The figure also shows the local maxima and minima in the soundwave, which occur at a frequency of roughly 113.73 hz and were found with the MATLAB function `findpeaks`.
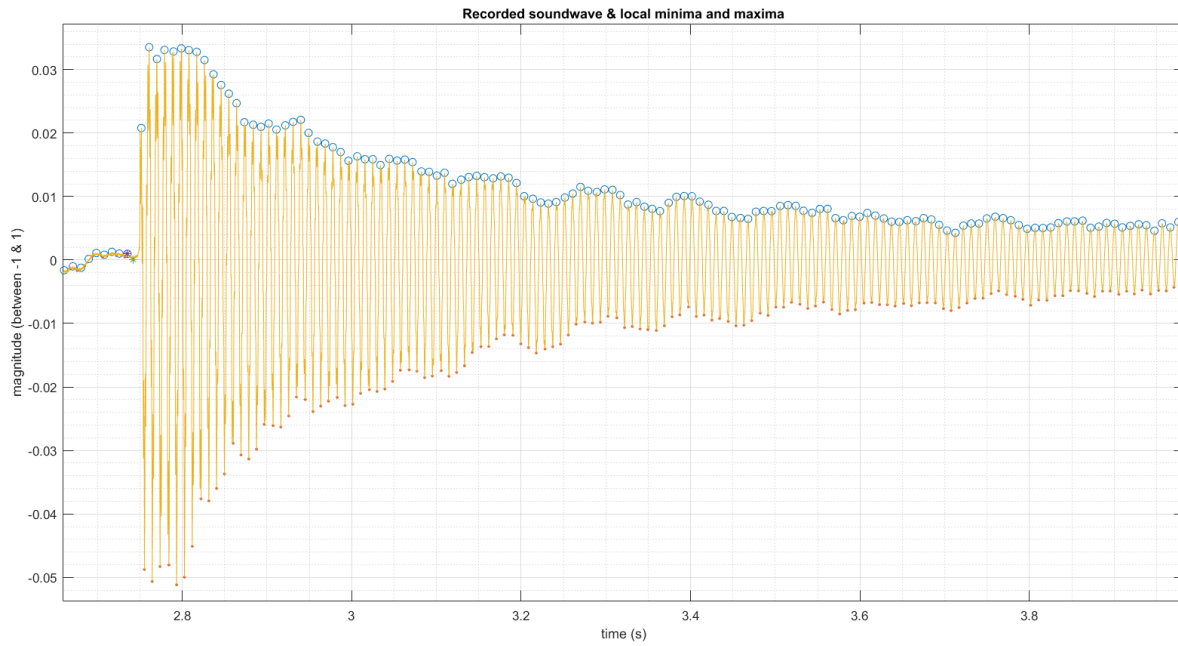
Figure 24: Local minima and maxima in time-domain soundwave from Figure 32

Each set of either local minima or maxima shown in Figure 24 can be fitted to an exponential function of the form given in equation (39), where a and b are real constants.

$$env(t) = a\mathrm{e}^{-bt} \tag{39}$$

It can also be shown that if structural damping is included in a FE cantilever beam, each of the nodal displacements in the beam decays in an exponential manner, as in equation (39). This is discussed in the following.

If $U(t)$ from equation (1) represents the nodal displacements of a FE cantilever beam model with damping, that vibrates in vacuum due to initial conditions, and its damping is modeled as proportional, then the generalized displacements $x_i(t)$ from equation (15) have the solution given in equation (17), which has an exponential decay component repeated in equation (40) for convenience.

$$x_{i,decay}(t) = \mathrm{e}^{-\xi_i \omega_i t} \tag{40}$$

To show the relative influence of each generalized displacement in the synthesis of $U(t)$ as stated in equation (15), a transient modal dynamic analysis of a cantilever beam with damping, vibrating in vacuum due to initial displacement conditions (the free end of the beam was displaced 2 mm in the transverse direction, just like in model Preload) was made in Abaqus and the generalized displacements corresponding to the first three natural frequencies of the beam shown in Table 8 were calculated. These are given by $x_i(t)$ with $i = 1,2,3$ and are shown in Figure 25. In yellow is shown $x_1(t)$; in red $x_2(t)$; and in black $x_3(t)$. In the beam, Rayleigh damping was defined with $\alpha = 1.642$ and $\beta = 0$, where α is the damping value determined from estimating the damping in the recorded soundwave as will be discussed later, setting $\beta = 0$ will also be discussed later.
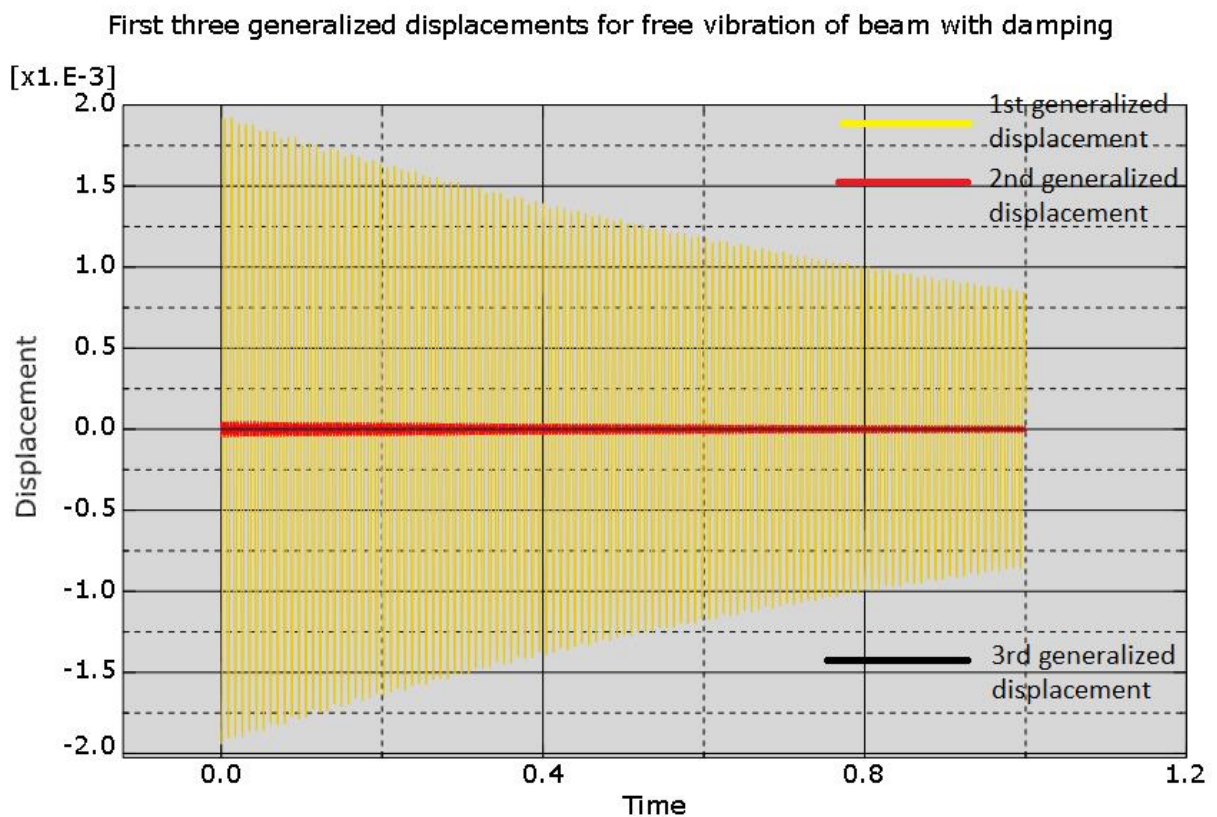
Figure 25: First three generalized displacements of a cantilever beam vibrating in vacuum due to initial conditions. Structural damping was defined for the beam

It is visible from Figure 25 that the first generalized displacement contributes the most to the synthesis of the nodal displacements vector $U(t)$. In view of the relative influence of each generalized displacement, $U(t)$ can be approximated as shown in equation (41), where only the first three eigenmodes are used since their eigenfrequencies are in the range from 100 hz to 2000 hz which was the range chosen to be studied in this work, as discussed in section 4.1.

$$U(t) \cong \sum_{i=1}^{3} \varphi_i x_i(t) \cong \varphi_1 x_1(t) \tag{41}$$

Equation (41) says that for the cantilever beam with structural damping, vibrating due to initial conditions, each of its nodal displacements' behavior is proportional to that of the first generalized displacement, so each nodal displacement decays as the exponential function given in equation (40) with $i = 1$, which is shown in equation (42)

$$x_{1,decay}(t) = e^{-\xi_1 \omega_1 t} \tag{42}$$

Thus, each of the nodal displacements in the beam decays in an exponential manner.

Additionally, if β is set equal to zero in equation (19) and $i = 1$, then it follows that $\alpha = 2\omega_1 \xi_1$. Thus equation (42) can be rewritten as in equation (43).

$$x_{1,decay}(t) = e^{-\frac{\alpha t}{2}} \tag{43}$$

Returning to the subject of estimating structural damping, particularly Rayleigh damping, since damping in the soundwave can be approximated as an exponential decay as in equation (39), and damping in the nodal displacements of a beam can also be approximated as an exponential decay as shown in equation (41) and equation (43), a correlation can be made between these two forms of damping by equating b from equation (39) to $\frac{\alpha}{2}$ from equation (43) and solving for α. This would define Rayleigh damping with a nonzero value for α and $\beta = 0$.

To define nonzero values of both mass and stiffness proportional terms in Rayleigh damping, two values of ξ_i would have had to be determined to solve for α and β in equation (19). However, only the value of ξ_1 could be determined by fitting either the local minima or maxima in Figure 24 to equation (39). Determining a second value of ξ_i is not straightforward and experiments beyond the scope of the present work would have to be performed on the physical system to get it. Rayleigh damping can still be defined with only one known value of ξ_i if β is set equal to zero, and this was done to get equation (43). This was also done for other reason: the abaqus analysis documentation states that the stiffness proportional damping term reduces the minimum time increment of an abaqus explicit dynamic step, which is used in the calculation of the numeric soundwave. Since the minimum time increment was found to be of the order of 3e-8 s by defining only mass proportional damping in the beam in model Free_X, it was already very small and making it smaller would yield the simulation that uses this model to calculate the numeric soundwave practically too long to be completed.

The effect of setting $\beta = 0$, is the following: by neglecting stiffness proportional damping, equation (19) shows that the damping ratios get smaller as ω_i increases, so the higher frequency components of $U(t)$ have smaller damping ratios than the lower ones. However, the product $\xi_i\omega_i$ from equation (17) is a constant equal to $\frac{\alpha}{2}$, so the generalized displacements of the beam, each corresponding to one frequency component, are equally damped. Put in other words, by setting $\beta = 0$, all the frequency components in $U(t)$ should be equally damped.

To estimate damping in the soundwave, the local maxima and minima in Figure 24 were each fitted to equation (39). Figure 26 shows the local maxima and the exponential function that fits them, whose equation and coefficient of determination (R^2) are also shown.
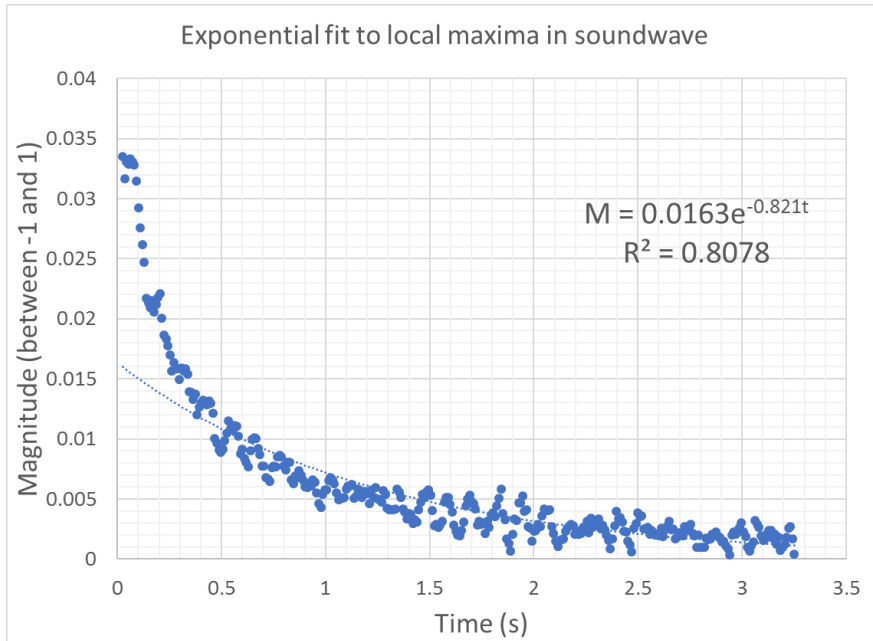
Figure 26: Exponential fit made to local maxima in soundwave

Figure 27 shows the exponential fit made to the local minima. Similarly, the exponential trendline's equation and coefficient of determination are given.
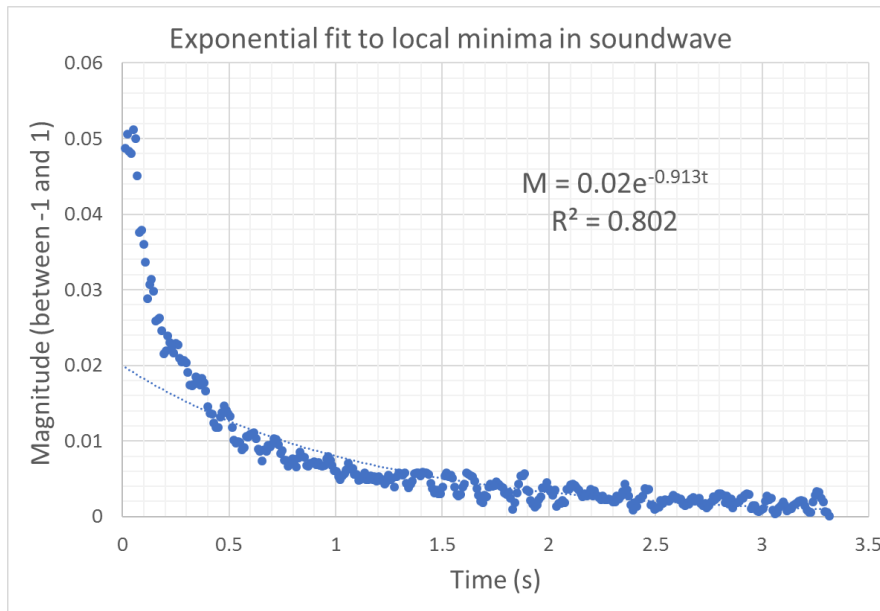
Figure 27: Exponential fit made to local minima in soundwave. The local minima were mirrored with respect to the time axis first

Figure 27 and Figure 26 show a coefficient of determination of roughly 80% for both set of data, which indicates that the data doesn't behave perfectly as an exponential function. However, it's still a high value. Given that the fit made to the local maxima has a slightly higher coefficient of determination, its exponential fit function was used to estimate the structure's mass proportional damping. By making b from equation (39) equal to 0.821 from the exponential fit function in Figure 26, and then equating b to $\frac{\alpha}{2}$ as discussed before, α was calculated as $\alpha = 1.642$.

A dynamic explicit analysis was made in Abaqus with the purpose of defining damping on the structure and validating that it was correctly defined. The analysis was the same as analysis FX_1 from model Free_X, but the air domain was excluded so that the beam would vibrate in vacuum. Additionaly, material "steel" was edited to include the material behavior "Damping", with Alpha = 1.642 and Beta = 0. The transverse displacement of set "free_edge" from Figure 18 was calculated as a function of time, and is shown in Figure 28. Also, in the figure is shown the exponential decay from equation (43) with the calculated value of α. The exponential decay, whose mirror with respect to the time axis is also plotted, is seen to be a good envelope of the underlying displacement curve from set "fixed_end". This validates that the structure's damping has been defined correctly.
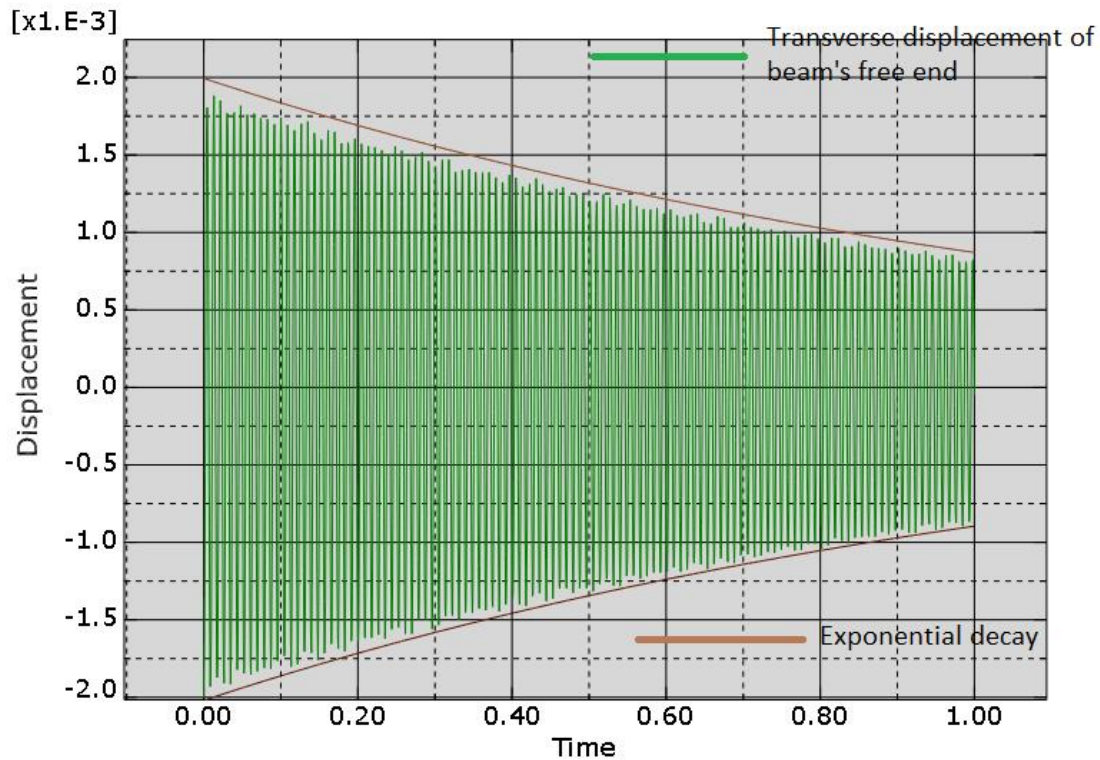
Figure 28: Transverse displacement of set "free_edge" from free damped vibration of beam as calculated in Abaqus explicit

This concludes the present section and chapter.

To calculate the actual numeric soundwave at the point in the air domain shown in Figure 20, which is the objective of this work, model Free_X was edited to include the values of α and β determined in this section, in the beam's material definition. Then an analysis named FXO_CPE4R_100-4 was created and submitted. The calculated soundwave is shown in section 5.1, Figure 37, and is discussed and validated by comparing it to a microphone recording from section 4.2 in all chapter 5.

4   EXPERIMENTAL SOUNDWAVE RECORDING

Acoustic measurements were done from the vise-beam system introduced in section 3.1 to define some parameters in the FE models from sections 3.5 and 3.8, and to validate the soundwave calculated with Abaqus, as stated at the end of section 3.8. This chapter explains

these measurements, which were made in two experiments. In the first experiment, described in section 4.1, the material damping for the beam in the vise-beam system was measured with a microphone, and then applied as Rayleigh damping to the FE beam from section 3.4, which was done in section 3.8. Also, the microphone measurements made in the experiment were used to define the air mesh from sections 3.5 to 3.7. In the second experiment, described in section 4.2, microphone measurements were made from the vibrations of the beam by exciting it at different positions. This was done to make a correspondence between the frequencies in the microphone measurements and the natural frequencies of the cantilever beam, which were obtained from a 3D FE beam model as will be explained. This allows one to distinguish the frequencies in the measurements that come from the beam's motions from any other frequency in the environment that might have been captured unintentionally, which is necessary when validating the FE soundwave with the microphone measurements.

4.1 Experiment for defining FE modeling parameters

The finite element model used to calculate the soundwave at a point in space consists of a structural domain and an air domain. The dimensions used for the structural domain were described in section 3.1. The dimensioning of the air domain, however, requires an analysis of the frequencies present in the sound radiated by the vibrations of the beam in air, and the reason for this is explained next. The physical beam-air system being modeled with the FEM can be categorized as an exterior acoustic radiation problem, which means that a structure vibrates in an unbounded fluid domain; in the present case, a beam vibrates in an unbounded air domain. To model unbounded domains using finite elements, the domain must be subdivided into two domains: domain A and B, which are shown in Figure 29.

Air domain B

Air domain A

Structure

Truncation surface
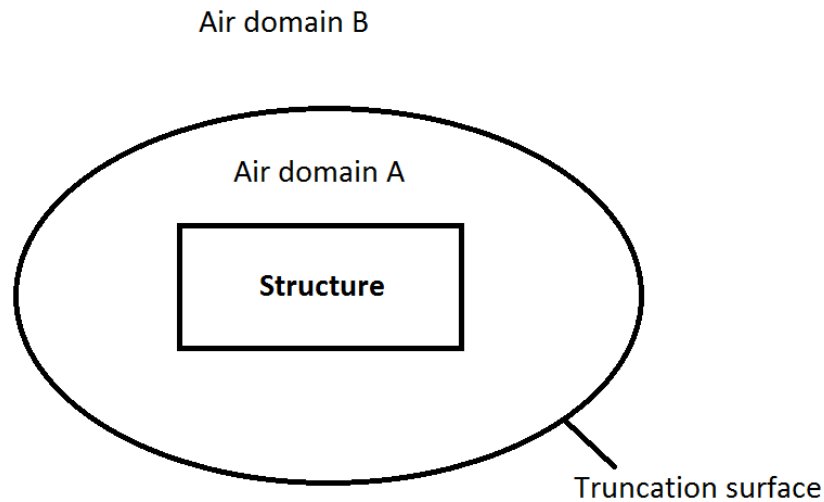
Figure 29: Exterior acoustic radiation problem diagram

Domain A can be modeled with Finite elements; domain B cannot, but its influence in the behavior of domain A can be modeled by placing either infinite elements or nonreflecting BCs in the truncation surface indicated in the figure. The use of infinite elements or nonreflecting boundary conditions, specially of these last, introduce an error in the solution that depends on how far from the structure the truncation surface is located, so the size of domain A must be chosen appropriately.

The Abaqus analysis documentation suggests some guidelines for choosing the size of the finite fluid domain which depend on the minimum and maximum frequencies excited in the system that are desired to be modeled accurately.

Because of this, the sound radiated by the beam from the vise-beam system (described in section 3.1) was recorded with a microphone. By analyzing the recorded signal in the frequency domain, taking its Discrete Fourier Transform (DFT), the frequencies present in the signal were determined. This allowed the determination of the minimum and maximum frequencies to be used when defining the (large) FE air mesh in section 3.5. The determination of these extremum frequencies was based on the relative influence of all the

frequencies found in the experimental magnitude spectrum. The experiment is further explained next, starting with a description of the experimental setup.

To record the sound produced by the beam in the vise-beam system, the vise was fixed to a table so that it wouldn't move when the beam was given an excitation. Figure 30 shows a diagram that indicates exactly how the vise was fixed. As can be seen in the figure, the vise was screwed to a piece of wood, using a piece of sponge in between, to isolate the vibrations of the vise-beam system. The vise was not screwed directly to the table so as not to damage it. The piece of wood was then clamped to the table, using sponges in between to further isolate the vise-beam system. The sponges used were simple, generic sponges.
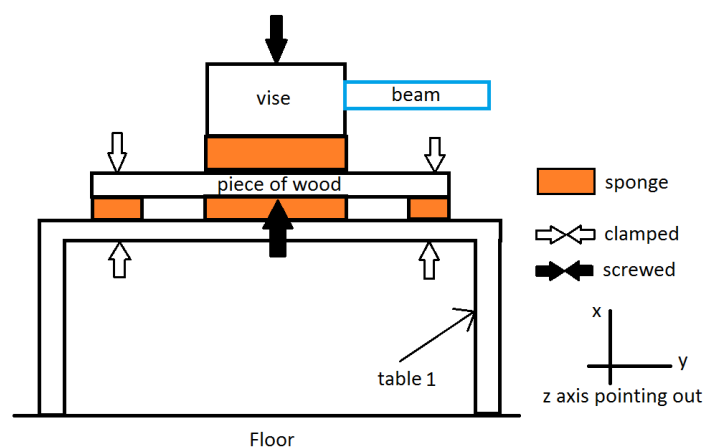
Figure 30: Diagram showing how the vise-beam system was fixed

Once the vise-beam system was fixed, a simple microphone (from a pair of earphones) was placed in front of the beam near its free end, at a distance of roughly 1 cm from the beam's surface as indicated in Figure 31. Next, the free end of the beam was given an initial displacement of roughly 2 mm in the transverse direction (the z direction in Figure 31), and subsequently, the beam was let to vibrate freely.
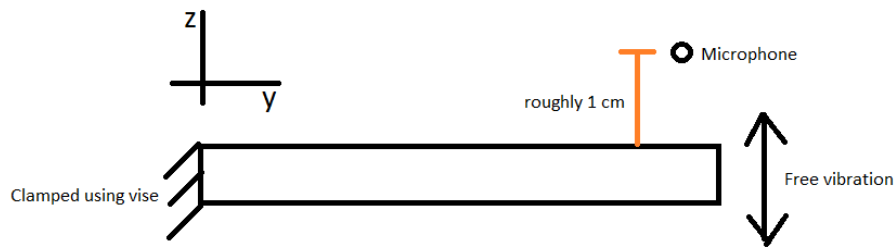
Figure 31: Set up of microphone and beam for experimental sound radiation measurements

A few recordings were performed, each with a duration of 9 seconds, using MATLAB. The MATLAB function `audiorecorder` was used to record the audio samples. This function has as input arguments the sampling frequency in hz (fs), the number of bits per sample (nbits) (which indicates the resolution of the recording), and the number of channels (nChannels). The values used for these arguments were fs = 44100, nbits = 16, and nChannels = 2; which correspond to the Compact Disk Digital Audio (CDDA) audio quality (The PC Guide, 2001), with the exception that the number of channels used was 1 instead of two, because setting nChannel to two results in two soundwave signals per recording, while only one is desired (nChannel = 2 corresponds to stereophonic recordings). The sampling frequency of 44100 hz allows frequencies up to 22050 hz to be captured accurately, which is more than enough since the maximum audible frequency for humans is 20 khz (Kinsler, Frey, Coppens, & Sanders, 2000).

Figure 32 shows a typical recorded soundwave in the time domain. The `audiorecorder` function gives unitless magnitude values in the range from -1 to 1. These values can be made to correspond to pressure values, but this would require a calibration to be done with the microphone.
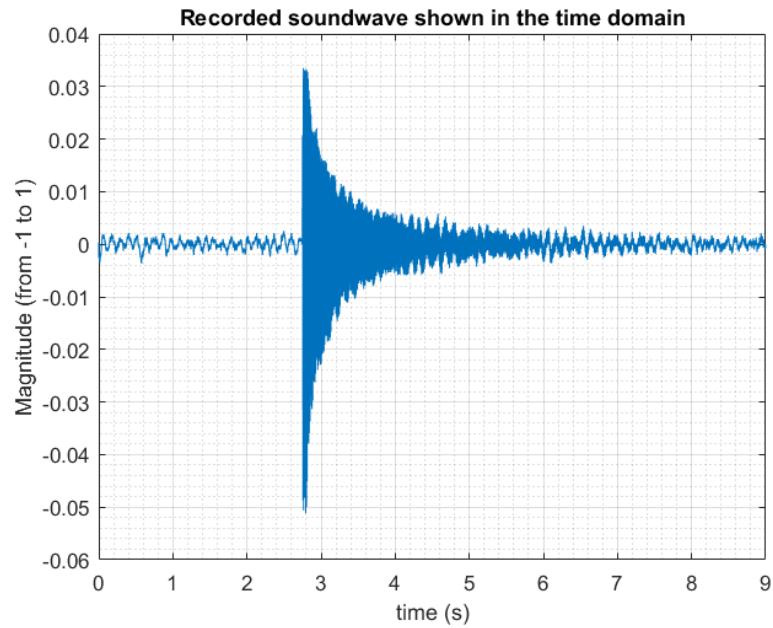
Figure 32: Time domain soundwave produced by the vibrating beam, captured with a microphone

After recording the soundwaves, the DFT was taken for each of them to see their frequency content, which was used to define the air-domain mesh dimensions and mesh density for the FE air model in section 3.5. To calculate the DFT of the time-domain waveforms, the MATLAB function `fft` was used. Figure 33 shows the magnitude spectrum of the DFT for the soundwave shown in Figure 32. The spectrum on the bottom of the figure is simply an amplification of that on the top. The DFT magnitude spectrum of the other soundwave measurements were very similar to the spectrum in Figure 33, so they are not shown.
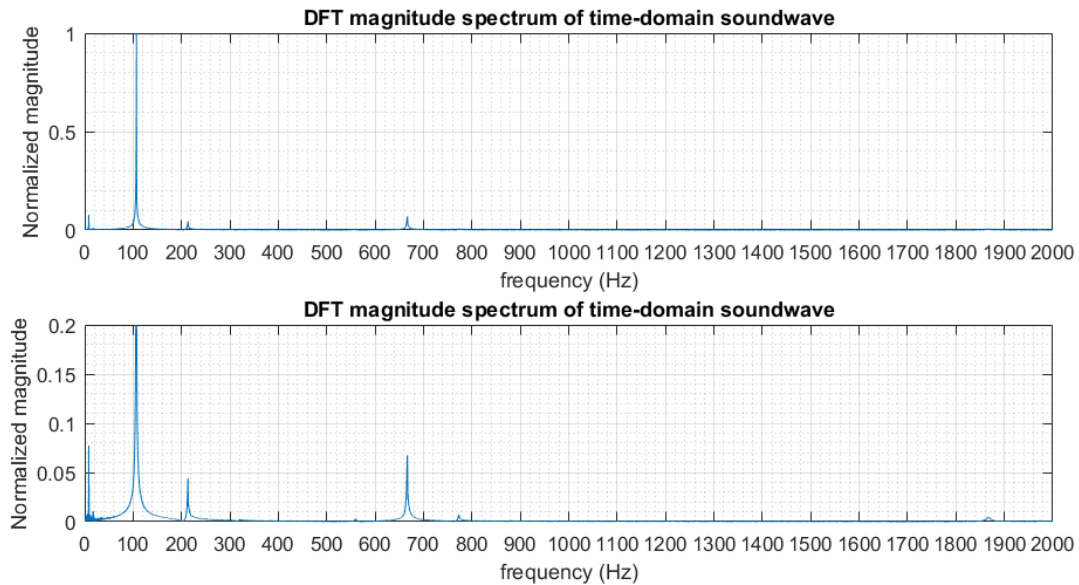
Figure 33: DFT magnitude spectrum of recorded soundwave

The magnitude spectrum in Figure 33 shows the largest peak at around 106 hz, and other significant peaks under 2000 hz. For frequencies greater than 2000 hz, the magnitude values were judged too small relative to those in the frequency range from 100 to 2000 hz. For this reason, it was decided to limit the finite element model, particularly the air domain mesh, to represent frequencies in the range from 100 hz to 2000 hz. A frequency in the range from 0 to 100 hz can also be seen, the origin of this frequency component is not known (it doesn't correspond to a beam's natural frequency), however, frequencies in this range are very low, and therefore may not be easily audible (Kinsler, Frey, Coppens, & Sanders, 2000).

4.2 Sound recordings for validating the FE soundwave

In chapter 5, the soundwave obtained with Abaqus was compared with the same soundwave produced by the beam in the vise-beam system from section 3.1 by exciting it in the same way as in the Abaqus model. This soundwave was recorded with a microphone, and is henceforth referred to as the recorded soundwave. To validate that the frequencies in the recorded soundwave corresponded to the beam's natural frequencies, and not to some sound

recorded from the environment, other microphone recordings were made by exciting the beam at different locations, chosen to excite particular beam mode shapes more energetically. These recordings, henceforth referred to as the auxiliary recordings, were then compared to the recorded soundwave in the frequency domain, and the frequencies in both sets of recordings were matched, thus concluding the validation. The validation procedure just described is detailed in this section.

To measure the recorded soundwave and the auxiliary recordings, the same setup described in section 4.1 was used for the beam-vise system. Since the recorded soundwave needed to be compared to the Abaqus soundwave, the UMM-6 USB measurement microphone by Dayton Audio was used to obtain the most accurate measurements. The microphone was mounted in a tripod and placed facing the beam, and on top of a table, which was not the same table from Figure 30, but was a separate one, which was done to isolate the microphone from any vibrations that the beam-vise system could have transferred to table 1 in the figure. MATLAB was used to do the recordings, with the `audiorecorder` function as explained in section 4.1.

Three auxiliary recordings were made by exciting the beam at three different locations. Figure 34 shows the three recordings, labeled as recordings 2, 3, and 4, and the position of beam excitation for each recording. The recorded soundwave is also shown in the figure as recording 1. The figure also shows the microphone positions for each recording. The microphone was placed in each case 7 mm away from the beam, since in Abaqus, this was the distance between set MIC and the beam, as shown in Figure 20. The exact positions of beam excitation and microphone placement is given in Table 20 for the 4 recordings, where the values are given relative to the coordinate system shown in Figure 34.
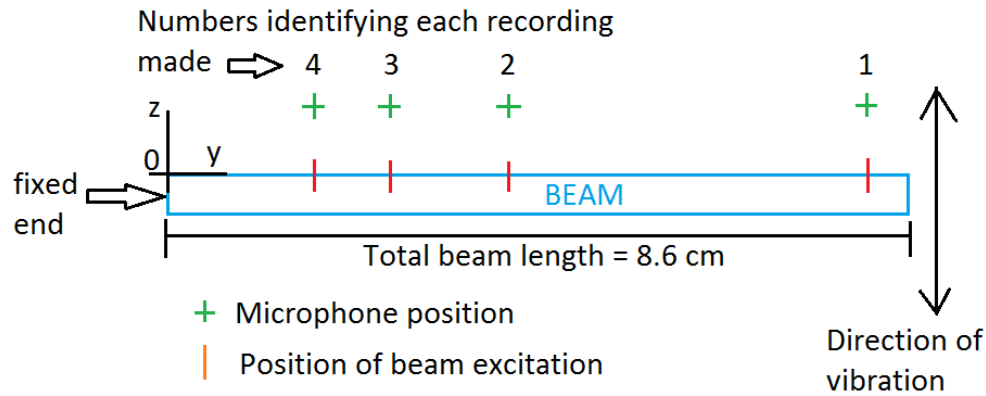
Figure 34: Locations along beam's lengthwise direction where the beam was excited, and microphone positioning for measuring the corresponding excitation

Table 20: Positions of microphone placement and beam excitation, indicated in Figure 34

# of measurement	Microphone placement in cm (y,z)	Position of beam excitation in cm (y,z)
1	(8,0.7)	(8,0)
2	(4.03,0.7)	(4.03,0)
3	(2.5,0.7)	(2.5,0)
4	(1.8,0.7)	(1.8,0)

The excitation positions for the auxiliary recordings were chosen as shown in the table because at these locations, modes 2, 3, and 4 of the beam have a (local) maximum displacement in the transverse direction, as can be seen in Figure 35. The figure shows the first four beam's mode shapes calculated with equation (31) from the Euler-Bernoulli model, and the X values are seen to be the excitation positions from Table 20. The implications of choosing these excitation positions are more easily explained using an example: by exciting the beam from the vise-beam system 4.03 cm away from its fixed end, mode 2 of the beam is strongly energized at this location and the corresponding microphone measurement, when seen in the frequency domain, should have a large peak at the frequency corresponding to

mode 2 of the beam. So, by doing this, it can be proven that the beam's eigenfrequency corresponding to mode 2 is contained in the microphone measurement. The same applies to the other auxiliary measurements.
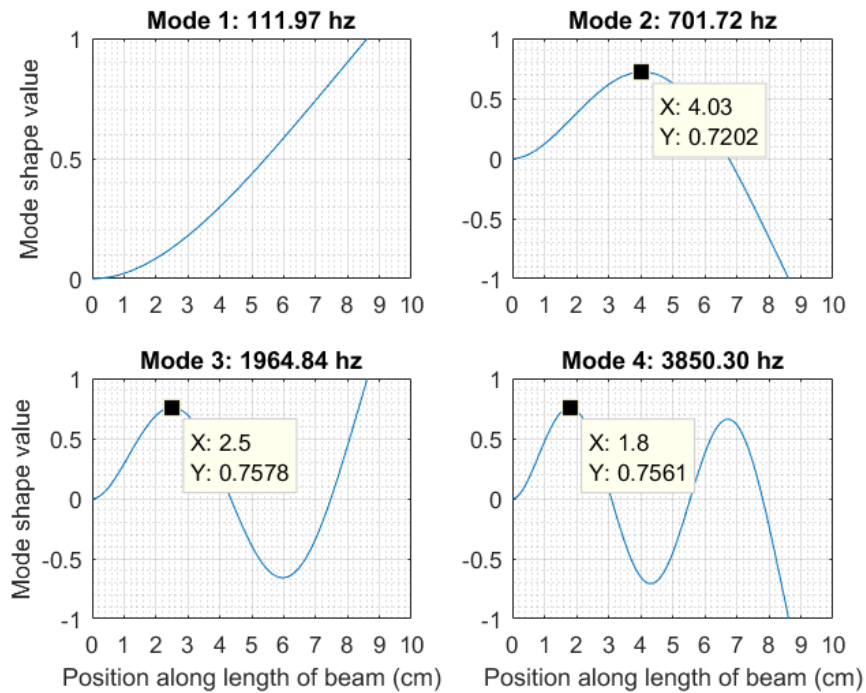
Figure 35: Locations where the first 4 mode shapes of the beam have the largest displacement

The DFT (or FFT) of the three auxiliary recordings and the main recorded soundwave were calculated, and their magnitude spectrum is shown in Figure 36 in blue, where for better visibility, only the relatively large peaks in the four spectrums are labeled with their frequency and magnitude values. Also, shown in the figure in red are the natural frequencies of a 3D FE model of the real-life beam in vacuum (whose dimensions were taken from section 3.1) that were calculated in Abaqus. Although only the frequency range from 100 to 2000 hz was analyzed in this work, the figure shows frequencies from 0 to 4200 hz.

As a note, the frequencies in Figure 36 labeled with a "T" are frequencies that a 2D FE model cannot calculate because they correspond to mode shapes that only a 3D FE beam model can

represent. The frequencies labeled with numbers from 1 to 4 are frequencies that a 2D FE

beam model can calculate, and are the same frequencies as in Figure 43 from section 5.3.
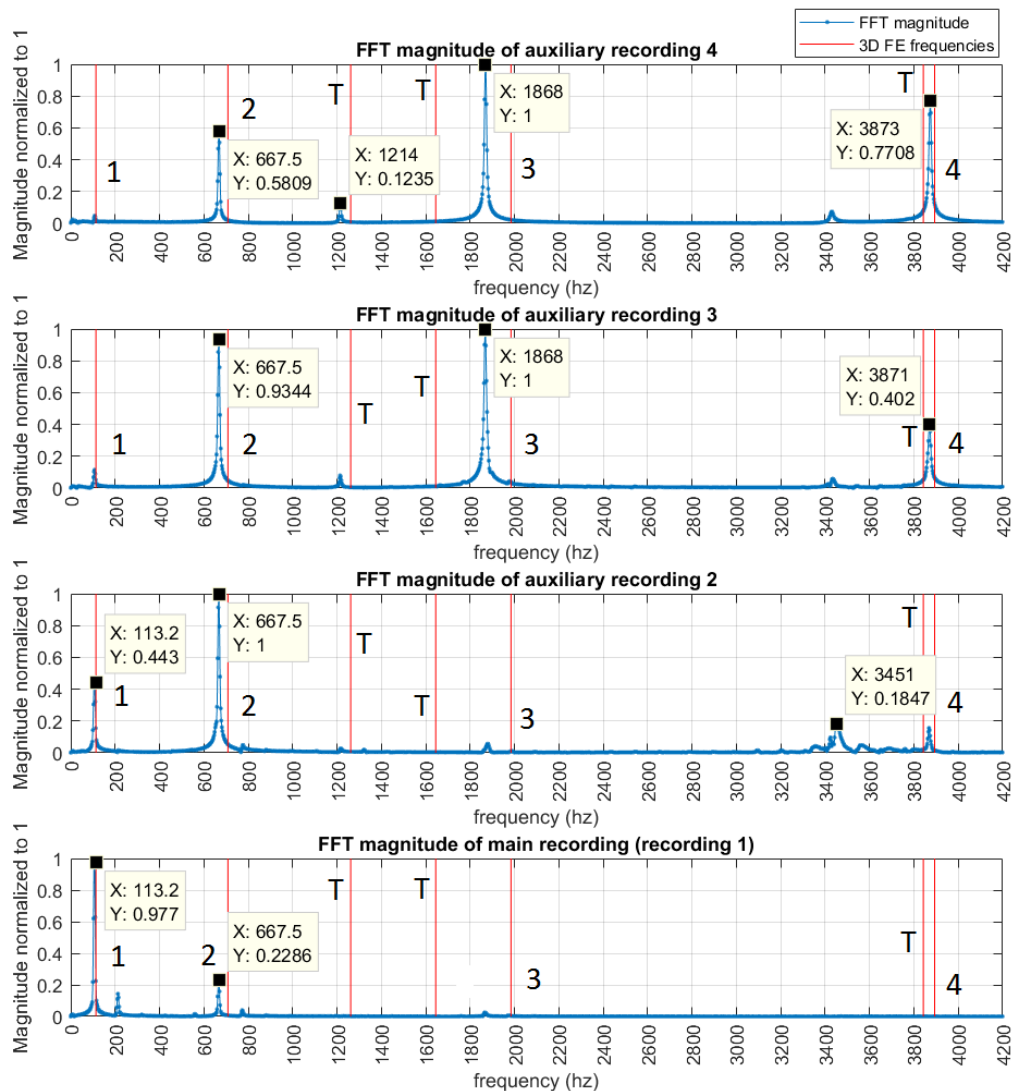
Figure 36: FFT magnitude of the main and auxiliary recordings. The beam eigenfrequencies from a 3D FE beam model are also shown

In Figure 36, it can be seen that there are 3 frequencies in the main recorded soundwave

(recording 1) that are also present in the auxiliary recordings: one at 113.2 hz (labeled as

frequency 1), other at 667.5 hz (frequency 2), and the last one at 1868 hz (frequency 3).

Although the frequencies 2 and 3 are not very noticeable in the main recorded soundwave,

they can be clearly seen in the auxiliary recordings. This proves that the frequencies in the

main soundwave are not any extraneous sound captured in the recording, but that indeed these frequencies correspond to the beam's natural frequencies. Table 21 shows the correspondence between the frequencies measured in Figure 36 (in blue) and the 3D FE beam frequencies in the same figure (in red). It must be noted that the number labels in Figure 36 don't correspond to the frequency numbers in Table 21. Frequency 4 in the table is not found in the measurements because it corresponds to an in-plane mode of the beam, and thus cannot be measured with the microphone since it vibrates perpendicular to the measurement direction.

Table 21: Matching between the 3D FE beam eigenfrequencies, and the frequencies in the microphone measurements from Figure 36

Frequency number	Abaqus Frequency values	Measured frequency values
1	113.175	113.175
2	708.254	667.529
3	1261.78	1213.934
4	1645.05	-
5	1984.22	1868.005
6	3842.48	3450.696
7	3893.19	3873.285

Finally, it must be noted from Figure 36 that for the main recording, there are some peaks in the spectrum at around 200 hz, 600 hz, and 800 hz. Since these peaks don't correspond to any of the natural frequencies from the 3D FE beam model, their origin is not known although it's discussed in section 5.3. Anyways, these frequencies should not be considered when validating the FE soundwave. Also, frequencies 3, 4, and 6 from Table 21, and labeled as "T"

in Figure 36, correspond to eigenmodes that involve displacements in three directions, for this reason these frequencies cannot be expected to be found in the Abaqus soundwave since this soundwave comes from a 2D model, which can only model eigenmodes with displacements in 2 directions.

5 RESULTS AND DISCUSSION

In this chapter, the acoustic soundwave calculated with the finite element model Free_X from section 3.7, referred to as the FE soundwave, is presented and compared to recording 1 from section 4.2 (Figure 34), referred to as the recorded soundwave in this chapter. In section 5.1, the FE soundwave is presented and its magnitude values discussed, and then, it's briefly compared to the recorded soundwave in the time domain. In section 5.2, the frequency component's values in both the FE and recorded soundwaves are compared and discussed. In section 5.3, the frequency components in the recorded and FE soundwaves are shown by calculating their Short Time Fourier Transform (STFT), and their magnitudes are compared within each soundwave and discussed. Finally, in section 5.4, the damping of the frequency components in both soundwaves is analyzed and discussed.

5.1 Time-domain comparison of FE and recorded soundwaves

In this section, the FE soundwave is first presented. Figure 37 below shows the time domain FE soundwave calculated with Abaqus, expressed in terms of the acoustic pressure p in pascals (see equation (23)). The signal was calculated at the node highlighted in red in Figure 20, which is located approximately 7 mm above the beam in that figure. The soundwave was calculated in several runs, using Abaqus' restart capability. Each colored segment in Figure 37 represents one run. Obtaining the soundwave in several runs was found to be faster than obtaining it in only one. Each colored segment with a duration of 0.5 s in the figure took around 6 hours to complete, and after simulating about 0.3 seconds of the soundwave in each

of these segments, the time increments of the Abaqus solver became about 2 times slower to complete.
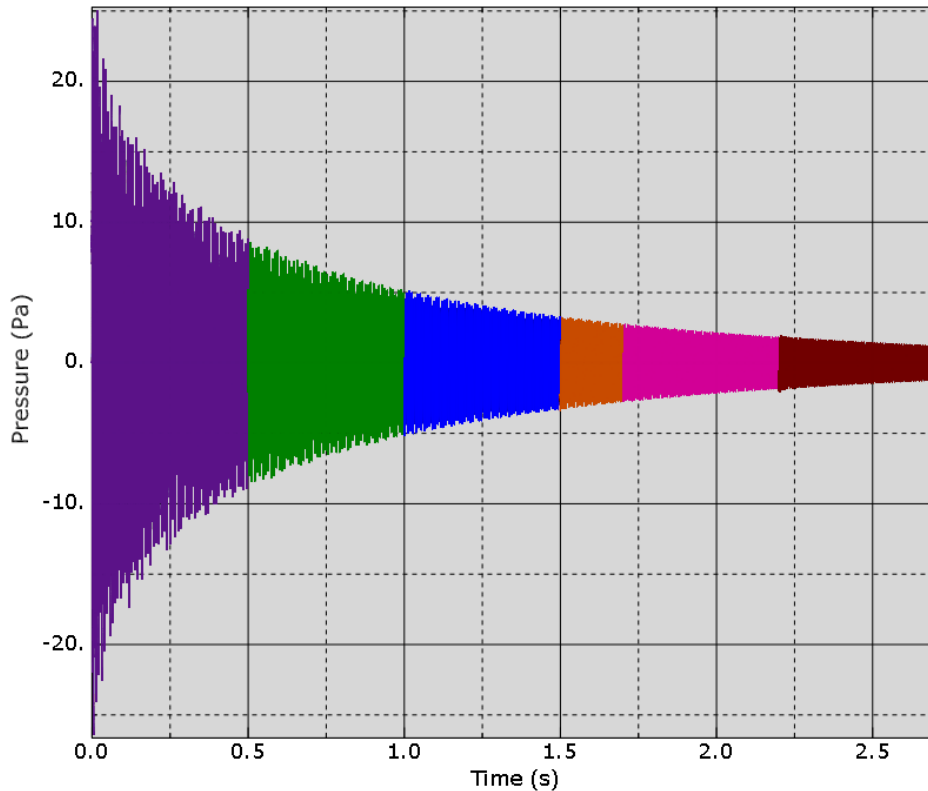
Figure 37: Time-domain soundwave calculated by Abaqus at the node highlighted in Figure 20

The maximum pressure value in Figure 37 is around 25 Pa and it corresponds roughly to the pressure amplitude of the lowest frequency component in the signal, the fundamental frequency component, which is the largest component in the recorded soundwave as discussed in section 4.1, and it also is the largest in the FE soundwave, which is seen in the DFT magnitude spectrum of Figure 22 from section 3.7. To see how large this pressure value is, its corresponding SPL value (equation (24)) was estimated by assuming that its RMS pressure value is that of an harmonic propagating plane wave, with an amplitude equal to 25 Pa. The SPL value is shown in equation (44), where $P_{max,RMS} = \frac{25}{\sqrt{2}}$ for the plane propagating

wave, and P_{ref} is a constant equal to 20 μPa, which is the reference for sound pressure in air (Kinsler, Frey, Coppens, & Sanders, 2000).

$$SPL = 20log_{10}\left(\frac{P_{max,RMS}}{P_{ref}}\right) = 20log_{10}\left(\frac{\frac{25}{\sqrt{2}}}{20E-6}\right) = 118.93 \; dB \; re \; P_{ref} \quad (44)$$

This SPL value corresponds approximately to hearing a chainsaw 1 meter away from it (The engineering toolbox, n.d.), so it says that the acoustic pressure of 25 Pa is relatively high. The reason why the maximum FE acoustic pressure amplitude is this high can be attributed to two factors: first and most importantly, the 2D FE model from which it was calculated assumes that the width of the FE beam is infinite; second, the distance away from the beam where the soundwave was calculated was 7 mm, and at this small distance the sound radiated by the beam would be judged as relatively loud. The first factor was verified by comparing the SPL value in equation (44), corresponding to the pressure of 25 Pa in Figure 37, with that produced by a beam of infinite length and width that vibrates in an up-and-down manner like a piston with a frequency equal to the fundamental (lowest) frequency component in the FE soundwave (113 hz, from Figure 39, section 5.2), and a displacement amplitude equal to 2 mm, the maximum amplitude of vibration of the FE cantilever beam (as defined in Table 17, section 3.6). The motion of this infinite beam, or piston, produces waves in air that propagate planarly, and theoretical results exist for the acoustic pressure produced. As shown in attachment A, the maximum acoustic pressure amplitude produced by the piston is of 592.24 Pa at any location in the air domain. As can be seen, the maximum amplitude pressure of 25 Pa in the FE soundwave is around 23 times smaller than the pressure produced by the piston, and this makes sense because although the beam that produced the pressure in the FE soundwave has infinite width, it also has finite length unlike the infinite piston. The exact

SPL value for the plane waves generated by the piston with the pressure of 592.24 Pa is given in equation (45).

$$SPL = 20log_{10}\left(\frac{P_{max,RMS}}{P_{ref,RMS}}\right) = 20log_{10}\left(\frac{\frac{592.24}{\sqrt{2}}}{20E-6}\right) = 146.42 \, dB \, re \, P_{ref} \quad (45)$$

This is the sound of a military jet take-off heard at a distance of 30 m (The engineering toolbox, n.d.). Thus, it's concluded that the relatively large pressure values in the FE soundwave are caused by the use of a 2D model which assumes that the beam has infinite width, and objects with a large surface area radiate more sound because the larger the area in contact with the air, the larger the amount of air that can be displaced.

Figure 38 compares the recorded and FE soundwaves in the time domain. To do the comparison, the initial time delay of ~2.25 s in the recorded soundwave between the beginning of the recording and the time when the beam started to vibrate had to be removed. This was done using the MATLAB function `alignsignals`. Furthermore, to do a damping comparison between the signals feasible, the magnitude values in each signal were normalized so that the maximum value (in the vertical axis) in each was equal to one. This was done since the signals didn't have the same units in the vertical axis: the recorded soundwave had unitless values in the range from -1 to 1 as discussed in section 4.1, and the FE signal was expressed in pascals, as can be seen in Figure 37.
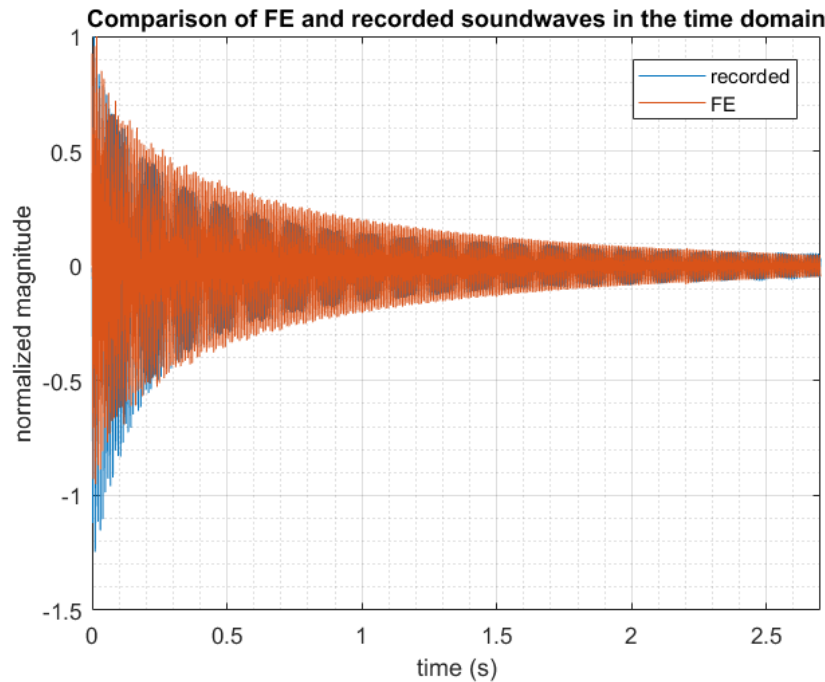
Figure 38:Comparison of recorded and FE soundwaves in the time domain

Figure 38 shows good agreement between the damping of the lowest frequency for both signals. It can be seen that the recorded signal does not have the symmetry with respect to the time axis unlike the FE soundwave. This may have been caused by the preload given to the real-life beam with the finger right before vibration. In the FE case, this preload consisted of the displacement of a single point in the beam in the transverse, or thickness, direction. In the experiment, however, using the finger may have imposed not only an initial transverse displacement on the beam's free end, but also displacement components in other directions. Most importantly, initial velocity components may have been imposed on the beam, and all these initial conditions were applied to a finite area of the beam, unlike in the FE case.

5.2 Comparison of FE and recorded soundwaves' frequency values

In this section, the frequencies in the FE and recorded soundwaves are compared. The following comparisons were made:

- First, to determine how the air affects the motions of the beam, which in turn affect the frequencies of the sound it produces, a comparison was made between the frequencies in the motions of the beam from model Free_X when it vibrates in vacuum vs when it vibrates in air. Structural damping was defined in both cases.

- Then, a comparison was made between the frequency values found in the FE and recorded soundwaves. Their differences were discussed.

- Finally, a comparison was made between the eigenfrequencies from the 3D FE beam model from section 4.2 and the frequencies in the recorded soundwave when the elastic modulus in the 3D FE model is varied. This was done to explain the differences in frequency values between the FE signal and the recorded signal.

Before making these comparisons, the frequencies found in both the FE and recorded soundwaves are shown in Figure 39 (repeated from Figure 43, section 5.3), which were obtained by calculating the DFT (or STFT) magnitude spectrum of the soundwaves in Figure 38. In the figure, the DFT spectrum of the recorded soundwave is shown on top, and on the bottom, the spectrum of the Abaqus soundwave is shown.
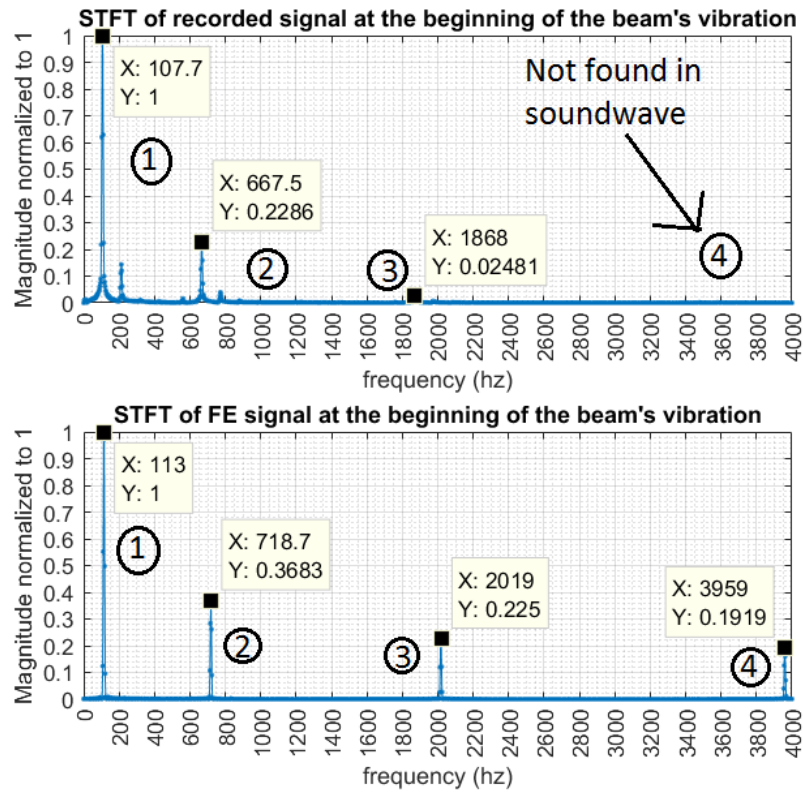
Figure 39: Frequencies in FE and recorded soundwaves from Figure 38. This is the same as Figure 43.

Only the frequencies labeled 1, 2, and 3 in Figure 39 (the same as those in Figure 36, section 4.2) were compared in this section since this work was limited only to the analysis of frequencies in the range from 100 to 2000 hz, as discussed in section 4.1. First, the frequencies in the displacements of the beam from model Free_X are compared, as discussed at the beginning of the section.

When a beam vibrates in vacuum due to initial conditions, the vibrations are not the same as when it vibrates in air because the air exerts forces on the beam which change its frequencies of vibration. To see how much the air changes these frequencies, an FE analysis was made using model Free_X in which the beam was set to vibrate in air in one case, and in vacuum in another case. In both cases, Rayleigh damping was included in the beam, as explained in section 3.8. The transverse displacement of the beam's free end (set "free_edge" in Figure 18,

section 3.6) was calculated as a function of time in both cases, and its frequency content was determined using the DFT.

The frequencies corresponding to the vibrations of the first three eigenmodes of the beam (the vibrations of these modes produce the soundwave frequencies 1, 2, and 3 in Figure 39) were determined from the DFT magnitude spectrum and are shown in Table 22, in columns 2 and 3 from left to right, for the case in vacuum and in air respectively. In column 4, the percent error between the two frequency sets is given relative to the frequencies of the beam vibrating in vacuum. As can be seen, the frequencies in the vacuum case are slightly higher than in the air case, which makes sense because by coupling the beam to the air, the air adds mass to the coupled beam-air system, and this makes the beam vibrate with smaller frequencies. The difference is not large, though, and is within 0.48 %, as indicated in the table. This happened because the air's added mass is not very large since its density is small compared to that of the beam.

The table also shows the frequencies in the FE soundwave in column 5 (from left to right). These are seen to be almost equal to the frequencies of the motions of the beam in air (column 3), which also makes sense since the soundwave was produced by the beam's vibrations in air. Since the frequencies of the soundwave are close to the frequencies of the beam's displacements in air, and these are only slightly smaller than the frequencies of the beam's displacements in vacuum, this suggests that the FE soundwave could also be calculated by uncoupling the vibrations of the beam from the air, instead of using a fully coupled acoustic-structural model to do so, as was done in this work: in one FE analysis, the vibrations of the beam in vacuum could be calculated, and then used as a BC to drive the pressures of the air in another FE analysis. The resulting soundwave's frequencies would be practically the same as the frequencies in the FE soundwave calculated in this work: they would be the same as the frequencies of the beam's vibrations in vacuum.

Table 22: Effect of the air on the frequencies of vibration of the beam. Also, the frequencies in the FE soundwave and the beam's eigenfrequencies from Table 8 are shown for comparison.

frequency number	Frequency (hz)		%e beam tip	Frequency (hz)	
	2D FE beam tip (in vacuum)	2D FE beam tip (in air)		FE soundwave	2D FE beam (natural frequencies)
1	114.1	114	0.09	113	117.48
2	722	718.5	0.48	718.7	735.76
3	2024	2018	0.30	2019	2058.13

It must be noted that the frequencies of the beam's displacements in vacuum should be practically equal to the natural frequencies of the beam, which are shown in Table 8 under the label "With plane_strain section". However, they're not exactly the same, as can be seen by comparing the frequencies in column 2 from Table 22 with the beam's natural frequencies from Table 8, repeated in Table 22 on column 6. The differences in the values of the frequencies were mainly caused by setting "yes" to the parameter "Update reference configuration" from Table 19, section 3.7, which was necessary for transferring the results from model "Preload" (section 3.6) to model "Free_X" (section 3.7), and it must be noted that the frequency differences disappeared almost completely if the parameter was set to "No", but by doing so, the tie constraint between the air and the beam made in model Free_X couldn't be done and consequently, the FE soundwave couldn't be calculated. This modeling step should be improved in future work. Other cause of the differences in the frequencies are the structural damping: the frequencies in column 2 of Table 22 were obtained with damping defined on the beam, while the eigenfrequencies in column 6 were obtained without defining any damping for the beam, however the effect of damping was judged to be negligible.

Next, the frequencies in the FE and recorded soundwaves were compared. Table 23 shows frequencies 1, 2 and 3 from the FE soundwave (column 3 from left to right) and recorded soundwave (column 2), taken from Figure 39. A percent error between the two frequency sets was calculated using equation (36), and is shown in column 4, where the error is given with

respect to the recorded soundwave's frequencies. The table shows that the FE soundwave

frequencies are within 8.08% of the corresponding frequencies in the recorded soundwave.

This error is explained in the following.

Table 23: Frequency comparison between FE and recorded soundwaves, and between eigenfrequencies of 2D and 3D beam FE models

Frequency number	Recorded soundwave (hz)	FE soundwave (hz)	Soundwave %e	3D FE beam (hz)	2D FE beam (hz)	Natural frequency %e
1	107.67	113.05	5.00	113.18	117.48	3.80
2	667.53	718.70	7.67	708.25	735.76	3.88
3	1868.00	2019.00	8.08	1984.22	2058.13	3.72

The frequencies in the FE soundwave must be similar to the natural frequencies of the beam

that was used to calculate the soundwave, so to explain the differences found between the

frequencies in the recorded and the FE soundwaves, the eigenfrequencies of the 2D FE beam

from model Free_X, whose vibrations produced the FE soundwave, were compared to the

eigenfrequencies of the 3D FE beam presented in section 4.2, which is a beam model that

describes the real-life beam better. The eigenfrequencies of both the 3D and 2D FE beams are

shown in Table 23 in columns 5 and 6 respectively, and in column 7, a percent error of the

2D beam's eigenfrequencies is given with respect to the 3D beam's. It can be seen in the

figure that the frequencies of the 2D beam are at most 3.88% larger than the same frequencies

in the 3D beam, which says that if the 3D beam model had been used to calculate the FE

soundwave, the resulting soundwave's frequencies would have been smaller than the

frequencies found in the FE soundwave calculated in this work (using the 2D FE beam), and

their values would have been approximately the same as those of the eigenfrequencies of the

3D FE beam shown in the table. This is because, as already stated, the frequencies in the

soundwave are similar to the eigenfrequencies of the beam since the air has only a small

influence on the motions of the beam due to its low density. One reason why the

eigenfrequencies from the 2D and 3D models were different may be the assumption of plain strain for the 2D model.

If it can be assumed that by calculating the soundwave with the 3D FE beam model, the soundwave frequencies would have been almost the same as the eigenfrequencies of the 3D beam shown in Table 23, the soundwave frequencies would still be larger than the frequencies present in the recorded soundwave obtained in this work, as can be seen in the table by comparing the 3D beam eigenfrequencies with the frequencies in the recorded soundwave. This can be explained at least partially by the fact that Young's modulus and Poisson's ratio used in Abaqus for all beam models, shown in Table 2, were not measured from the real-life beam, but were rather estimated from the literature, using as a reference the beam's material, which was known from the datasheet of the plate from which the beam was manufactured.

Finally, to show the effect of changes of an elastic property, like Young's modulus, on the beam's eigenfrequencies (which affect the frequencies in the soundwave), the 3D FE beam's eigenfrequencies are compared in Table 24 with the frequencies from the recorded soundwave from Table 23, using different values of Young's modulus for the FE beam and Poisson's ratio set to 0.3. The table gives the % error values between the recorded soundwave's frequencies and the 3D beam's eigenfrequencies when Young's modulus is set to 200 GPa in one case, and in another, when it's set to 190 GPa. The % error values are given with respect to the FE beam's eigenfrequencies in both cases. It's noted that the eigenfrequencies calculated with the elastic modulus set to 200 GPa are the same as those shown in Table 13.

Table 24: Comparison between frequencies in recorded soundwave and eigenfrequencies of a 3D FE beam. Young's modulus is varied in the FE beam

Natural frequency number	Frequency (hz)			% error, E = 200 Gpa	% error, E = 190 Gpa
	3D model, E = 200 Gpa	3D model, E = 190 Gpa	Recorded soundwave		
1	113.18	109.14	107.67	4.87	1.35
2	708.25	683.95	667.53	5.75	2.40
3	1984.22	1915.09	1868.00	5.86	2.46

As can be seen from Table 24, the error in the frequency values in the soundwave decrease by decreasing the value of the FE beam's elastic modulus. This shows that indeed, variations in the elastic material properties could have caused the differences observed in the frequency values between the FE and recorded soundwaves in Table 23.

5.3 Comparison of frequency component magnitudes in FE and recorded signals

In this section, the frequency components in both the FE signal and the recorded signal are determined from their STFT, and their magnitudes are discussed.

The STFT of the recorded soundwave, which had a duration of 9 s, was calculated and is shown in Figure 40 in the form of a spectrogram. As can be seen in this figure, the beam started to vibrate sometime between 2 and 2.5 seconds after the recording started because sometime in this time interval, there's a sudden appearance of frequencies in the spectrogram.

Also, in this figure there are some low frequency components ($< 100\ hz$) in the soundwave. These components, however, are present in the spectrogram even before the beam started to vibrate, so they are not really part of the sound radiated by the beam's vibrations. In the spectrogram, several frequency components can be observed: the relatively large components at around 100 hz, 700 hz, and 1900 hz were verified to be associated with the beam's natural frequencies in section 4.2. There are also other frequency components in the spectrogram

surrounding these three frequencies, as stated at the end of section 4.2, but it's not known why these frequencies are present in the spectrogram since they don't match any of the beam's natural frequencies calculated with a 3D model as was shown in Table 21, section 4.2. For example, there's no natural frequency for the beam near 200 hz as can be seen in Table 21, however, there's a relatively large frequency component at this value in Figure 40. These unknown frequency components might be reflections of the beam's radiated acoustic waves with the microphone since it was placed quite closely to the beam. They might also be natural frequencies from the coupled vise-beam system, or frequencies in the sound produced by the interaction between the finger and the beam. Also, it must be noted that the fixed-end beam's boundary condition that was tried to be imitated in the experiments by holding the beam with a vise was not perfect: the edges of the vise's jaws that were holding the beam in place might have had a small misalignment, for example, and this may have changed the beam's frequencies to some extent. Lastly, there may be a possibility that these unknown frequency components are a result of aliasing of higher frequency components, but this is very unlikely since the aliased frequencies would have had to be greater than 22050 hz because of Niquist's sampling theorem and the fact that the sampling frequency used to record the signal was 44100 hz. Besides, it's seen from the spectrogram that the frequency components past 2000 hz are hardly present in the signal.
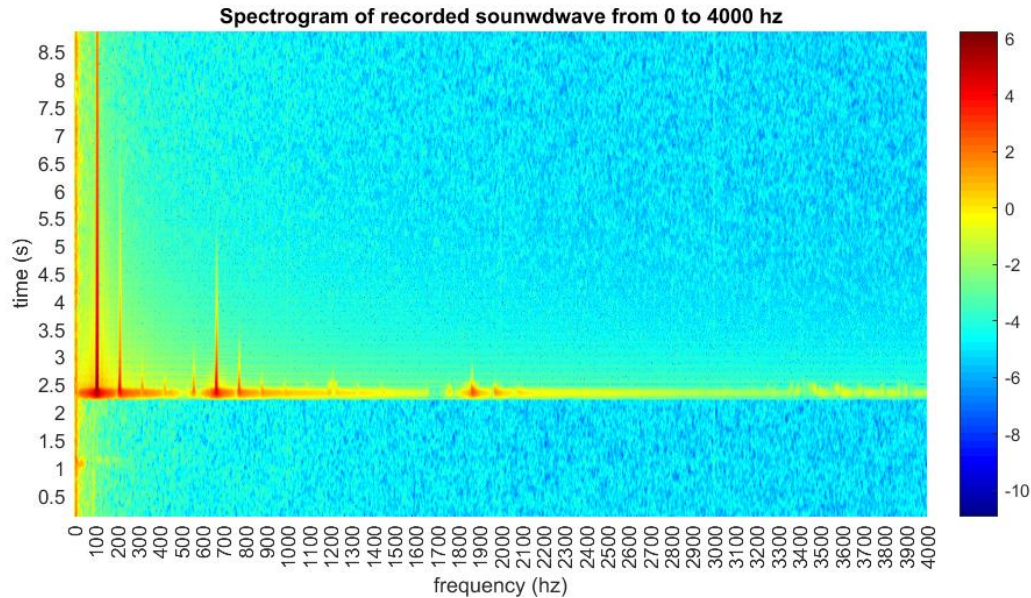
Figure 40: STFT of recorded soundwave from the beginning of recording

Figure 41 and Figure 42 show the STFT of the recorded and FE signals from Figure 38, with the natural logarithm of the STFT magnitude shown in colors. The figures show that the frequency components of roughy 100 hz, 700 hz and 1900 hz are present in both soundwaves, and that the 700 hz and 1900 hz frequency components are more present in the FE signal as the time progresses than in the recorded soundwave. This may be due to two factors: either the magnitudes of the frequency components are larger in the FE soundwave than in the recorded one from the beginning of the beam's vibrations, or the damping of the same frequency components is lighter in the FE soundwave. A combination of these two factors is also possible.
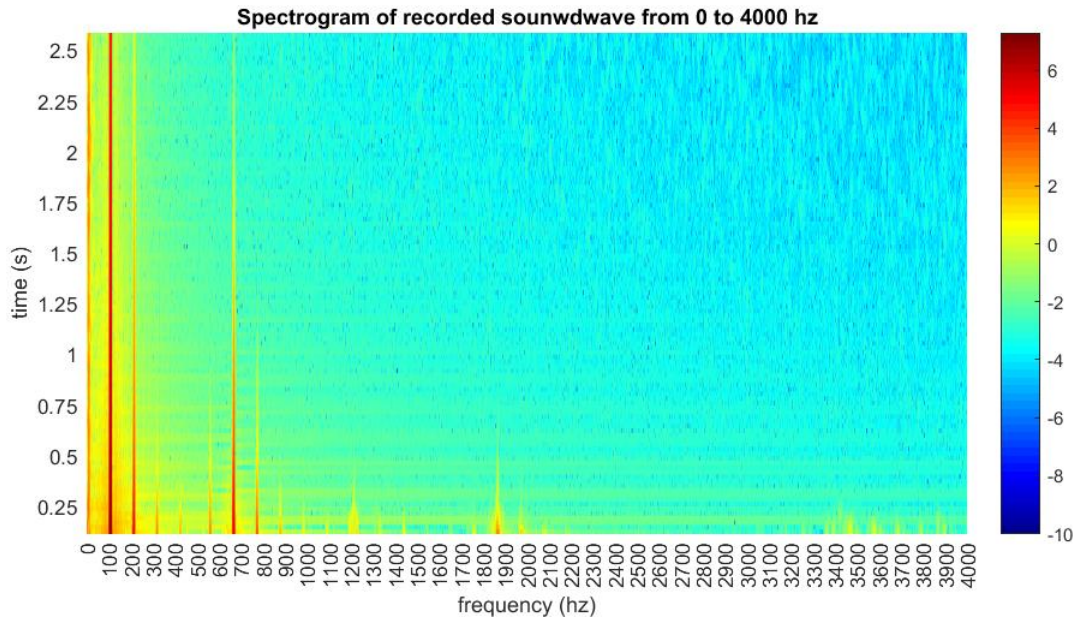
Figure 41: Spectrogram of recorded soundwave for the duration of the FE soundwave. The natural logarithm of the magnitude of the STFT is shown in colors.
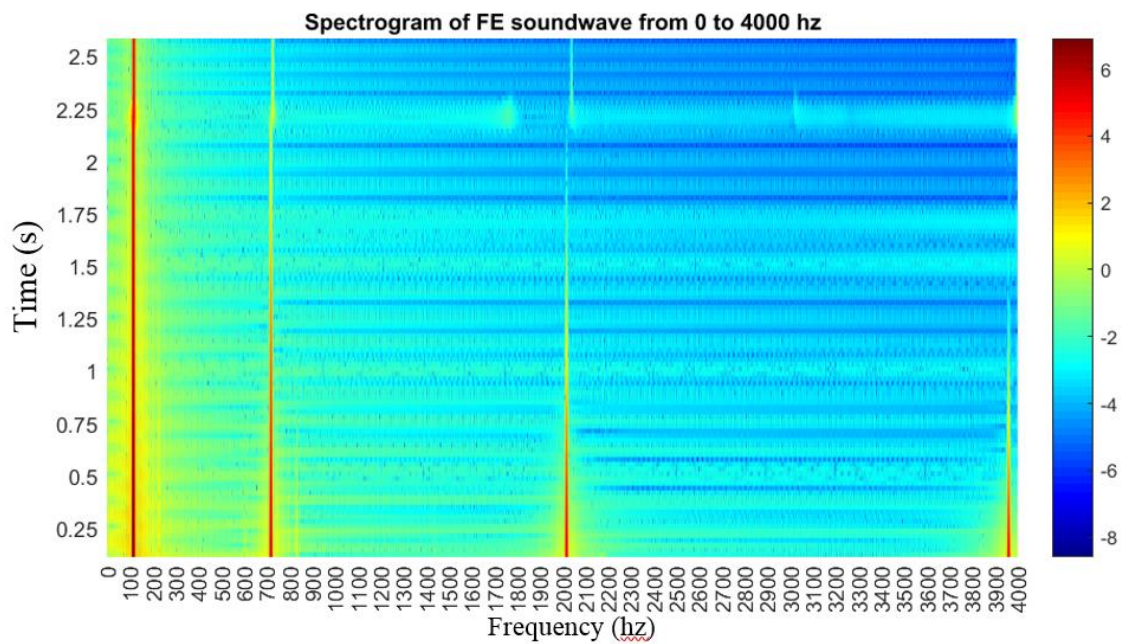
Figure 42: Spectrogram of FE soundwave. The natural logarithm of the magnitude of the STFT is shown in colors

From Figure 41 and Table 21 from section 4.2 it can be noted that the following frequencies from the 3D FE beam model from section 4.2: 1645.05 hz and 3842.48 hz, are not present in the spectrogram of the recorded soundwave, and the frequency of 1261.78 hz is only slightly

present. It's reminded here that these three frequencies correspond to modes that can only be represented by a 3D FE beam model in Abaqus, and cannot be obtained with a 2D FE frequency extraction procedure due to the symmetry conditions inherent to a 2D FE model. It's concluded, then, that in the frequency range from 0 to 4000 hz, the frequencies corresponding to 3D mode shapes are practically absent in the recording, and thus, a 2D FE model is sufficient to synthesize all the frequencies excited by the real-life beam in the given frequency range. The reason why the frequency of 1261.78 hz is only slightly present in the spectrogram of the recording may be that its mode shape doesn't displace air as effectively as the other modes, like the first mode. The same argument explains why the other two frequencies (1645.05 and 3842.48 hz) do not appear in the spectrogram. The magnitudes of the frequency components in both the FE and recorded soundwaves are analyzed next.

Figure 43 shows a comparison of the STFT's magnitude spectrum from Figure 41 and Figure 42 around time zero, when the beam just starts to vibrate and the magnitudes of all frequency components are the highest in both the FE and recorded soundwaves. The magnitude of the STFT is shown without taking its natural logarithm and it was normalized to 1 in both cases

for convenience. The frequencies in the figure that correspond to a beam's natural frequency

are numbered, from lowest to highest frequency, just as in Figure 36, section 4.2.
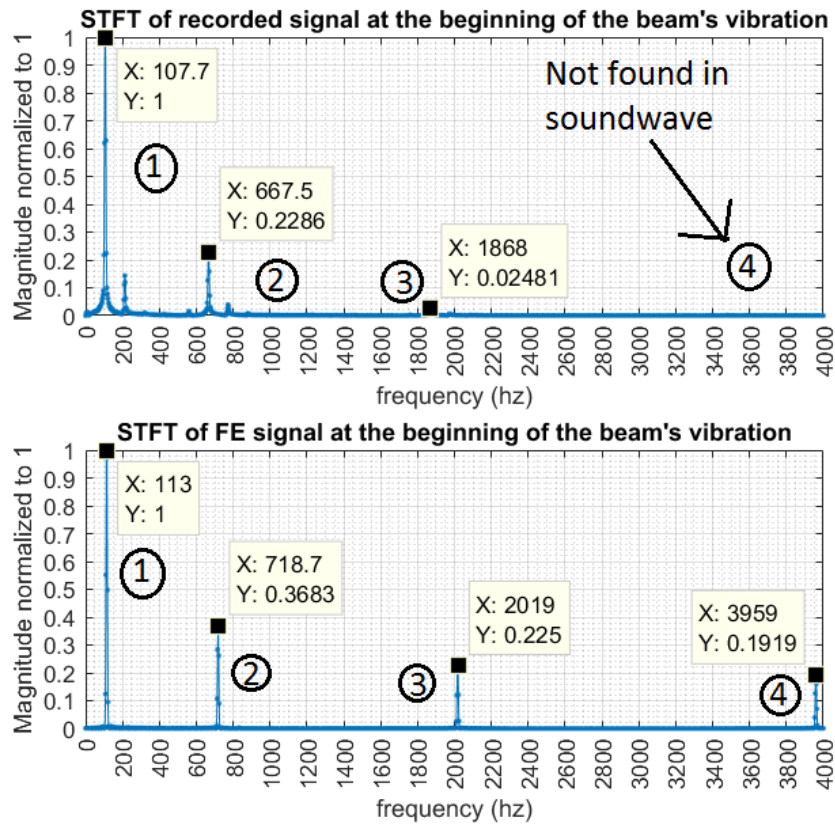
Figure 43: Comparison of STFT magnitude of FE and recorded soundwaves at the beginning of the beam's vibration. The different frequency components are labeled in the figure for both signals

From Figure 43, it is visible that for both signals, the lowest frequency component (frequency

1) is the largest relative to the other components in each signal. This makes sense for two

reasons: first, as discussed in section 3.8, the beam's generalized displacement with the

largest influence on its overall motion is the one corresponding to its lowest eigenfrequency,

so it should not be surprising that the lowest frequency in the soundwave, produced by the

vibration of the lowest beam eigenfrequency, would also be the most influential on the

behavior of the soundwave. Second, both soundwaves were obtained close to the beam's free

end, where some of the beam's modes have nodes (opposite to antinodes). This means that at these locations these modes would radiate sound least effectively.

Another important thing to notice from Figure 43 is that in the case of the FE soundwave, the magnitude of frequencies 2, 3, and 4 represent a larger fraction of frequency 1's magnitude than do the same three frequencies in the case of the recorded soundwave, with respect to frequency 1 in that soundwave. For example, in the case of the FE signal, the magnitude of the second lowest frequency component (of roughly 718 hz) is roughly 37% the magnitude of the first component (of roughly 113 hz), while in the recorded soundwave, the second lowest component (of roughly 667 hz) is only 23% of the lowest frequency component in that signal. As for frequency 4 in the recorded signal, its magnitude is so small that it can't even be seen in Figure 43.

The fact that in the recorded signal, frequencies 2, 3, and 4 are relatively smaller than in the FE signal may be caused by several factors:

First, damping could have caused the frequency components in the recorded signal to be relatively small because it must be noted that in the experiment the beam was coupled to the vise, and some of the beam's vibrations were transmitted to the vise. This loss of energy was not modeled with Abaqus and could have limited the magnitude values of the frequency components in the recorded signal.

Second, as already discussed, the preload given to the beam's free end in the FE model is just an idealization of the actual preload given in the experiment, so this difference in the nature of both preloads may have caused a difference in the relative magnitudes of the frequency components in both signals.

Third, according to the datasheet of the microphone used, its frequency response should be flat, meaning that the sensitivity of the microphone, which is the ratio of its output to its input

values, should be the same for all the frequencies in the microphone's operating frequency range. In practice, however, the microphone's frequency response might not have been perfectly flat, which would have given different magnitudes for each frequency component in the recorded data, even if in reality these components had been present in the soundwave with the same magnitude or intensity.

There's also the possibility that the beam's generalized displacements obtained from the 2D model, and shown in Figure 25, might have different magnitudes than those found in a 3D beam model, and the 3D model is a better representation of the real-life beam since it doesn't have the plain strain assumption that the 2D model has. If a soundwave was calculated using a 3D beam model, and the beam's generalized displacements were substantially different from those found in the 2D beam model used to calculate the soundwave from this work, then the frequency component magnitudes in the soundwave obtained from the 3D model would be definitely different from those found in Figure 43 for the FE soundwave.

The Abaqus and recorded soundwaves in Figure 38 were played using an audio system, and after hearing them, it was found that in the Abaqus signal, the fundamental frequency was not as noticeable as the higher frequencies. In contrast, in the case of the recorded soundwave, the fundamental frequency stood out over the higher frequencies. The impact of the frequency component magnitudes of each soundwave in their sound perception is discussed next.

From the equal level loudness contours explanation given in section 2.3, high and low frequency tones in the range from 0 to 10000 hz require a higher SPL to sound equally loudly as the mid frequency tones. And since SPL is an increasing function of pressure, it can be concluded that high and low frequency tones require a larger pressure amplitude to sound equally loud as the mid frequency tones. The relation between this and the results from this

section is the following: From Figure 43, frequencies 2, 3, and 4 in the FE soundwave, in proportion to frequency 1 in the same signal, are larger than in the case of the recorded soundwave.

The implications of this is that if the two soundwaves were listened to by playing them with an audio system, frequencies 2, 3, and 4 in the FE signal might stand out over frequency 1, and this effect wouldn't be as noticeable in the recorded signal. This actually happened in the case of the FE signal when the soundwaves were played using MATLAB's built-in function `soundsc`. In the case of the recorded signal, frequency 1 stood out over the other frequencies. This happened presumably because according to Figure 1 in section 2.3 (equal loudness level contours plot), frequencies 2, 3, and 4 in both sound signals require a lower SPL level, hence, a lower pressure amplitude, to sound as loudly as frequency 1. So, the amplitudes of frequencies 2, 3, and 4 in the FE soundwave may have been large enough to be heard more loudly than frequency 1. Since frequencies 2, 3, and 4 in the recorded soundwave represent a smaller fraction of frequency 1 than is the case in the FE signal, even though they require a lower pressure amplitude to be heard as loudly as frequency 1, their relatively small amplitude wasn't enough to make them stand out above frequency 1, as was judged from playing the sound.

5.4   Damping comparison between the two soundwaves

In this section, several damping estimations and comparisons were made, and are detailed next:

- First, the damping of frequencies 1, 2, and 3 from Figure 43 for the Abaqus soundwave was estimated from the spectrogram of the time-domain signal. The damping of these frequencies was compared between them. It was hypothesized that infinite elements damp more heavily the higher frequencies.

- To prove that air infinite elements damp more heavily higher frequencies, the transverse displacement of the beam from model Free_X from section 3.7 was calculated at its free end, when the beam vibrates in air and in vacuum, which was done in section 5.2, and the damping of the frequencies in both displacements was estimated from their STFTs and compared. It was verified that infinite elements damp higher frequencies more heavily.

- The damping in frequencies 1, 2, and 3 from the recorded soundwave were then estimated from the corresponding STFT and compared to the damping of the corresponding frequencies in the FE soundwave.

First, the damping in the Abaqus soundwave was analyzed. Figure 44 shows the STFT of the FE soundwave with the natural logarithm of the magnitude in the vertical axis (Figure 42 viewed from a different perspective). The decay of each frequency component is visible in the figure. The same three frequency components (1, 2, and 3) shown in Figure 43 are indicated in Figure 44.
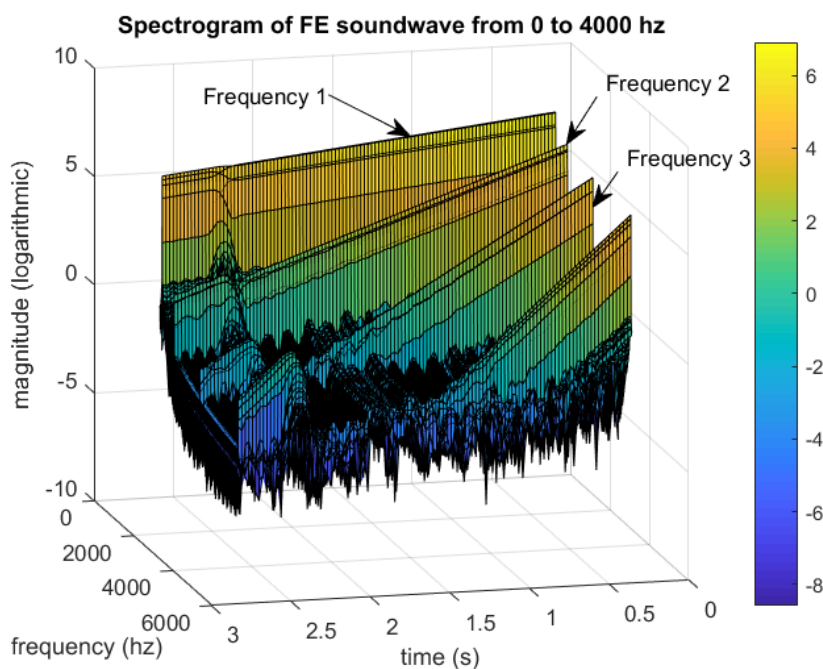
Figure 44: Spectrogram of FE soundwave from 0 to 4000 hz
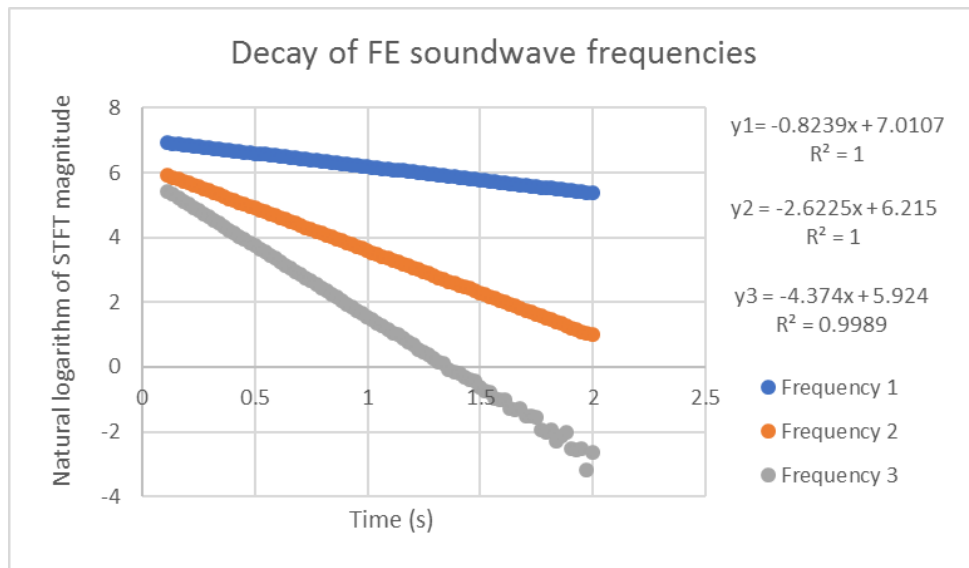
Figure 45: Decay of FE soundwave frequencies as a function of time. The STFT magnitudes come from Figure 44

In Figure 44, there can be seen a sudden jump in magnitude for all frequencies at around 2.3 s. This is explained by the fact that the time-domain soundwave in Figure 37 (from which the spectrogram is shown) was not calculated in a single Abaqus analysis, but several restart analyses were performed to get it. At around 2.3 s from Figure 44 one restart analysis concluded and another began, and apparently the transfer of results from the first analysis to the second caused the disturbance that can be seen in the figure. In Figure 37 this disturbance is also visible, and an amplified view of it is shown in Figure 46.
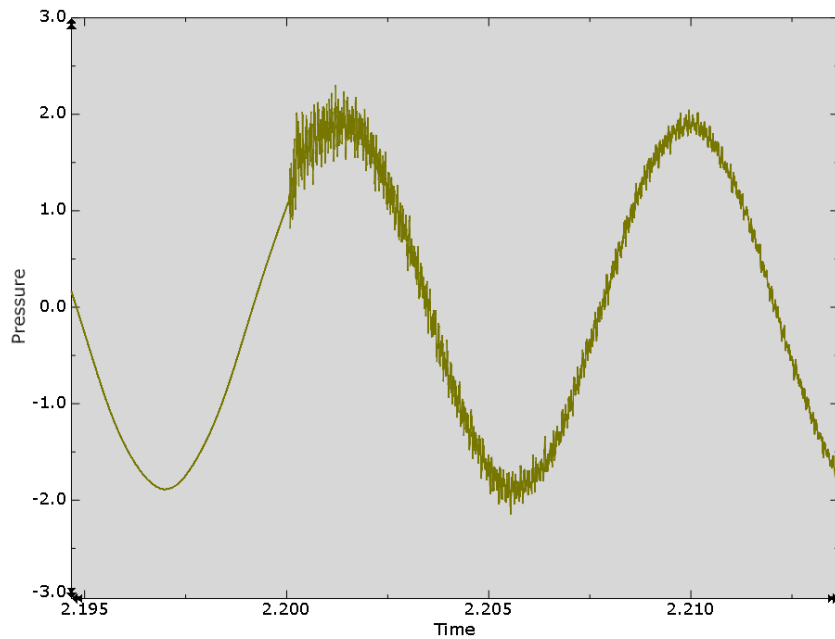
Figure 46: Amplified view of the disturbance in the Abaqus soundwave from Figure 37

The magnitude of an STFT is proportional to the magnitude of the time-domain signal from which it was calculated, so if the different frequency components in the time-domain FE soundwave each have a magnitude that decays exponentially with time, then their STFT magnitude must also decay exponentially with time, and the logarithm of these magnitudes must decay linearly with time. This is shown to happen in Figure 44 for all frequency components in the range from 0 to 4000 hz. Figure 45 shows more clearly how the peaks in Figure 44 for frequencies 1, 2, and 3 decay linearly as a function of time. Also, a linear fit was made to each set of data in the figure and the equation of the fit is shown; the slope of the equations represents how fast each frequency component decays, and the R^2 value for each equation shows how well each linear fit fits the data.

Since the R^2 values in Figure 45 are practically equal to 1, it can be concluded that all three frequency components' magnitude decays exponentially with time. This was expected since their damping is related to the Rayleigh damping defined for the FE beam, which produces an exponential decay type of damping.

One important thing to be noted from Figure 44 and Figure 45 is that while the logarithm of the magnitudes of the three frequencies shown decay linearly with time, the rate of decay is not equal for all frequencies and it increases as the frequencies increase. This is more clearly seen by the fact that the slopes of the linear fits in Figure 45 increase in magnitude as the frequency increases. This implies that the higher frequency components are more damped than the lower ones. This was not expected: since only mass proportional damping (α value in Rayleigh damping) was defined for the structure in the FE model, the product $\xi_i \omega_i$ from equation (19) is equal to $\frac{\alpha}{2}$ for all values of i, which means that all generalized displacements of the beam in equation (17) must have had the same exponential decay term equal to $e^{-\alpha/2}$, and as a consequence from equation (15), all beam's nodal displacements must have been composed of n frequency components, each damped with the same exponential decay term of $e^{-\alpha/2}$. And since the frequency components in the FE soundwave should behave in a similar way as those in the displacements of the beam, the soundwave frequencies should also have been equally damped, but this is not what happens in Figure 44 or Figure 45.

To prove that in fact, the frequencies in the beam must be equally damped because of the Rayleigh damping, a 2D FE analysis was made of the cantilever beam vibrating in vacuum using model Free_X from section 3.7 (without considering the air part), and only mass-proportional Rayleigh damping was defined for the beam. The transverse displacement of the beam's free end, taken as the displacement of the node in set free_edge from Figure 18, was calculated as a function of time (the same was done in section 5.2), and its STFT was calculated and is shown in Figure 47 with the natural logarithm of the magnitude in the vertical axis. In the figure, the lowest three frequency components are shown (associated with frequencies 1, 2, and 3 in Figure 44), and only one second of vibration was calculated.
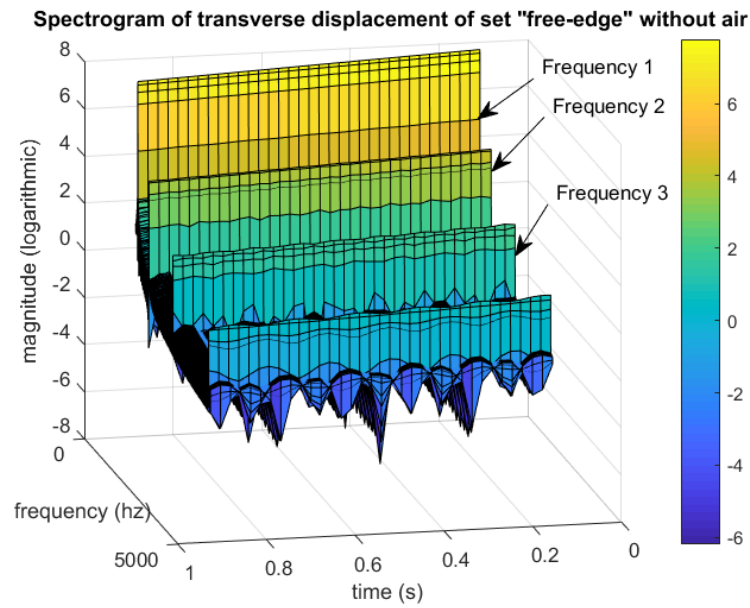
Figure 47: STFT of transverse displacement of FE beam's free end for the beam vibrating in vacuum

Figure 48: Decay of beam displacement frequencies as a function of time for beam vibrating in vacuum with Rayleigh damping. The STFT magnitudes come from Figure 47

Figure 47 shows that each frequency component decays linearly with time, and the rate of decay is the same for all frequencies. This is more clearly seen in Figure 48, which is similar to Figure 45 but refers to Figure 47. In the figure, the three lines have practically the same slope, so the three corresponding frequencies are equally damped.

The transverse displacement of the beam's free end (more precisely of set free_edge from Figure 18) was calculated again, but this time with the beam vibrating in air. The STFT of this displacement function is shown in Figure 49.

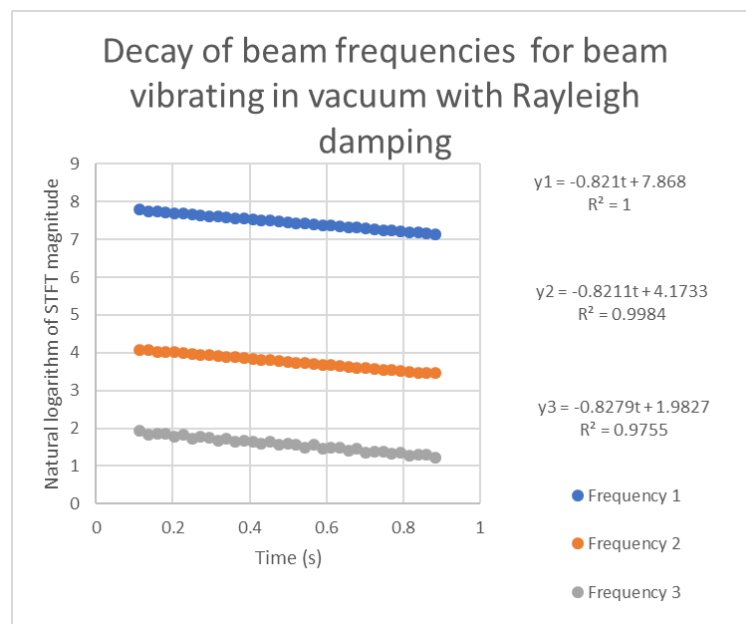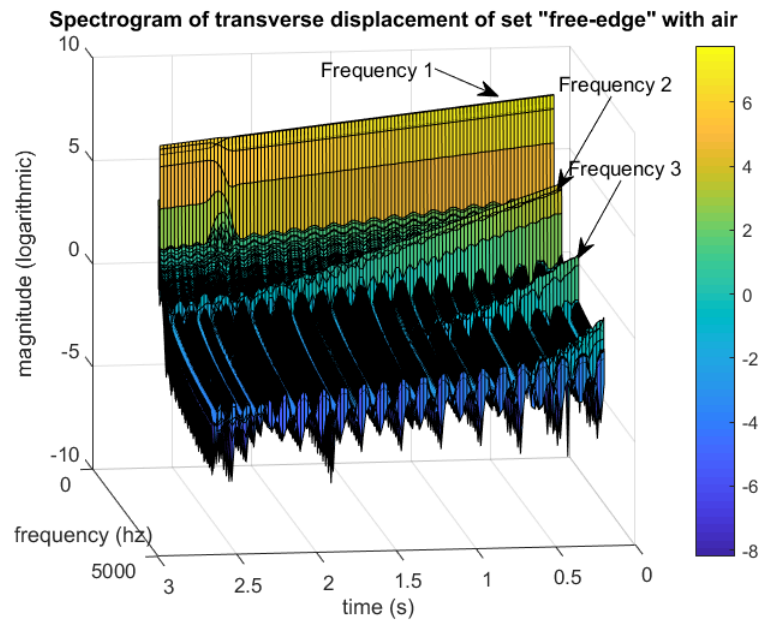*Figure 49: Spectrogram of transverse displacement of set "free_edge" when the beam vibrates in air*
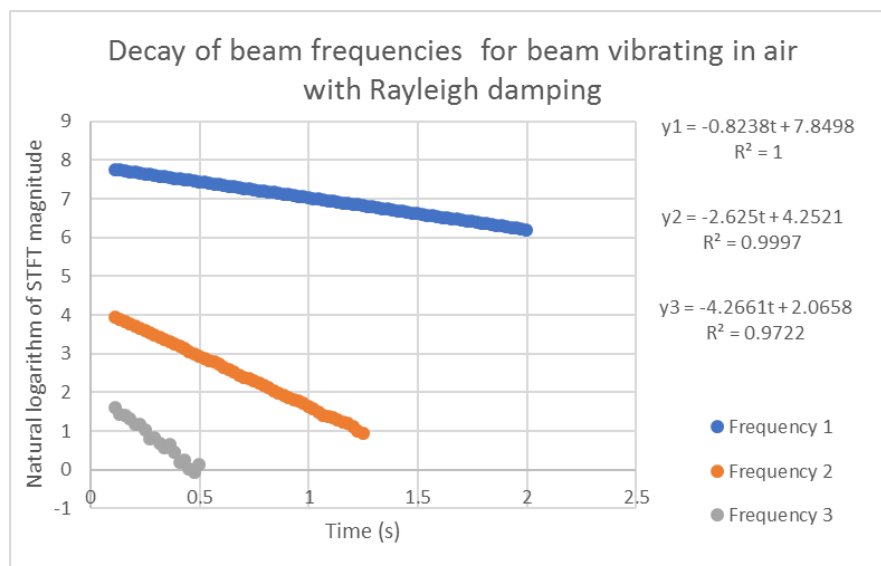

Figure 50: Decay of beam displacement frequencies as a function of time for beam vibrating in air with Rayleigh damping.

The STFT magnitudes come from Figure 49

Figure 49 shows the same three frequency components as Figure 47 and Figure 44. Figure 50 shows better the decay of the frequency peaks in Figure 49 as a function of time. Figure 50 shows that each frequency component in Figure 49 decays more rapidly as the frequency increases.

Figure 47 shows equal damping for the three frequencies; in contrast, Figure 49 does not. The only difference in both cases is that in Figure 47 the beam vibrated in vacuum and in Figure 49 it vibrated in air, so it can be concluded that the air damps the higher frequencies more heavily. Since the only damping found in the air is the one that comes from the infinite elements, it can be concluded that infinite elements damp the higher frequencies in the transverse motion of the tip of the beam more heavily, and consequently, they also do this for the frequencies in the soundwave as indicated in Figure 44.

From Figure 47 and Figure 49, it can also be concluded that if the FE soundwave was calculated by uncoupling the structural and air domains, the damping in the frequency components from the resulting soundwave would be different than in the FE soundwave calculated with the structural and fluid domains coupled, which was done in this work. This is because in the uncoupled case, the damping behavior of the beam would be as in Figure 47, while in the coupled case, the damping behavior of the beam is as in Figure 49, and the soundwave behavior depends heavily on the behavior of the beam. So, if the uncoupled model was used to calculate the soundwave, even though the frequencies in the resulting sound signal would be practically the same as the ones in the FE signal obtained in this work, as discussed in section 5.2, the damping would be different.

Figure 51 shows the STFT of the recorded soundwave, and as before, the natural logarithm of the magnitude is shown in the vertical axis. From the figure, it can be seen that in the beginning, the frequency components don't decay as straight lines as in the FE soundwave.

This means that the frequency components don't have an exact exponential decay, and this was confirmed for the lowest frequency component of the soundwave in Figure 24, section 3.8, by looking at the coefficient R^2 from Figure 26 and Figure 27, which is not exactly equal to 1. The frequency components in Figure 51 appear to decay as a straight line for the larger time values, though. As in the case of the FE soundwave, the rate of decay of each frequency component in the recorded soundwave also increases with increasing frequency. Figure 52 shows the decay of the three frequency peaks in Figure 51 as a function of time. In the figure, it's clearer that the logarithm of the STFT magnitudes of the three frequency components in Figure 51 do not decay linearly with time exactly, which is shown by the fact that the R^2 values are not exactly equal to 1. Also, the rate of decay is seen to increase as the frequencies increase because of the larger magnitude of the slopes of the linear fits in the figure as the frequencies get larger.

By comparing the slopes of the line equations in Figure 45 and Figure 52, it can be seen that frequencies 1 and 2 are similarly damped in both FE and recorded soundwaves. However, the third frequency is more heavily damped in the recorded signal than in the FE signal.
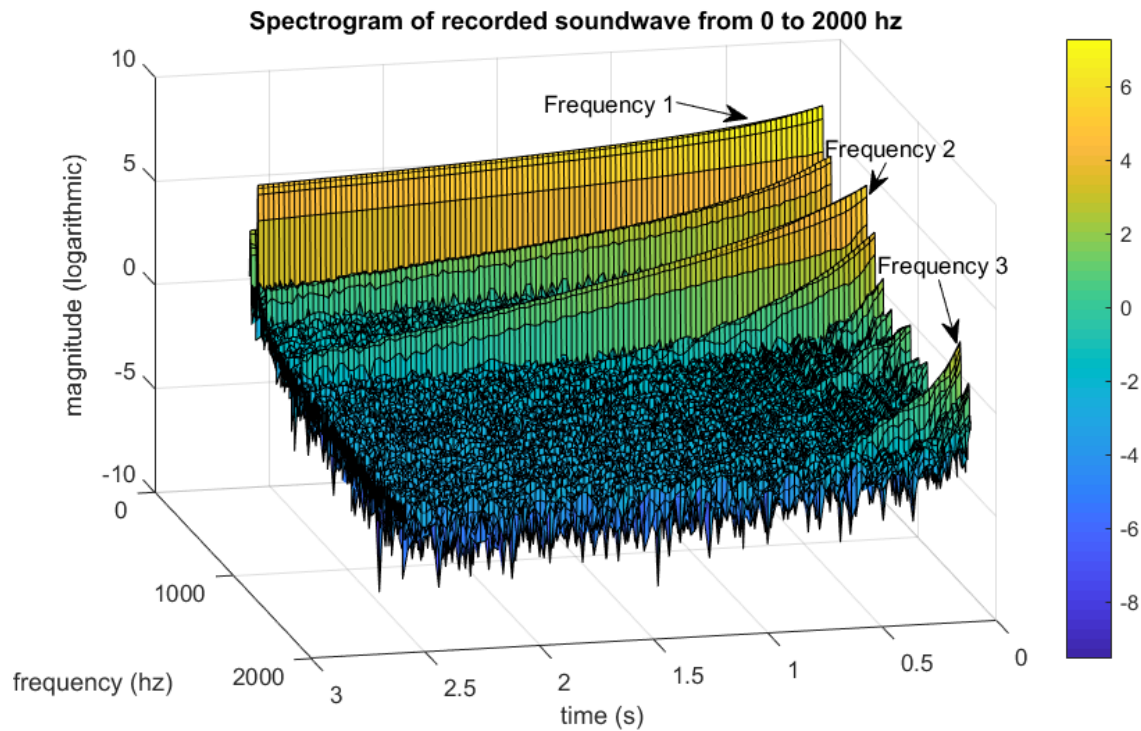
Figure 51: Spectrogram of recorded soundwave from 0 to 2000 hz

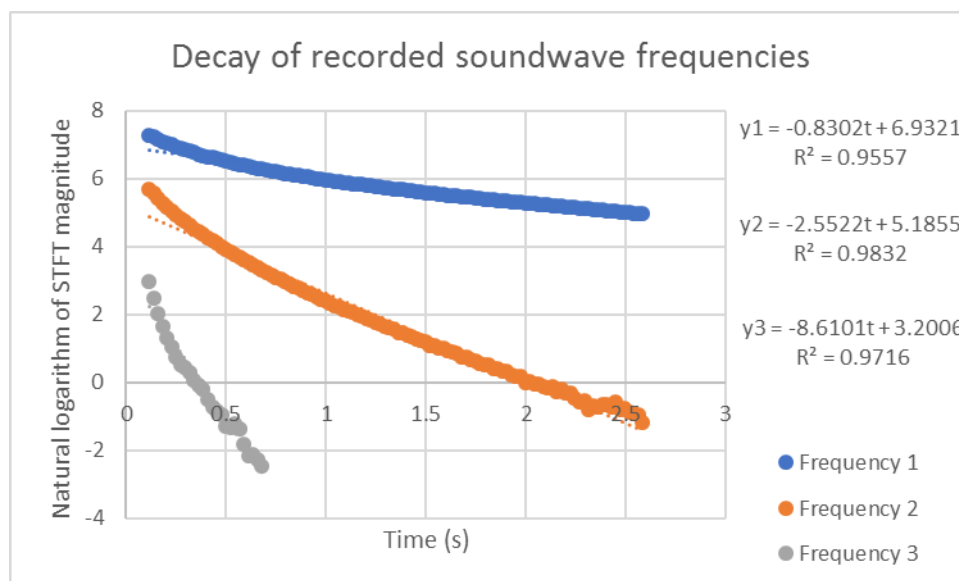*Figure 52: Decay of recorded soundwave frequencies as a function of time. The STFT magnitudes come from Figure 51*

Finally, Table 25 shows the damping ratios and natural frequencies extracted from the slopes

of the linear functions in Figure 45, Figure 48, Figure 50, and Figure 52, by making each

slope equal to $-\xi_i \omega_i$, assuming the exponential decay of each frequency component in these

figures behaves as $e^{-\xi_i \omega_i t}$, like in the case of the underdamped sinusoid in equation (17). The frequency values in Table 25 for the beam's free end displacements were obtained from Table 22, section 5.2, and the frequencies for both soundwaves were obtained from Table 23 in the same section. As can be seen, for the beam's tip displacement, the damping ratios of each frequency are larger when the beam vibrates in air than when it vibrates in vacuum, which is due to the damping from the air infinite elements.

Table 25: Natural frequencies and damping ratios extracted from the rate of decay of the beam's tip displacement frequencies in air and in vacuum, and from the rate of decay of the recorded and Abaqus soundwave frequencies

Beam's free end with air		Beam's free end in vacuum		FE soundwave		Recorded soundwave	
frequency (hz)	damping ratio (%)	frequency (hz)	damping ratio (%)	frequency (hz)	damping ratio (%)	frequency (hz)	damping ratio (%)
114	0.115010	114.1	0.114519	113	0.116042	107.7	0.122684
718.5	0.058146	722	0.018100	718.7	0.058075	667.5	0.060853
2018	0.033646	2024	0.006510	2019	0.034480	1868	0.073359

6   CONCLUSIONS AND RECOMMENDATIONS

In the following chapter, conclusions are drawn from the discussion of the results in chapter 5. Then recommendations for improving the work presented in this document are given.

6.1   Conclusions

The objective of synthesizing the sound of a vibrating cantilever beam with finite elements was accomplished in three ways: first, the frequencies in the calculated soundwave were found to differ from the corresponding frequencies in the recorded soundwave by a maximum of 8.08% in the analyzed frequency range from 100 to 2000 hz, which is satisfactory. Second, the damping of the frequencies in both soundwaves was found to be similar in that higher frequencies were more damped than lower ones. And third, in both soundwaves, it was found that the frequency with the largest magnitude was the fundamental, and the magnitude decreased as the frequencies increased.

The frequencies in the recorded soundwave were found to be a little lower than in the FE soundwave. This was attributed in part to the fact that the elastic properties of the beam used to obtain the recorded soundwave were not measured but estimated from the literature. Also, by using a 2D FE model of the beam with the assumption of plain strain to calculate the soundwave, its frequencies may have been slightly larger than they would have, had a 3D FE beam model been used to calculate the soundwave instead, which would represent reality better. This is because by comparing the 2D FE beam eigenfrequencies with those from a 3D FE model, the eigenfrequencies from the 2D model were found to be at most 3.88 % larger than the eigenfrequencies from the 3D model, and the eigenfrequencies of the beam affect the frequencies in the calculated soundwave. Differences in the eigenfrequency values may have been present between the 2D and 3D models due to the assumption of plain strain for the 2D model.

The FE soundwave obtained in this work was calculated using a coupled structural-acoustic FE model. The soundwave could have been calculated from a 3D model, but the computational cost of doing so would have been too high because of the increased number of equations that would result from modeling a 3D region, and also because of the high cost of using a direct integration procedure to advance the FE solution in time. It's important to mention, though, that the frequencies corresponding to mode shapes that can only be represented with a 3D model were not present in the recorded soundwave, but only those that the 2D model could represent. So, the 2D model was enough to calculate a soundwave with all the frequencies present in the recording.

It must be noted that when comparing the eigenfrequencies of the 2D FE beam used to calculate the FE soundwave, obtained with model F, with the frequencies in the vibrations of this beam in vacuum due to initial conditions, obtained from model Free_X, it was found that the beam's eigenfrequencies were a little larger than the frequencies of the beam's vibration

in vacuum. The difference between these frequencies in reality should be close to zero, and it was found to be caused mainly by updating the reference configuration of the beam when transferring results from model "Preload" to model "Free_X". This modeling procedure should be improved in future work.

If the FE soundwave had been calculated by decoupling the structure and acoustic domains, very similar frequencies as the ones found in the FE soundwave calculated in this work would have been present in the resulting signal since it was found that the air surrounding the beam doesn't have an important influence on the frequencies of its vibrations. However, the damping of the different frequency components in the signal may have changed substantially from the damping observed in the soundwave calculated in this work, because of the damping of the infinite elements that affects the motions of the beam. Besides, it was found that the infinite acoustic elements damp more heavily the high frequency components than the lower ones.

The soundwave calculated with Abaqus has a maximum amplitude of roughly 25 Pa for the lowest frequency component in it, which is a relatively large value. This, however, was expected since the 2D FE model from which the soundwave was calculated assumes that the beam is infinite in the width direction. By comparison, if the beam had infinite length and width, and was vibrating in an up-and-down manner like a piston, at the same frequency as the lowest one in the FE calculated soundwave, it would produce planar soundwaves with a magnitude of 592.24 Pa.

By comparing the relative magnitudes of the frequency components in both the FE and recorded soundwaves in the range from 0 to 4000 hz, it was found that in the FE soundwave the second, third and fourth frequency components had a larger magnitude in proportion to the first component than in the recorded soundwave. Because of the behavior of the human

ear, this may explain the fact that when playing the FE soundwave with an audio system, the higher frequency components stand out over the fundamental frequency, unlike the recorded soundwave, which when played shows that the fundamental frequency stands out over the other frequencies. The differences in the relative magnitudes of the frequency components in each soundwave should be further researched, but they could be attributed to several factors, like the fact that the energy dissipated by the real-life beam through the vise was not modeled in Abaqus, the nature of the preload given to the beam in real life and in Abaqus, the fact that a 2D beam model with infinite width was used to approximate the behavior of a 3D structure of finite dimensions, and the microphone used in the recording not having a perfectly flat frequency response.

Finally, by analyzing the recorded soundwave in the frequency domain, it was found that it contained some frequencies that did not correspond to any of the natural frequencies obtained from a 3D FE beam model (which is the only model that can capture all of the beam's natural frequencies). The presence of these frequencies in the soundwave may have been caused by the fact that the fixed-end boundary condition on the beam that the physical system tried to imitate by using a vise was not perfect: The edges of the vise's jaws that were holding the beam still were not perfectly aligned with each other, for example. Furthermore, it must be noted that the recorded soundwave was not exactly the result of the vibrations of a cantilever beam alone, but of the beam-vise coupled system, so it is possible that this coupled system had natural frequencies of its own that were captured with the microphone. Also, these unknown frequencies in the recorded soundwave might have been soundwaves reflected from the microphone; this could have happened since the microphone was placed quite closely to the beam. They could have also been frequencies present in the sound produced by the interaction of the finger and the beam, when preloading it.

6.2   Recommendations

To improve the work presented in this document, the ideas given in the following can be tried:

To obtain a soundwave with Abaqus whose frequency components are more similarly damped as the corresponding frequency components in the recorded soundwave, the following can be done: an uncoupled acoustic-structural analysis can be used to calculate the soundwave with Abaqus, in which the damping in the beam is defined so that it takes into account the damping from the air infinite elements in addition to the structural damping. Since the motions of the beam would be uncoupled from the air, this last would not further damp the motions of the beam, unlike in a fully coupled acoustic-structural analysis, as shown in this work. This would produce a soundwave with frequency components similarly damped as the corresponding frequency components in the motions of the beam, which comes from the observation that the frequencies in the FE soundwave from this work (Figure 45) had similar damping as the corresponding frequencies in the motion of the beam (Figure 50). This observation can also be used to define damping in the beam as described above: the damping of the beam's eigenfrequencies can be defined to be equal to the damping of the corresponding frequencies in the recorded soundwave (Figure 52). The beam's damping matrix C can be calculated from the damping ratios of the frequency components in the recorded soundwave, using the Caughey series, as described in the literature (Bathe, 1996).

Apart from this, to obtain a FE soundwave faster, beam elements can be used instead of 2D plain strain elements for the beam. This might augment the minimum time increment from the explicit dynamics Abaqus solver, which could give a more computationally inexpensive FE model.

The FE soundwave calculation could be performed by using a modal dynamics Abaqus procedure instead of a direct integration procedure as done in this work. Since the modal dynamics procedure is less computationally demanding than direct integration, it may yield results faster, although this type of procedure cannot account for nonlinear effects like large deformations for the beam.

Finally, when making a recording with the microphone, the use of an analog antialiasing filter is recommended so that aliasing does not take place. Also, Abaqus has an antialiasing filter for calculating the acoustic soundwave and its use may make the simulation less computationally expensive.

7 REFERENCES

(2001, April 17). Retrieved from The PC Guide: http://www.pcguide.com/ref/cd/formatCDDA-c.html

Bathe, K.-J. (1996). *Finite Element Procedures.* New Jersey: Prentice-Hall.

Bertrand, T., Kaczmarek, K., & Wilen, L. (2015). Musical Acoustics and Instrument design: When Engineering Meets Music. *International Computer Music Conference Proceedings*, 114-117.

Bestle, P., Eberhard, P., & Hanss, M. (2017). Musical instruments - sound synthesis of virtual idiophones. *Journal of Sound and Vibration*, 187-200.

Bilbao, S. (2009). *Numerical Sound Synthesis.* United Kingdom: John Wiley & Sons, Ltd.

Bilbao, S. (2010). Percussion Synthesis Based on Models of Nonlinear Shell Vibration. *IEEE Transactions on Audio, Speech, and Language Processing*, 872-880.

Bruyns, C. (2006). Modal Synthesis for Arbitrarily shaped objects. *Computer Music Journal*, 22-37.

Debut, V., Carvalho, M., Figueiredo, E., Antunes, J., & Silva, R. (2015). The sound of bronze: Virtual resurrection of a broken medieval bell. *Journal of Cultural Heritage*, 544-554.

Fahy, F., & Gardonio, P. (2006). *Sound and Structural Vibration.* Academic Press.

Fletcher, N. H., & Rossing, T. D. (1998). *The Physics of Musical Instruments.* New York: Springer.

Kinsler, L. E., Frey, A. R., Coppens, A. B., & Sanders, J. V. (2000). *Fundamentals of Acoustics.* John Wiley & Sons, Inc.

Lu, Y., D'Souza, K., & Chin, C. (2005). *Sound Radiation of Engine Covers With Acoustic Infinite Element Method.* SAE Technical Paper. doi:10.4271/2005-01-2449

MatWeb Material Property Data. (n.d.). Retrieved April 6, 2017, from Matweb: http://www.matweb.com/search/DataSheet.aspx?MatGUID=ff6fd4ea327e47d9b838ac044c580693

Nowak, L., & Zielinski, T. G. (2012). Acoustic radiation of vibrating plate structures submerged in water. *Hydroacoustics*, 163-170.

O'Brien, J. F., Shen, C., & Gatchalian, C. M. (2002). Synthesizing sound from Rigid-Body Simulations. *ACM SIGGRAPH Symposium on Computer Animation*, 1-7.

Rao, S. S. (2011). *Mechanical Vibrations.* Singapore: Pearson Education.

Serway, R., & Jewett, J. (2005). *Física para ciencias e ingenierías.* México, D. F.: Thomson.

The engineering toolbox. (n.d.). Retrieved April 26, 207, from The engineering toolbox: http://www.engineeringtoolbox.com/sound-pressure-d_711.html

ATTACHMENT A: ANALYTICAL CALCULATION OF PLANE WAVES PRODUCED BY A PISTON (PLATE) OF INFINITE DIMENSIONS

Here, the acoustic pressure p produced by a rigid piston (plate) of infinite width and length vibrating in air at a given amplitude x_0 and frequency f is calculated. The air's bulk modulus $\mathcal{B}$ and density ρ_0 are given in Table 26 below, as well as the values of the frequency f and displacement amplitude x_0.

The displacement $x(t)$ of a piston oscillating with simple harmonic motion at the circular frequency ω can be expressed in complex exponential notation as in equation (46), where x_0 is the displacement amplitude, which is defined here to be equal to 2 mm (the initial displacement given to the FE beam in section 3.6, Table 17).

$$x = x_0 e^{j\omega t} \tag{46}$$

The speed of oscillation u is the derivative of equation (46) and is given in equation (47)

$$u = \frac{dx}{dt} = j\omega x_0 e^{j\omega t} \tag{47}$$

Since the piston is of infinite dimensions, it produces planar soundwaves with acoustic pressure p. The acoustic pressure is related to the speed of vibrations of the piston by the acoustic impedance z, which is given in equation (48) for plane propagating waves as in the present case. The acoustic pressure is obtained from equations (47) and (48) as given in equation (49), where it's seen that the acoustic pressure is a harmonic function with amplitude p_0. This is the pressure amplitude at the interface between the piston and the air, and if viscous damping is not included in the fluid, the amplitude is the same everywhere in the fluid (Kinsler, Frey, Coppens, & Sanders, 2000).

$$z = \rho_0 c \tag{48}$$

$$p = zu = j\omega\rho_0 c x_0 e^{j\omega t} = \omega\rho_0 c x_0 e^{j\left(\omega t + \frac{\pi}{2}\right)} = p_0 e^{j\left(\omega t + \frac{\pi}{2}\right)} \tag{49}$$

The amplitude p_0 can be calculated from equation (50)

$$p_0 = \omega\rho_0 c x_0 = 2\pi f \rho_0 c x_0 = 2\pi f \rho_0 \sqrt{\frac{B}{\rho_0}} x_0 = 2\pi f x_0 \sqrt{\rho_0 B} \tag{50}$$

In equation (51) the pressure amplitude is calculated using the parameter values in Table 26 and equation (50). The frequency value was chosen to be the lowest frequency of the FE soundwave as shown in Figure 39, section 5.2

Table 26: Physical parameters needed for acoustic pressure calculation

$f \; (hz)$	113
$x_0 \; (m)$	2e-3
$\rho_0 \; \left(\dfrac{kg}{m^3}\right)$	1.225
$B \; (Pa)$	142000

$$p_0 = 592.24 \; Pa \tag{51}$$

ATTACHMENT B: MATERIAL DATASHEET OF THE BEAM MANUFACTURED IN THIS WORK

The material properties of the steel plate are highlighted in orange (1 mm thickness)

产 品 质 量 证 明 书
MILL TEST CERTIFICATE

PAGE 2 OF 3

Customer: CORPORACION ABC ENTERPRISES
品 名: Commodity STAINLESS STEEL COILS
牌 号: Type 430
表 面 加 工: Surface Finish BA/PE
标准: Specification ASTM240/ASTM480
号: Invoice No. MY-EC160929
发行日期: Date 2016/11/17

序号 No.	货物编号 Product No.	厚度 Thickness MM	宽度 Width MM	长度 Length MM	数量 Package Number	重量 Weight Kg	屈服强度 0.2% YS N/mm²	抗拉强度 TS N/mm²	延伸率 EL %	表面硬度 Hardness HRB	炉批号 HEAT NO.	C	Si	Mn	P	S	Cr	Ni
		产品尺寸 Product Size					拉伸试验 Tensile Test					化 学 成 分 (%) Chemical Composition (%)						
3	16111703	0.4	1219	C	1	3145	292	476	28	78	TFE244	0.0380	0.2900	0.4200	0.0290	0.0030	16.520	0.2300
4	16111704	0.4	1219	C	1	3052	292	476	28	78	TFE244	0.0380	0.2900	0.4200	0.0290	0.0030	16.520	0.2300
5	16111705	0.6	1219	C	1	1905	295	478	28	77.5	TFE656	0.0390	0.3300	0.4300	0.0300	0.0020	16.400	0.2500
6	16111706	1.0	1219	C	1	2039	296	480	29	78	TFE664	0.0390	0.3200	0.4100	0.0280	0.0020	16.410	0.0255
7	16111707	1.5	1219	C	1	2000	298	479	28	78.5	TFE541	0.0370	0.2800	0.4300	0.0310	0.0020	16.420	0.0260

备注（Remarks）：
1. 尺寸和表面：合格
   Size and Surface : Guaranteed

签证明所列产品均符合订单和标准的制造要求
WE HEREBY CERTIFY THAT THE MATERIAL HEREIN HAS BEEN MADE IN ACCORDANCE WITH THE ORDER AND SPECIFICATION
*批报告仅可完全复制
*The report can only be copied completely

技 术 本 部
TECHNICAL DEPT.

Authorized Signature(s)